
On-bottom Stability Analysis of a Subsea Pipeline in Irregular Waves and Currents

Lanjing Li, 220440
Universitetet i Stavanger
Spring 2016

Supervisors
Professor Muk Chen Ong, UiS
Dr. Guomin Ji, MARINTEK

Acknowledgement

This thesis is a reflection to my Master of Science in offshore structure and material engineering at University of Stavanger.

Firstly I would like to show my appreciation for the education I have received in University of Stavanger. I felt home as an international student.

Foremost I would like to express my most sincere gratitude to my supervisors Dr.Guomin, Ji and Professor Muk Chen Ong, for the continuously academical support illuminating inspiration and immense knowledge. They have always been there with great patience when I was confused or stuck. I could never have had better guidance if it was not for them.

Moreover I am grateful to my beloved parents who have been giving me the unconditional support through out my whole life, especially during my study abroad.

Without all that mentioned above, there would be neither me as a person I am now, nor the academical contribution this thesis is to make. Thank you!

Abstract

Pipelines in a subsea environment are exposed to a very complex system of hydrodynamic reaction. The on-bottom stability has long been an important study for offshore practice. The soil types, wave conditions as well as the structure itself are considered to be the main focus of the on-bottom stability analysis for a subsea pipeline.

The objective of this thesis is to study the on-bottom stability in a series of complex environmental conditions through the dynamic analysis, as well as the generalized stability method and absolute lateral static stability method. The effect of different parameters regarding stability is investigated through the sensitivity analysis. Models will be built using PONDUS, a software developed by MARINTEK for the dynamic on-bottom stability analysis. The linear wave theory, the JONSWAP spectrum and the energy-based soil model will be considered for irregular waves and soil-pipe interactions respectively. Based on the different case set-ups, the results will be compared and discussions will be made on the methodology of pipeline stability analysis, considering the sensitive variables as follows.

Both regular waves and irregular waves have been studied in the past. Behaviours of the pipe in irregular waves are studied further in this thesis based on the previous research. Important development patterns and characteristic values such as displacement, forces and velocity will be compared between cases with regular and irregular waves. The mechanisms are further discussed based on simulation results. Same values taken for the wave height and wave period of regular waves, the significant wave height and the peak wave period of irregular waves. Results indicate that the maximum wave-induced water particle velocity is larger in irregular waves. It suggests that when considering the environmental condition, 10-year return currents and 100-year return irregular waves is the most critical load combination. These recommendations are important to obtain a more realistic and reliable model among all the cases in the present study for the on-bottom stability analysis. Furthermore, the stair-like development pattern of dynamic displacement is quite distinguishable when the pipeline is exposed to underwater environment with irregular waves.

The pipe-soil interaction is also investigated in this thesis. Past studies took only one single type of soil for the investigation of pipe-soil interactions. However, the seabed soil condition is actually more complicated in reality, considering that pipes run a very long distance and will pass several areas of different soil types. Three typical values of the friction coefficient are applied for the pipe-clay model and pipe-sand model respectively.

The maximum displacement seems to decrease as the friction coefficient increases for both the pipe-sand model and the pipe-clay model. The friction coefficient and the relative velocity between the pipe and the water particles, and the penetration will interact with each other. While for the pipe-sand model, the different friction coefficients do not seem to affect the displacement in the same way as it is for the pipe-clay model. This is likely due to the varying residual force that interacts differently and further leads to a different interaction between the soil resistance force, the relative penetration and the displacement. It appears that the displacement and friction coefficient does not interact with each other in any explicit pattern. But in general, the penetration and accumulated displacement tends to grow larger as the friction coefficient decreases.

It appears that there are few common features for both the pipe-clay and pipe-sand models:

- The friction coefficient will affect the soil resistance force, and further changes the initial time when the pipeline starts to move in lateral direction. The time history of displacement for the pipeline is changed for different friction coefficients.
- The relative velocity between water particles and the pipeline is different at time instance when the pipeline has significant movement
- The penetration is related to the accumulated displacement of the pipeline which is reduced for large friction coefficients.
- The penetration and accumulated displacement tend to grow larger as the friction coefficient decreases.

The simulation results for both clay and sand further prove that the pipe-soil reaction has a non-linear behaviour, and the relative penetration contributes in a non-linear way to the stability of the pipe by inducing a trench-like surrounding under the pipe, which reduces the movement of the pipe and diffuses the soil resistance force to shear forces along the circumference of the trench. As sand is stiffer and less permeable than clay, the penetration depth is subsequently larger for the pipe-clay model than that for the pipe-sand interaction.

Under the same hydrodynamic environment, the near-bed water velocity remains the same for all cases as the properties of the pipe and the characteristic parameters for the wave condition are the same, while the friction coefficient will affect soil resistance force, which decides when the lateral movement of the pipeline will be initiated. The time history of displacement for the pipeline varies with different soil friction coefficients. The instantaneous relative velocity between water particles and the pipeline is different when pipeline has significant movement. The penetration is related to the accumulated displacement of the pipeline as well. The larger the soil friction coefficient is, the smaller the displacement of the pipeline will be, as the pipeline penetrates the soil deeper and creates a kind of soil berm. This is likely the reason for deviations of forces as well as the displacements between the cases with different soil conditions.

Furthermore, the soil condition along the route is divided into 2-3 sections with different combinations of clay and sand. Deviations for different cases on displacements, soil forces and relative penetrations will be compared and studied for the sensitivity level. With the relatively large amount of designed cases, sufficient data are provided to support the discussion and conclusion.

When conducting the on-bottom stability analysis, the procedure itself can also affect the result. There are mainly three types of procedures applied nowadays:

- Standard 3-hour simulation procedure with default initial penetration calculated by PONDUS
- Procedure recommended by the PONDUS user manual[8]

- Procedure recommended by DNV-RP-F109[5]

Apart from the data collection and comparisons based on simulations, different design procedures for the simulations are tested for a best fit. The initial penetration in procedure 2 is computed step-by-step with several iterations. The penetration used for the design storm analysis for the current case is similar for procedure 2 and procedure 3. The 3-hour design storm analysis shows that the pipeline is stable when the stabilized initial penetration is used in analysis. Overall, procedure 2 has the largest accumulated displacement and is recommended for engineering practice.

The procedure recommended by DNV considers the build-up effect of the initial penetration before the storm. It could be applied in the analysis when the penetration is stabilized after the start-up time (20% of 3-hour).

In the end, different mitigation measurements are investigated when the virtual stability criteria is considered for the pipeline design. Proper mitigation methods will be taken to fulfill the criterion. It appears that the allocation of anchors along the pipe is also essential for the reaction mechanism and improvisation of the on-bottom-stability.

Taking account of the cost and viability of operations, weight coating should be considered first as a primary stabilization method. It should also be noted that the increase of self-weight due to weight coating will affect the initial penetration. The increase of the outer diameter of the pipeline will alter the hydrodynamic coefficients and the hydrodynamic loads.

Contents

1	Introduction	8
1.1	Objective and scope	10
2	Background	12
2.1	Current effects	12
2.2	Wave effects	13
2.3	Effects of hydrodynamic Loads	17
2.4	Effects of soil resistant forces	18
2.5	Methodology	19
2.5.1	An introduction to PONDUS	20
2.5.2	Limitations	23
2.6	Design data for the base case	24
2.7	Numerical set-up	26
3	On-bottom stability analysis in regular waves plus current and irregular waves plus current	28
3.1	Combined regular waves plus currents	32
3.1.1	Pipelines under combined load of 10-year return currents and 100-year return regular waves	34
3.1.2	Pipelines under combined load of 100-year return currents and 10-year return regular waves	41
3.2	Combined irregular waves plus currents	45
3.2.1	Pipelines under combined load of 10-year return currents and 100-year return irregular waves	46
3.2.2	Pipelines under combined load of 100-year return currents and 10-year return irregular waves	50
3.3	Comparison of the pipeline with combined regular waves and currents versus combined irregular waves and currents	54
3.3.1	10-year return currents and 100-year return waves	55
3.3.2	100-year return currents and 10-year return waves	58
4	Study on soil coefficients	66
4.1	Pipe-soil interaction with uniform soil types	72

4.1.1	Pipe-clay model	72
4.1.2	Pipe-sand model	82
4.2	Summary for pipe-soil interaction with uniform soil types	93
4.3	Pipe-soil interaction with multiple soil types	94
4.3.1	Mixed soil types of 50% sand and 50% clay	94
4.3.2	Mixed soil-types case	98
4.4	Summary for pipe-soil interaction with multiple soil types	103
5	Comparison on different procedures	105
5.1	Standard 3-hour simulation procedure with default initial penetration calculated by PONDUS	106
5.2	Procedure recommended by the PONDUS user manual	107
5.2.1	Step 1, 800 waves	107
5.2.2	Step 2, 500 waves	108
5.2.3	Step 3, 500 waves	109
5.2.4	Step 4, 3-hour design storm analysis	110
5.3	Procedure recommended by DNV-RP-F109	112
5.4	Comparison and discussion	113
6	Mitigation methods	114
6.1	Weight coating	114
6.1.1	Pipelines under combined load of 10-year return currents and 100-year return irregular waves with increased layer	115
6.1.2	Pipelines under combined load of 100-year return currents and 10-year return irregular waves with increased concrete layer	117
6.2	Anchoring	119
7	Conclusion and future work	122
7.1	Conclusion	122
7.2	Future work	123
	References	125
A	PONDUS input file for Case 1.3	127

1 Introduction

Subsea pipelines are used to develop subsea hydrocarbon resources. The pipeline system can be built in various forms such as a single-pipe, pipe-in-pipe, or a bundled system. The term of subsea flow lines describes the subsea pipelines carrying oil and gas products from the well to the riser base.

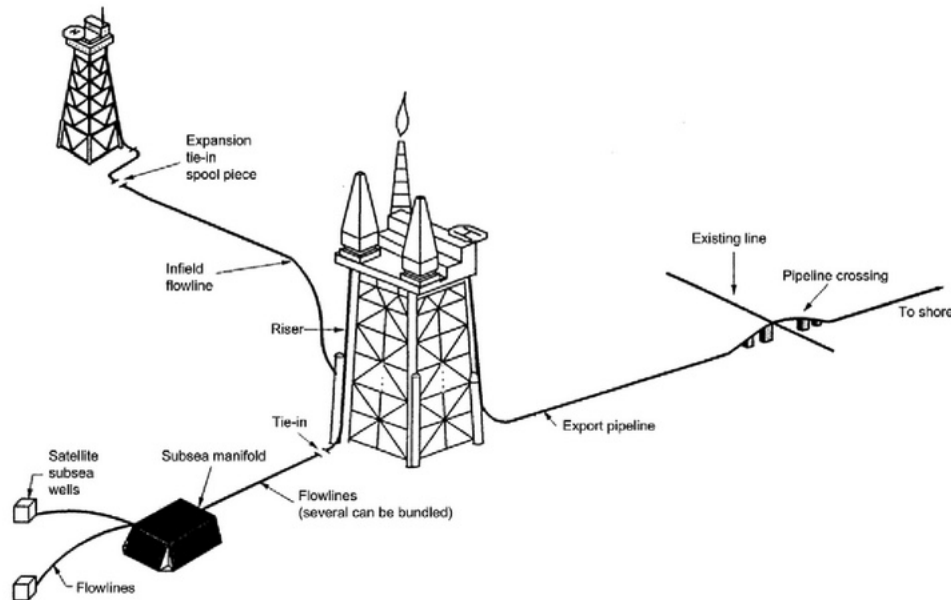


Figure 1.1: Subsea pipeline. Bai and Bai[15]

The pipelines laid on the seabed are exposed to forces generated by waves and current, apart from other internal and external loads. Substantial displacement of the pipeline leads to severe structural damages, consequential ecological and economic loss. As an important virtual link between the subsea field and onshore platform, the pipeline needs to be kept stable under the most critical conditions specified in relevant standards.

The design process for different types of lines (figure 1.1) is the same in general. There are usually 3 stages performed in the design of pipelines:

- Conceptual design engineering
- Front-end engineering design (FEED) engineering
- Detail design engineering

The objective and scope for each stage can vary by the operator and the size of the project. There are few decisive parameters for the design process such as:

- Pipeline internal diameter
- Pipeline wall thickness
- Grade of pipeline material

- Type of coating-corrosion and weight
- Coating wall thickness

The design analysis can be described as in figure 1.2.

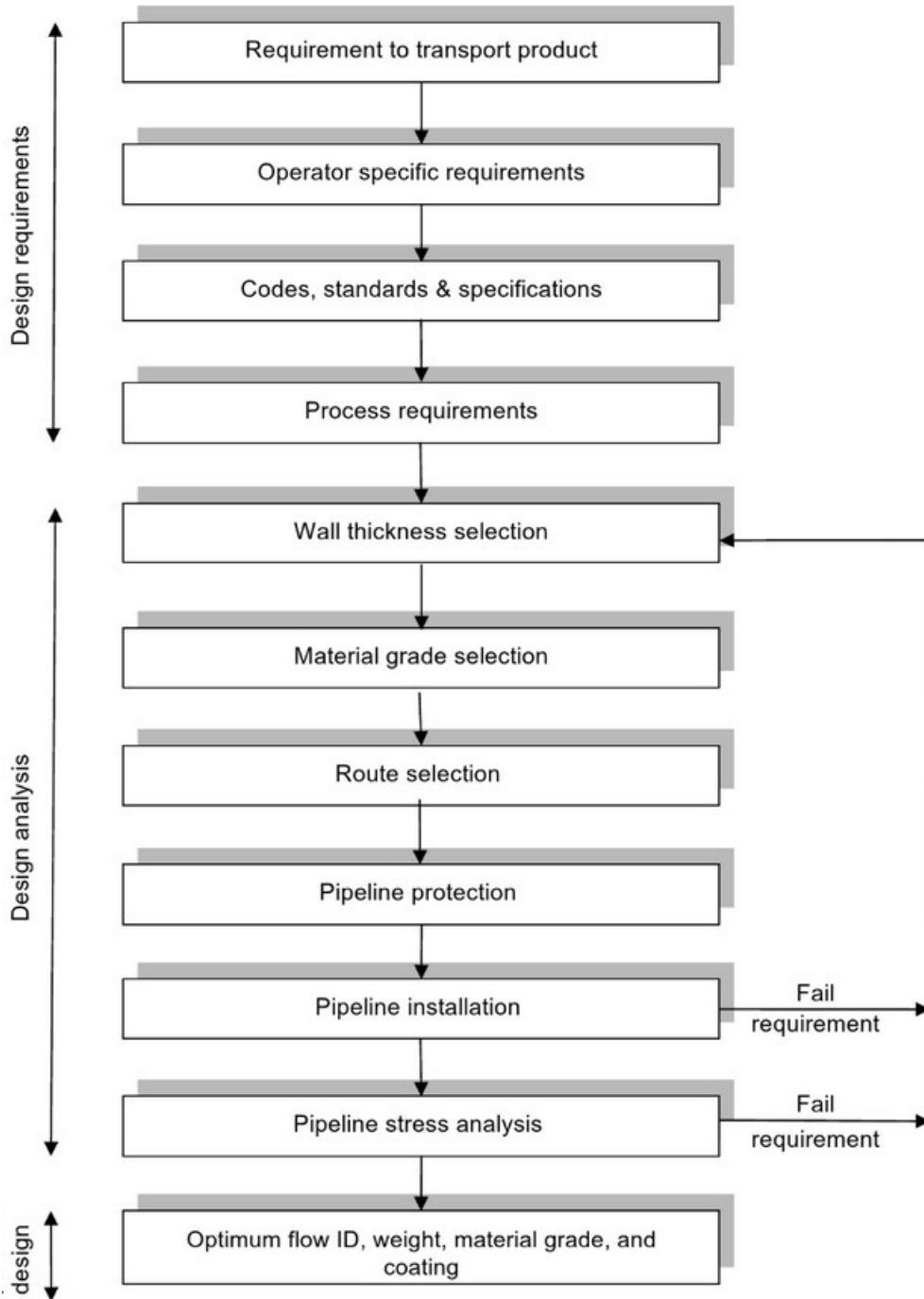


Figure 1.2: General design process. Bai and Bai[15]

The offshore and subsea industries are constantly experiencing technical revolutions in

the design process. Advanced methods and models are developed to achieve a more sophisticated design approach. Modern materials and revised design codes provide solid support to the limit state design concepts and the assessment for reliability.

The most recent developed method is called design through analysis (DTA), where the finite element method (FEM) is adopted to run simulations for the global behavior of the pipeline and the local structural strength. This concept includes a two-step process as a complementary measure to determine the dominating limit state, which intends to optimize one particular design.

Design guidelines developed by DNV (Det Norske Veritas) are widely used. It covers the general design context, where the uncertainties in the parameters and the application of various analysis methods are taken into account. The structure and load combinations are accurately modeled as well. However, the codes could be overly conservative for some particular design situations. Therefore, the FEM model should be considered to simulate the structural behavior more properly. It allows specific mitigation measures to be further applied and documented. The FEM analytic tools support the through-life behavior of the entire pipeline system. It helps to identify the most critical sections or components and gives indications of optimizations. A software PONDUS, which is developed by MARINTEK, will be used to build FEM models and to provide proper assessments for the on-bottom stability of the subsea pipeline. More details on PONDUS will be given in Chapter 2.5.

For the selection of the analytical method, the simulation of global response and the local strength are often necessary. The design parameters and local environment are quite project-oriented.

A subsea pipeline is subject to complicated load conditions due to the specific installation process, seabed features, various operating conditions etc. The cyclic loading and displacement can be verified by simulations. The simulation results will be further evaluated for the assessment of the on-bottom stability of the pipeline. Simulations of the pipeline behavior in a realistic environment obtained by measurement can support the identification of the strength and weaknesses of the pipeline design. It further helps to obtain safe and cost-effective solutions.

The on-bottom stability analysis of a subsea pipeline in irregular waves will be discussed in this study. Based on the finite element method, simulations and investigations will be made with respect to the important parameters such as structure properties of the pipe, the environment conditions at the seabed level and the design procedure. The scope of work is presented in Chapter 1.1.

1.1 Objective and scope

The objective of this thesis is to study the on-bottom stability in a series of complex environmental conditions through the dynamic analysis, as well as the generalized stability method and absolute lateral static stability method. The effect of different parameters regarding stability is investigated through the sensitivity analysis. Models will be built using PONDUS, a software developed by MARINTEK for the dynamic on-bottom sta-

bility analysis. The linear wave theory, the JONSWAP spectrum and the energy-based soil model will be considered for irregular waves and soil-pipe interactions respectively. Based on the different case set-ups, the results will be compared and discussions will be made on the methodology of pipeline stability analysis.

Based on the design concepts and principles for the on-bottom stability of a subsea pipeline in irregular waves described above, the following topics will be further investigated and discussed:

- Comparison and discussion on the reaction of the pipeline in regular waves plus currents and irregular waves plus currents.
- The effect of different soil friction coefficients for the on-bottom stability are studied for the pipe-clay model and pipe-sand model. Multiple soil types is further applied to the pipeline in different sections with varied combinations. The important simulation results will be compared and discussed respectively.
- Based on the available of guidelines and standards, different procedures for the on-bottom stability analysis of the pipeline will be evaluated.
- When the virtual stability criterion is considered, the application of different mitigation methods is studied to fulfill the criteria.

The design guideline and methodology adopted in this study are based on the literature as follows:

- HYDRODYNAMICS AROUND CYLINDRICAL STRUCTURES [13]
- DNV-RP-F109 October 2010 [5]
- DNV-RP-C205 April 2014 [4]
- PONDUS technical manual 1994 [7]
- PONDUS user manual 1994 [8]
- Linear wave theory NTNU 2000 [11]

2 Background

A subsea pipeline is exposed to combined loads such as bending, axial force, and external pressure during installation due to the dynamic vessel motion. This motion is caused by the unique subsea environment, which is affected by the aspects as follows.

2.1 Current effects

The steady current flow at the seabed level consists of:

- Tidal current
- Wind-induced current
- Storm surge induced current
- Density driven current

If current coexists with waves, the presence of current may affect the waves. The problem of wave-current interaction is an important issue in its own right. Detailed reviews of the subject are given by Peregrine [16], Jonsson [17] and Soulsby et al. [21].

The effect of coexisting current on forces has been investigated by several authors. These investigations include those by Moe and Verley [20], Sarpkaya and Storm [22], Justesen et al.[18], Bearman and Obasaju [18] and Sumer, Jensen and Fredsøe [23]. In on-bottom stability design, the current impact is accounted for the boundary layer effect and its directionality.

- Boundary layer effect: the friction force towards the seabed reduces the velocity
- Directionality: only the force component perpendicular to the pipe introduces significant loads

As shown in Figure 2.1, only the perpendicular force component will try to move the pipe.

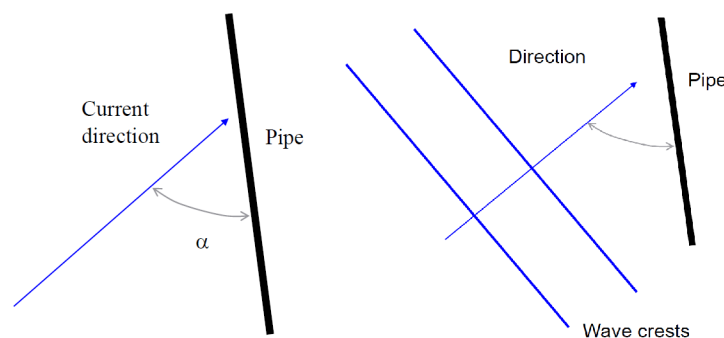


Figure 2.1: Current and waves attacking the pipe. Chen[1]

which gives

$$U_{effective} = U \sin(\theta) \quad (2.1)$$

The current(velocity and direction) is considered constant with respect to time, where the components(x and y) of the current velocity will be added to the wave velocity components in the time series.

The boundary layer correction to estimate an effective current velocity is calculated according to the procedure described in DNV-RP-F109[5].

2.2 Wave effects

There has been a large amount of studies conducted on forces on a cylinder in a plane oscillatory flow. Real waves differ from the case of plane oscillatory flow in several aspects. While the water particles in the case of plane oscillatory flow travel over a straight-line trajectory, and the trajectory of the orbital motion of water particles in the case of waves is elliptical, where the elliptical motion may vary between 0 (the straight-line motion) to 1 (the circular motion). It suggests that the forces on a cylinder will subject to a real wave, and influenced by the presence of the orbital motion.

The wave induced oscillatory wave condition at the seabed level can be calculated by using numerical or analytical wave theories. The wave theory describes the conditions at the pipe location. The short-term, stationary, irregular sea states may be described by a wave spectrum (i.e. the power spectral density function of the sea surface elevation). Wave spectra may be given in table form, as a measured spectra, or in an analytical form.

The mostly used wave spectrums are namely the Pierson-Moskowitz spectrum and the JONSWAP (Joint North Sea Wave Observation Project) spectrum. The JONSWAP spectrum is similar to the Pierson-Moskowitz spectrum, except that waves continues to grow with distance (or time), and the peak in the spectrum is more pronounced. The wave peak turns out to be particularly important. It leads to enhanced non-linear interactions and a spectrum that changes in time. The JONSWAP spectrum is considered in this thesis and the analytic form is expressed as follows.

The directional frequency spectrum $S(f, \theta)$ of the surface wave elevation $\eta(t)$ is defined as:

$$S(f, \theta) = S(f)D(\theta) \quad (2.2)$$

$$S(f) = K_1 f^{-5} \exp[-1.25(f/f_p)^{-4}] \gamma^\beta \quad (2.3)$$

where

$$\beta = \exp[-(f - f_p)^2 / (2\sigma^2 f_p^2)] \quad (2.4)$$

$$\sigma = \begin{cases} 0.07 & \text{for } f < f_p \\ 0.09 & \text{for } f > f_p \end{cases}$$

$$D(\theta) = K_2 \cos^{2s}(\theta - \theta_0) \quad (2.6)$$

where

γ : peak enhancement factor
 f_p : peak frequency
 θ_0 : mean wave direction
 s : directional spreading parameter
 K_1, K_2 : scaling factors

In this study, surface waves are transferred to sea bottom level using Airy linear wave theory.

Regular waves used in this study are specified in terms of the wavelengths, the amplitudes and the phase factors. The dispersion relation defined the angular frequency.

The velocity and acceleration time series are generated at specified points(grid points) along the actual pipeline section modeled. A rectangular grid is used to describe short-crested wave conditions. Only one grid point is used(one time series) for a complete description of the ocean wave environment when a long-crested sea state propagates with a specified direction to the pipeline. The theoretical basis for modeling of the analytic surface spectrum is given according to DNV-RP-F109 [5]. The mechanism is described as in Figure 2.2

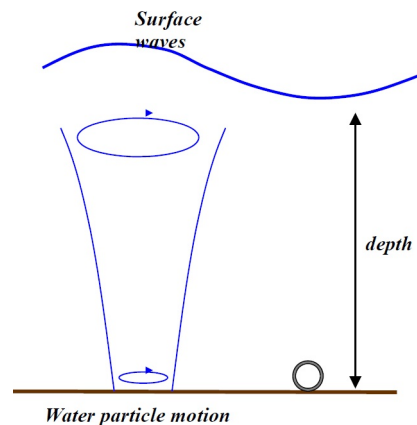


Figure 2.2: Wave mechanism. Chen[1]

The effects from waves can be identified considering the wave velocity. The velocity U_m is calculated according to DNV-RP-F109 [5].

$$U_m = u_{max} \quad (2.7)$$

where

$$u = \frac{\sqrt{2}}{2} \frac{\pi H}{T} \frac{\cosh(k(z+h))}{\sinh(kh)} \cos(\omega t - kx) \quad (2.8)$$

It should be noticed that since the angle of attach is assumed 90 degrees, equation 2.8 is multiplied with 1. k is the wave number given by $k = 2\pi/L$. The wave length L is determined by solving equation 2.9:

$$\sqrt{gk \tanh(kh)} = \frac{2\pi}{T} \quad (2.9)$$

where T is the wave period.

The wave is also characterized by the Keulegan-Carpenter (KC) number, which describes the *size* of a wave. The water particles move in ellipses, and KC indicates how large this ellipse is relative to the diameter. It ranges from zero to infinity and is important to determine the force coefficients such as the drag force coefficient, the lift force coefficient, the inertia force coefficient and the friction force coefficient. According to Sumer and Fredsøe [13], KC number is calculated as

$$KC = \frac{U_m T}{D} \quad (2.10)$$

Where T is the wave period and D is the outer diameter of the pipe.

Small KC numbers therefore mean that the orbital motion of the water particles is weak relative to the total width of the cylinder. When KC is very small, separation behind the cylinder may not even occur.

While large KC numbers indicate that the water particles travel quite large distances relative to the total width of the cylinder, resulting in separation and probably vortex shedding. For very large KC numbers ($KC \rightarrow \infty$), we may expect that the flow for each half period of the motion resembles that experienced in a steady current.

In this study, the KC number for regular waves is taken as a major reference when reading the force coefficients (the drag coefficient C_D , the inertia coefficient C_M and the lift coefficient C_L) in figure 2.3 according to Sumer and Fredsøe[13].

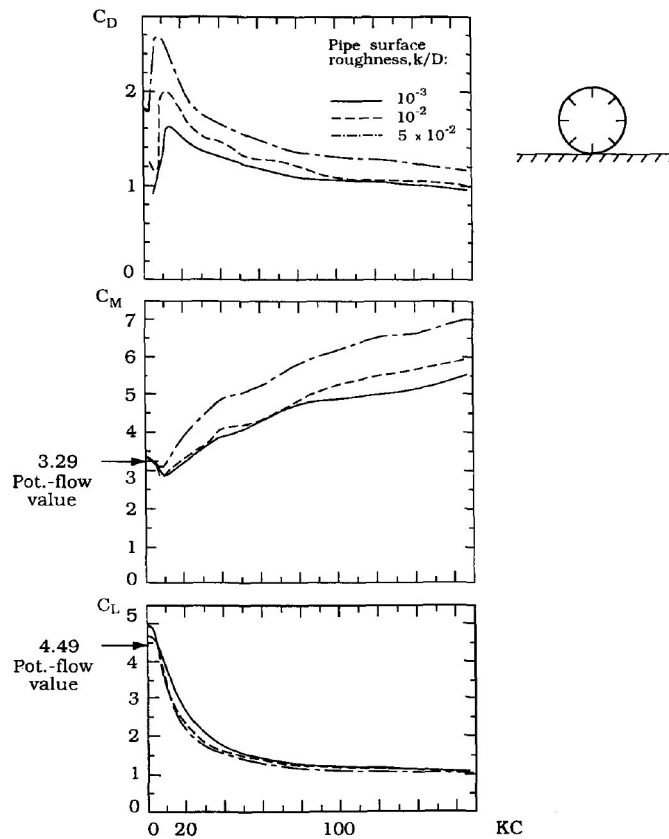


Figure 2.3: Force coefficients for a wall-mounted cylinder. $Re = (0.5 - 3.6) * 10^5$. Sumer and Fredsøe[13]

According to the linear wave theory [11], the waves on a windy day are far from being regular, and it is impossible to keep track of as an individual wave crest for more than a few periods. It thus appears that the theory developed with regular waves will be of little or no use in this situation.

The only waves in the ocean, which resemble what we considered in regular waves, are swell generated by a distant storm. Swell can be surprisingly regular, but never pure sine waves. In order to model a sea surface consisting of a wind sea and swell, we must introduce what is commonly referred to as irregular waves. This is a description which, in a way, is not as detailed as the full description of the surface motion we considered in regular waves. Nevertheless, linear irregular wave theory is basically the theory in regular waves put in a irregular or probabilistic setting. Knowledge of elementary probability theory is therefore necessary for the understanding of the theory.

The most important concept for irregular waves is the wave spectrum. Within the approximations which are built into linear wave theory itself, the spectrum basically provides all properties needed about the waves. It defines the so-called the sea state. Under normal conditions the wave spectrum and hence the sea state are likely to be constant over half an hour. The properties of the sea for a constant sea state are covered by short term wave statistics. Short term wave statistics deals with the properties of the individual waves, for example the probability distributions of wavelength, period, height and so on.

For time periods longer than a few hours, the sea state is likely to vary. Variations in the sea states are covered by a (different) irregular theory and described by long term wave statistics. For coastal and ocean engineering, it is very important to know how rough conditions the structures are likely to encounter during their lifetime, and this part of the long term statistics is treated by extreme wave statistics. Extreme wave statistics provides methods to estimate how rough conditions are likely to happen at a given location over a time span of, as in 100 years.

2.3 Effects of hydrodynamic Loads

The hydrodynamic force consists of a horizontal force and a lift force. These forces are defined to represent the integration of the dynamic pressure acting on the pipe per unit length. It is supposed that the hydrodynamic forces can be expressed as a function of a certain water particle and pipe velocity and acceleration. The numerical modeling of hydrodynamic forces is illustrated as follows (equations and definitions refer to the PONDUS user manual [8]).

The horizontal force per unit length may be written as:

$$F_h = F_h(u, \dot{u}, \dot{v}, \ddot{v}) \quad (2.11)$$

where

- u : effective total water velocity
- \dot{u} : effective total water acceleration
- \dot{v} : pipe velocity
- \ddot{v} : pipe acceleration

The lift force per unit length is written as a function of water and pipe velocity .

$$F_l = F_l(u, \dot{v}) \quad (2.12)$$

Based on the previous studies on regular waves, there are some universal attributes that seem to be applicable on irregular waves as well.

- Lift force is not in phase with flow
- Lift force amplitude depends on the previous waves
- Hydrodynamic force consists obviously of more than one harmonic component
- A small current does not shift the mean horizontal force as predicted by the *Morrison's* formulation

Morrison's formulation with constant coefficients may be used to describe the hydrodynamic forces. The classical *Morrison's* formulation is in particular relevant for a free pipe section, e.g. not in contact with the seabed.

Previous studies on the hydrodynamic model are mostly based on the *Morrison's* formulation, though this model is applicable with a certain limitation. There are several available models in PONDUS and the database model is adopted in this study as it is by far the most properly developed model based on empirical data collection. This model will be further illustrated in the introduction of PONDUS.

2.4 Effects of soil resistant forces

The resistant force is generally consisted of:

- One pure Coulomb friction part
- Passive resistance F_R due to soil penetration
- Anchors etc. (which is rare)

In this study, different models for friction force is applied. The simple Coulomb friction models is adopted for the comparison on regular and irregular waves, while more complexed soil models are designed for the investigation on the sensitivity level of soil parameters.

According to Irman [12], a non-linear soil model is typically employed when investigating a complex pipe-soil interaction problem. Two main pipe-soil interactions are frequently studied: the vertical pipe-soil interaction, and the lateral pipe-soil interaction during the lateral buckling of the pipeline.

The interaction often is represented using a force-displacement curve found by fitting a high number of test data points. In the lateral direction, the soil model developed by Verley and Sotberg [10] is widely used in industry for assessing pipeline walking.

In lateral non-linear pipe-soil interaction, two main components of soil resistance are encountered.

- The first component, friction force, is also known as the Coulomb model.
- The second component is called soil passive/remaining resistance. The soil passive resistance appears to be time-dependent and a function of soil penetration and vertical force.

The related soil model of soil passive resistance generally can be divided into three main paths.

- The elastic regime: the soil force can be found from the soil elastic stiffness
- The plastic regime: the pipe starts to dig into the soil and stimulates high soil resistance.
- The residual force path: the pipe breaks out of the soil trench and begins to drag soil along the way. The dragged soil provides resistance on top of the friction force, and if lateral displacement is quite large, it will build up the soil berm, which gives a rather high lateral resistance.

2.5 Methodology

The instability of a subsea pipeline is likely to be compromised due to the complicated hydrodynamic load, and the main failure modes are described as follows:

- The pipeline moves excessively sideways under the action of hydrodynamic forces. (main focus)
- The pipeline floats in water.
- The pipe sinks.
- The pipe floats in liquefied soil when it is intended to be buried.

Referring to the failure modes described above, the displacement and force equilibrium system is essential in the on-bottom stability design.

According to DNV-RP-F109 [5], there are three design methods mainly applied for the lateral on-bottom stability analysis:

- dynamic lateral stability analysis
- a generalized lateral stability method based on data base results from dynamic analyses/simulations
- an absolute lateral static stability method

The dynamic lateral stability analysis satisfies the general requirements with respect to a time domain simulation of pipe response, which includes hydrodynamic loads from an irregular sea-state and soil resistance forces.

While the generalized lateral stability method and the absolute lateral static stability method give detailed specific design results for two approaches to stability design.

According to DNV-RP-F109 [5], there are normally two criteria used for the generalized stability. One is described as $L_{stable} < D/2$, while the other one is $L_{stable} < L_{10}$, where L_{stable} is the acceptable displacement, L_{10} is 10 times of the outer diameter of the pipe D .

The generalized lateral stability method is based on an allowable displacement in a design spectrum of oscillatory wave-induced velocities perpendicular to the pipeline at the pipeline level. The design spectrum is characterized by spectrally derived characteristics U_s (oscillatory velocity), T_u (period) and the associated steady current velocity V . As a special case, the virtually-stable case is considered whereby the displacement is limited to about one half pipe diameter and is such that it does not reduce the soil resistance and the displacements do not increase no matter how long the sea-state is applied for.

The absolute lateral static stability method is a "design – wave" approach, i.e. it ensures absolute static stability for a single design (extreme) wave-induced oscillation. The design oscillation is characterized by oscillatory velocity amplitude U^* and period T^* and the associated steady component V^* . Often $V^* = V$, however some hydrodynamic models

account for a local mean velocity V^* within a wave-induced oscillation and this may be different to the overall mean velocity V .

In this study, the dynamic method is applied with the criteria of relative stability. While for the discussion on mitigation method, the general method with the virtually-stable criteria is considered.

The dynamic analysis is applied in this study as well as in PONDUS model as it provides a much better and realistic way to estimate the pipeline response by applying suitable hydrodynamic load and *soil – interaction* models and provides a more accurate assessment for the necessary stability requirements to ensure the pipeline safety under irregular waves and steady currents. The related on-bottom stability criteria is defined as $L_{stable} < L_{10}$, and L_{10} is referred as 10 times of the outer diameter of the pipe. (Section 2.5 in DNV-RP-F109 [5])

According to Sumer and Fredsøe [13], there has been a number of studies and experiments showing that the stability of a pipeline is particularly sensitive to a few variables as soil properties, hydrodynamic loads and structural design.

The pipe itself will be defined with constant initial properties. Based on the past studies and hydrodynamic principles, further investigations will be conducted with irregular waves presented. Moreover, pipe-soil interaction models with better of soil types will also be applied for a parametric study that is more compatible for the seabed soil conditions in reality.

With the subsea environment surrounding the pipe, it is identified that waves and currents will generate hydrodynamic loads. The relationships between the different active components will be discussed in this study based on the outcome from PONDUS.

2.5.1 An introduction to PONDUS

PONDUS is a software developed by MARINTEK, focusing specifically on the dynamic lateral response of offshore pipeline subject to a combined action of wave and current on a horizontal seabed.

The typical format of the PONDUS input files are IWAV, IPRE, and IPON(input files of typical cases are attached in Appendix A and Appendix B). These input files are written to run the corresponding modules. There are 4 modules in PONDUS(i.e. WAVESIM; PREPONDUS; PONDUS; PLOTPO) and they are described in the flow chart in figure 2.4:

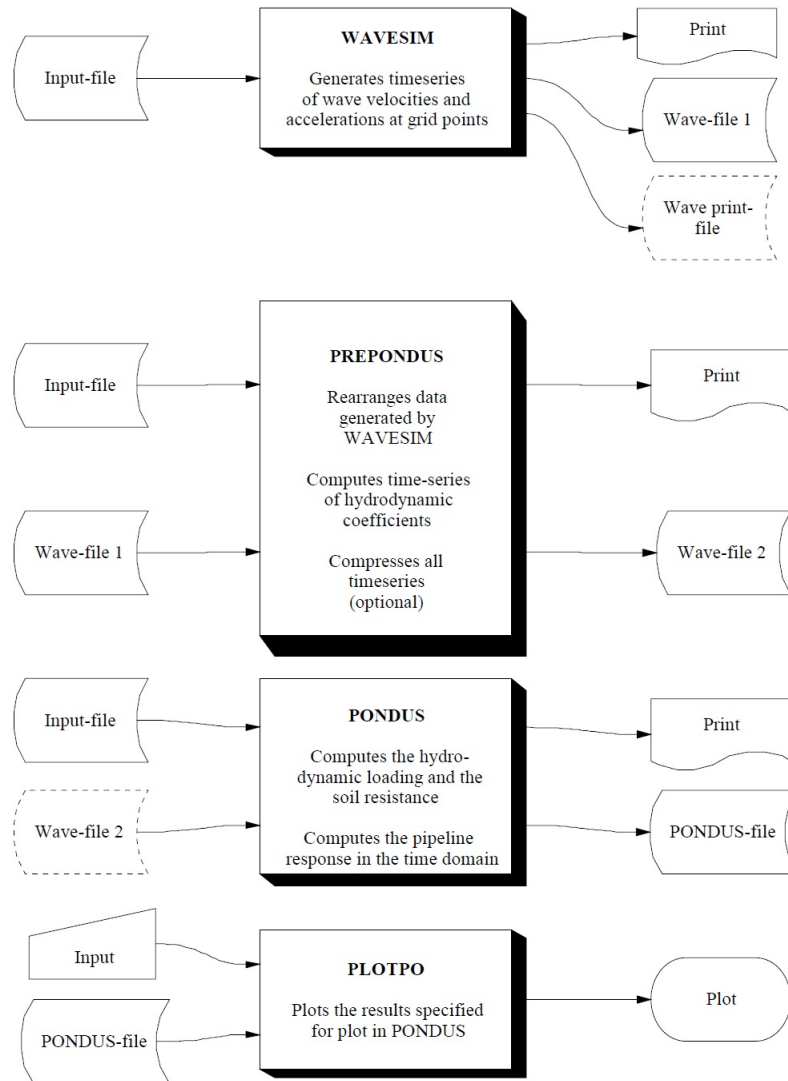


Figure 2.4: Flow chart of the 4 modules in PONDUS. PONDUS user manual [8]

- **WAVESIM**

- Format of the input file: IWAV.
- Format of the output file: OWAV.

The WAVESIM module is used to:

- Specify the directional frequency spectrum $S(f, \theta)$ of the surface wave elevation $\eta(t)$
- Calculate of irregular phase set and complex wave elevation amplitude
- Transform from surface to sea bottom level by using Linear Airy wave theory
- Calculate the Fourier amplitude with summation over one or more directions per frequency, and transfer to time series by inverse Fast fourier Transformation (FFT), generate the velocity and acceleration time series at specified points (grid points) along the pipe section

- PREPONDUS

- Format of the input file: IPRE.
- Format of the output file: OPRE.

PREPONDUS is an interface module which rearranges data generated by WAVESIM in a form compatible with the input of PONDUS.

- PONDUS

- Format of the input file: IPON.
- Format of the output file: OPON.

Main features are:

- Straight pipeline on horizontal sea bottom
- Beam element with two degrees of freedom (DOF) at each node (lateral displacement and rotation about the z-axis)
- Small deflection theory (small rotations) for the beam elements (no updating of nodal coordinates according to hydrodynamic force)

- PLOTPO

- Plots the results specified for plot in PONDUS
- Input to the PLOTPO module is the data stored for plot on the PONDUS-file and the control data given by the user during execution of PLOTPO.

Main features of PONDUS software are listed as follows.

- Calculation of the wave kinematics from 3-D irregular waves for medium and deep water
- Calculation of the hydrodynamic force by load models
- Use of 2-D beam elements with small deflection theory in the finite element formulation
- Calculation of the soil resistance forces by soil model
 - *Sand soil*
 - *Clay soil*
- Computation of the dynamic response of pipeline subject to waves and current in time domain for the pipeline on horizontal seabed

The water particle velocities used to calculate hydrodynamic forces correspond to either a regular or irregular wave time series. A preprocessor to the analysis(PREPONDUS) allows input of wave velocities from the 3-dimensional wave simulation module(WAVESIM). Through the input data different wave spectra model can be specified. The sea state is considered to be stationary for the time period of the simulation. By using an inverse FFT (Fast Fourier Transformation) algorithm, wave kinematics are generated. A cosine

wave directional spreading function $\cos^n(\theta - \theta_w)$, where θ_w is the mean wave propagation direction, can be applied. The irregular nature of the waves is described through a irregular phase angle for each individual wave frequency or alternatively both irregular phase and amplitude.

The model is based on a data-base of Fourier-coefficients obtained by decomposition of force data from extensive laboratory tests conducted in combined steady current and regular waves. It is a mathematical approach which describes a measured force signal by superposition of a number of harmonic components. The force coefficients are made non-dimensional as follows:

$$\frac{F(t)}{\frac{1}{2}\rho d_h u_w^2} = C_0 + \sum_{n=1}^N C_n(\omega t + \phi_n) \quad (2.13)$$

where

$F(t)$: total force

ρ : water density

d_h : hydrodynamic diameter(outer diameter of coating)

u_w : effective amplitude of water velocity

C_0, C_n, ϕ_n : Fourier coefficients and phase angles

By decomposing the time-series of bottom wave velocities in irregular waves into zero-upcrossing and zero-down-crossing half-wave cycles, local wave parameters such as K and M are defined. Each irregular half-cycle is treated as a regular wave with their own amplitudes.

2.5.2 Limitations

As PONDUS is not specifically designed to consider the free span, it should be noticed that the numerical model in PONDUS includes free-span. The current solution is to apply the *Morrison's* formulation partially to the free-span and the force model to the rest part of the pipe.

As the database hydrodynamic force model is applied in PONDUS, the validation of the linear wave theory needs to be performed for relative small water depth referring to Airy linear wave theory [6].

For the validation of the linear wave theory, the Ursell number or Miche breaking criterion will be a limitation for the use of the database model. This limitation can be expressed for narrow-band random waves as:

Ursell number:

$$\left(\frac{kH_{rms}}{2}\right)/(kh)^3 \leq 0.2 \quad (2.14)$$

Miche criterion:

$$\left(\frac{kH_{rms}}{2}\right) \leq \pi * 0.142 \tanh(0.875kh) \quad (2.15)$$

where

k : the the wave number
 U_{rms} : the rms of U_s , ($U_{rms} = U_s/\sqrt{2}$)
 h : the water depth

In the shallow water ($kh = \pi/10$) to deep water ($kh = \pi$) range it appers that equation 2.14 is the most restrictive for ($\pi/10 \leq kh \leq 1.2$), while equation 2.15 is most restrictive for ($1.2 \leq kh \leq \pi$).

H_s^{max} is found by modifying equation 2.14 and equation 2.15.

Ursell number:

$$H_s^{max} \leq (0.2 * \sqrt{2} * 2 * k^2 h^3) \quad (2.16)$$

Miche criterion:

$$H_s^{max} \leq 2 * \sqrt{2} * \pi * 0.142 \tanh(0.875kh)/2 \quad (2.17)$$

The limitation of the wave theory may be normalized with respect to gT_z^2 , and it can be expressed in terms of U_s and T_u as follows:

Ursell number:

$$\left[\frac{kU_{rms} \sinh(kh)}{\omega_z} \right] / (kh)^3 \leq 0.2 \quad (2.18)$$

Miche criterion:

$$\left[\frac{kU_{rms} \sinh(kh)}{\omega_z} \right] \leq \pi 0.142 \tanh(0.875kh) \quad (2.19)$$

where

k : the the wave number
 U_{rms} : the rms of U_s , ($U_{rms} = U_s/\sqrt{2}$)
 ω_z : the mean zero-crossing frequency $\omega_z = 2\pi/T_u$
 h : the water depth

U_s^{max} is found by modifying equation 2.18 and equation 2.19.

Ursell number:

$$U_{rms} \leq (0.2 * \sqrt{2} * 2\pi * k^2 h^3) / (T_u \sinh(kh)) \quad (2.20)$$

Miche criterion:

$$U_{rms} \leq 2 * \sqrt{2} * \pi^2 * 0.142 \tanh(0.875kh) / [kT_u \sinh(kh)] \quad (2.21)$$

If the criteria is not satisfied, other wave theories can be applied to generate wave kinematic and then applied as input to PONDUS. Alternatively, a wave spectrum that is compatible for the equivalent wave kinematics can be applied.

2.6 Design data for the base case

The on-bottom stability analysis is conducted with several representative models built in PONDUS, where the structural properties and environment factors are defined with reasonable assumptions described as follows.

Given a oil-filled pipe lying on the seabed, the on-bottom stability is analyzed for filled pipe under operating condition.

Here it is assumed that the pipeline has a roughness factor k/D of 0.001.

The pipe shown in table 2.5 is laying on the seabed. The layout follows the material conventions, where the pipe is made of steel and coated with concrete to achieve its stability. Assume the internal content is oil. At the spot where the pipe lies, following conditions are predefined.

- The dominant current is due to the tidal event
- The direction of this dominant current is at right angle to the pipeline
- The dominant waves is at an angle of 90° to the pipe.

Pipe-soil data, densities of materials and environmental data are shown in table 2.1, 2.2 and 2.3.

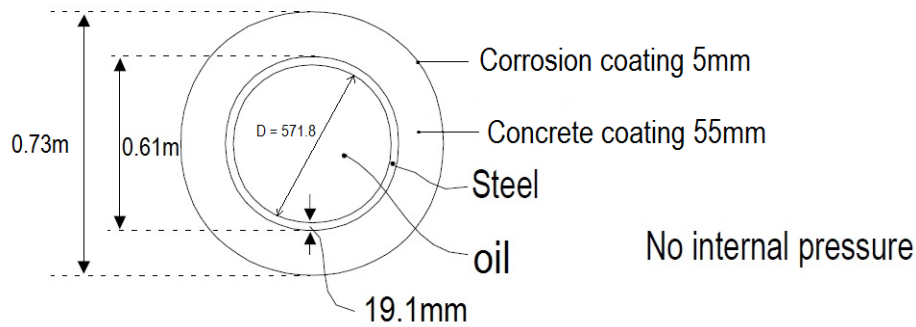


Figure 2.5: Cross-section of pipeline

Table 2.1: Pipe and soil data

Pipe and soil data		
Friction coefficient, μ	0.6	-
Int. diameter of pipe, D_{in}	571.8	mm
Concrete coating, t_{con}	55	mm
Wall thickness, t_{wall}	19.1	mm
Corrosion allowance, t_{cal}	1.5	mm
Corrosion coating, t_{cc}	5	mm
Marine growth, t_{mg}	0	m
Pipe roughness, k/D	0.001	-

Table 2.2: Material densities

Densities of materials		
Steel density, ρ_{steel}	7800	kg/m ³
Concrete density, $\rho_{concrete}$	3000	kg/m ³
Oil density, ρ_{oil}	800	kg/m ³
Corrosion coating, ρ_{cor}	930	kg/m ³
Marine growth, ρ_{mg}	0	s
Gravity coeff., g	9.81	m/s
Sea water, ρ_{water}	1030	kg/m ³
Kinematic viscosity of salt water at 20°C, ν	1.05	mm ² /s

Wave and current		Value		
		1 year	10 year	100 year
Regular waves	Wave Height H [m]	10.3	12.6	14.8
Regular waves	Wave period T [s]	13.2	14.7	15.9
Irregular waves	Significant wave height Hs [m]	10.3	12.6	14.8
Irregular waves	Peak wave period Tp [s]	13.2	14.7	15.9
Current velocity (1m above the seabed) [m/s]		0.36	0.51	0.66
Water depth [m]		104		
Current height Zr [m]		1.00		

Table 2.3: Environment data

2.7 Numerical set-up

Based on the various wave-current combinations from DNV-RP-F109[5] and the soil studies (see Lund [9] and Verley [10]), the related wave-current and soil parameters are applied as the inputs of each case.

An overview of the numerical set-up for this study is shown as follows:

Case description for comparison of regular/irregular waves						
Case no.	Wave type	Return period of current [year]	Return period of wave [year]	Wave height H [m]	Peak period T [s]	Current velocity U_0 [m/s]
1.1	Regular	10	100	14.8	15.9	0.51
1.2	Regular	100	10	12.6	14.7	0.66
Case no.	Wave type	Return period of current [year]	Return period of wave [year]	Significant wave height H_s [m]	Peak period T_p [s]	Current velocity U_0 [m/s]
1.3	Irregular	10	100	14.8	15.9	0.51
1.4	Irregular	100	10	12.6	14.7	0.66
Case description for soil parametric study						
Case no.	Soil model description					
2.1	Pipe-clay model					
2.2	pipe-sand model					
2.3	50%sand and 50% clay					
2.4	30%sand + 40%clay +30%sand					
2.5	30%clay + 40%sand +30%clay					
Case description for different procedures						
Case no.	Procedure description					
3.1	Standard 3-hour simulation procedure with default initial penetration calculated					
3.2	Procedure recommended by the PONDUS user manual[7]					
3.3	Procedure recommended by DNV-RP-F109[5]					
Case description for mitigation measurements						
Weight coating with the original pipe outer diameter 0.73m						
Case no.	Increased outer diameter [m]	Return period of current [year]	Return period of wave [year]	Significant wave height H_s [m]	Peak period T_p [s]	Current velocity U_0 [m/s]
4.1	0.75	10	100	14.8	15.9	0.51
4.2	1	100	10	12.6	14.7	0.66
Anchoring						
Case no.	Number of anchors			Maximum displacement [m]		
4.3	1			2.3		
4.4	2			1.4		
4.5	3			0.7		
4.6	4			0.23		

Table 2.4: Case overview

3 On-bottom stability analysis in regular waves plus current and irregular waves plus current

According to Sumer and Fredsøe[13], experiments and numerical studies were made by three progressive tests, namely 1) the regular, sinusoidal oscillatory flow tests, 2) the irregular oscillatory flow tests with a narrow-band spectrum and, 3) that with a broad band spectrum. A JONSWAP type spectrum was used in this study for irregular waves. The fundamental mechanisms of flow around a cylinder in the irregular oscillatory flow was classified into three categories:

- the vortex-pair regime which occurs in the range $0(1) < KC < 7$.
- the transverse-vortex-street regime which occurs in the range $7 < KC < 15$.
- the vortex-street regime which occurs for $KC > 15$. While for $KC < 0(1)$, the flow is unseparated.

With the same methodology adopted by Sumer[13], using regular waves as a cornerstone, force parameters (i.e. the lift force coefficient, the inertia force coefficient and the soil friction coefficient) affecting forces on pipelines is investigated for combined regular waves plus current and irregular waves plus current. Results obtained from the cases with regular waves will be compared with the ones with irregular waves.

According to DNV-RP-F109[5], section 2.2, there are two load combinations for filled (permanent/operation) conditions.

- 10-year return condition for waves and 100-year return condition for current
- 100-year return condition for waves and 10-year return condition for current

Table 3.1 presents the 4 cases that are designed based on those two criteria above and following studies will be made with those as a guideline.

Case description for comparison of regular/irregular waves						
Case no.	Wave type	Return period of current [year]	Return period of wave [year]	Wave height H [m]	Peak period T [s]	Current velocity U_0 [m/s]
1.1	Regular	10	100	14.8	15.9	0.51
1.2	Regular	100	10	12.6	14.7	0.66
Case no.	Wave type	Return period of current [year]	Return period of wave [year]	Significant wave height H_s [m]	Peak period T_p [s]	Current velocity U_0 [m/s]
1.3	Irregular	10	100	14.8	15.9	0.51
1.4	Irregular	100	10	12.6	14.7	0.66

Table 3.1: Case overview for the comparison between load combinations with regular and irregular waves

In order to obtain a specific and clear comparison of the pipe under different types of hydrodynamic load combinations, the simple Coulomb friction model is selected in PONDUS.

The Morrison coefficient is used for regular wave, and the database force model is used for irregular wave.

The database force model gives a very good fit to experimental, measured data. The model is based on a data base of Fourier-coefficients obtained by decomposition of force data from extensive laboratory tests conducted in combined steady current and regular waves. It is a mathematical approach which describes a measured force signal by superposition of a number of harmonic components. The force coefficients are made non-dimensional as follows:

$$\frac{F(t)}{\frac{1}{2}\rho d_h u_w^2} = C_0 + \sum_{n=1}^N C_n(\omega t + \phi_n) \quad (3.1)$$

where

$F(t)$: total force

ρ : water density

d_h : hydrodynamic diameter(outer diameter of coating)

u_w : effective amplitude of water velocity

C_0, C_n, ϕ_n : Fourier coefficients and phase angles

According to the PONDUS technical manual [8], the database model decomposes the time-series of bottom wave velocities in irregular waves into zero-uncrossing and zero-down-crossing half-wave cycles, local wave parameters such as k and m are defined. Each irregular half-cycle is treated as a regular wave with an amplitude determined as follows.

Consider the full cycle from t_a to t_c in figure 3.1, and the forces in second half. An appropriate local mean velocity is found as:

$$u_{loc} = \int_{t_b}^{t_c} u dt \quad (3.2)$$

The velocity amplitude in the second half U_2^* is presented in 3.1.

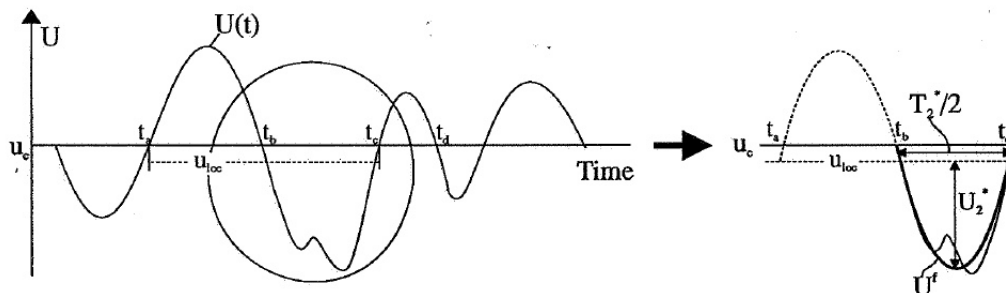


Figure 3.1: Development of wave velocity. PONDUS technical manual [7]

The period T_2^* is determined by fitting a sinusoid through two points: passing through t_c and u_{loc} and with an amplitude U_2^* . Figure 3.1 shows that U_2^* and T_2^* and the fitted sinusoidal velocity. The values obtained, $K = U_2^*T_2^*/d_h$ and $M = u_{loc}/U_2^*$ are used between t_b and t_c and used to obtain the appropriate Fourier force coefficients in the data base.

The airy linear wave theory [6] suggests that the water velocity has a positive correlation with the significant wave height and a negative one with the peak wave period.

As it is mentioned in the introduction of PONDUS, the database force model is adopted. It provides more a specified algorithm for the the calculations of the important parameters described as follows [7]:

- Horizontal force

For the horizontal force the data base finds the drag component, obtained by subtracting an inertia force with $C_m = 3.29$, from the measured force in the experiments. When using the model, an inertia force based on the measured acceleration is added to the drag force. The horizontal force on a fixed stationary pipe subjected to harmonic waves of velocity amplitude U_2^* and period T_2^* is given as:

$$F_h(t) = F_d(t) + F_I(t) \quad (3.3)$$

$$= 1/2\rho d_h |U_2^*| U_2^* [C_{h0} + \sum_{n=1}^N C_{hn}(\omega t + \phi_{hn})] + \frac{\pi}{4} \rho d_h^2 C_m \dot{u}(t) \quad (3.4)$$

where

$F_h(t)$: total horizontal force

$F_d(t)$: drag force

$F_I(t)$: inertia force

U_2^* : fitted water velocity amplitude

C_m : inertia coefficient(=3.29)

$\dot{u}(t)$: water particle acceleration

C_0, C_n, ϕ_n : Fourier coefficients and phase angles

Equation 3.3 indicates that the drag force is positively proportional to the fitted water velocity amplitude and the inertia force to the near-bed water particle acceleration.

- Vertical force

The vertical lift force on a fixed stationary pipe due to the fitted, sinusoidal velocity is given by:

$$F_l(t) = 1/2\rho d_h U_2^* [C_{l0} + \sum_{n=1}^N C_{ln}(\omega t + \phi_{ln})] \quad (3.5)$$

where

$F_l(t)$: lift force

C_0, C_n, ϕ_n : Fourier coefficients and phase angles

According to equation 3.5, the lift force is positively proportional to the near-bed water velocity.

- Relative velocity modification

In order to determine forces on a moving pipe it is necessary to determine the wave induced near-bed velocity near the pipe (i.e. modified for the effects of the wave behind the pipe being washed over the pipe at flow reversal). It has been shown that forces on a stationary pipe may be represented by:

$$F_x = 1/2\rho d_h |U_e| U_e + 1/4\rho d_h^2 C_M \dot{u} \quad (3.6)$$

$$F_z = 1/2\rho d_h C_l U_e^2 \quad (3.7)$$

Thus the time dependent effective velocity $U_e(t)$ is determined using constant values of C_d and c_m as:

$$U_e(t) = \sqrt{\left| \frac{F_h(t) - \pi/4\rho d_h^2 C_m \dot{u}}{1/\rho d_h C_d} \right| \text{sgn}(F_h(t) - \pi/4\rho d_h^2 C_m \dot{u})} \quad (3.8)$$

For a moving pipe, assuming that the movements changes neither the coefficients C_d and C_l nor the effective velocity U_e , the total forces included relative drag and inertia terms can be written as:

$$F_{hm}(t) = 1/2\rho d_h |U_e - \dot{v}|(U_e - \dot{v}) + \pi/4\rho d_h^2 (C_m \dot{u}(t) - C_d \ddot{v}) \quad (3.9)$$

$$= F_h(t) - 1/2\rho d_h C_d (U_e |U_e| - |U_e - \dot{v}|(U_e - \dot{v})) - \pi/4\rho d_h^2 C_d \ddot{v} \quad (3.10)$$

$$F_{lm}(t) = 1/2\rho d_h C_l(t) (U_e - \dot{v})^2 \quad (3.11)$$

$$= F_l(t) - 1/2\rho d_h C_l(t) (2U_e \dot{v} - \dot{v}^2) \quad (3.12)$$

where

$F_{hm}(t)$: horizontal force on a moving pipe

$F_{lm}(t)$: lift force on a moving pipe

$C_l(t)$: time dependent value of the lift force coefficient

\dot{v} : pipe velocity

\ddot{v} : pipe acceleration

$U_e(t)$: effective velocity

The second term in the second part of equation 3.9 and equation 3.11 is the hydrodynamic damping, and the last term in equation 3.9 is the added mass. The constant C_d value and the $U_e(t)$ and $C_l(t)$ time histories are used for the hydrodynamic damping calculations. Equation 3.3 to equation 3.11 shows that the selection of C_d and C_m is important to the hydrodynamic damping and response.

These algorithms and principles described above are considered to be the cornerstone of the following analysis and the differences between regular wave cases and irregular wave cases.

3.1 Combined regular waves plus currents

The dynamic response of the pipeline will be studied under regular waves plus currents. A structural model is designed as in figure 3.2 to accommodate the FEM method in PONDUS.

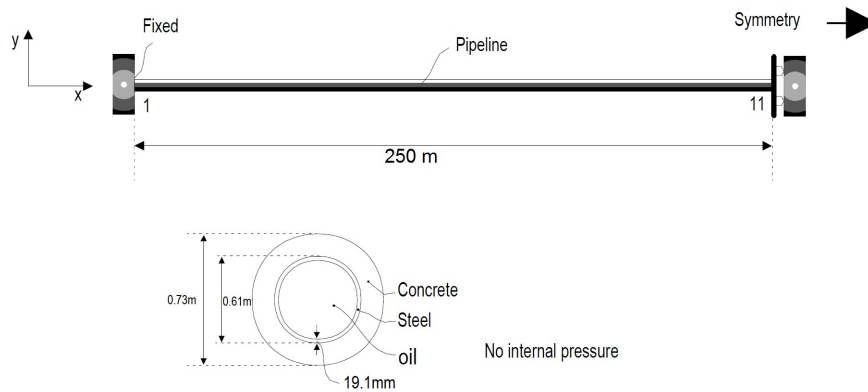


Figure 3.2: Structural model of the pipe. PONDUS user manual [8]

According to the user manual [8], the simulation is set as 2400 sec. The boundary conditions are defined as follow:

- Fixed in translation and rotation at the left end.
- Fixed in rotation at the right end.
- Free in translation at the right end.

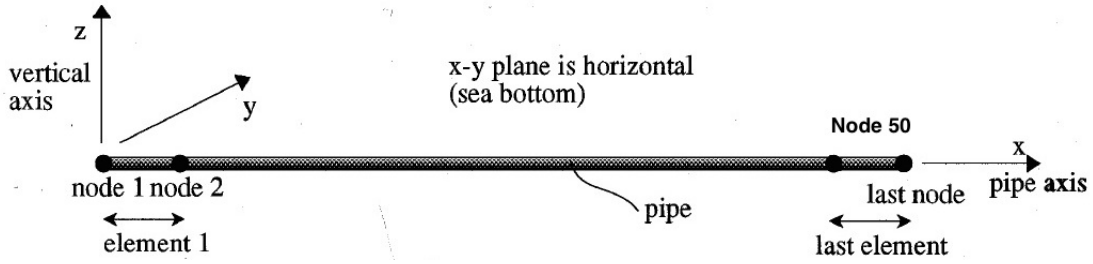


Figure 3.3: Calculation model of the pipe with 50 elements. PONDUS user manual[8]

The pipe is 250m long and divided into 50 elements of equal length. The pipe is assumed to be clamped at node 1 while node 51 is simply supported, which means node 1 is fixed in statical equilibrium state in both translational and rotational aspects. While at node 51 there will be a rotational reaction. Axial force is acting along the element at both ends. Material and environment data in the table below is applied for the following cases.

Material and environment data		
Steel Yielding stress	415	MPa
Soil elastic stiffness	65 000	N/m^2
Depth	104	m
Simulation time	3	hours
Time increment	0.01	s (1 080 000 time steps)

Referring to the PONDUS user manual [8], the plot graph is categorized as pipe length dependent and time-dependent, which indicates the pipe reaction relationships in terms of pipe length (P-result) or time (T-result).

Simulations are performed by following the guide line of PONDUS user manual[8]. Important parameters and specified values will be presented in details further in the following sections. Input files are attached in appendix A.

As the current velocity $U_c(z_r)$ is given at 1m above the seabed, the mean perpendicular current velocity U_c over a pipe diameter is determined as in equation 3.13 according to DNV-RP-F109[5].

$$U_c = U_c(z_r) \frac{(1 + \frac{z_0}{D}) \ln(\frac{D}{z_0} + 1) - 1}{\ln(\frac{z_r}{z_0} + 1)} \sin(\theta) \quad (3.13)$$

where

z_r is the reference measurement height over sea bed.

z_0 Bottom roughness parameter.

D is the outer diameter of the pipe.

The forces acting on the pipe are shown in fig. 3.4. U is the flow velocity acting on the pipeline, F_L is the lifting force, $F_{in-line}$ is the in-line force, F_μ is the friction between the pipeline and the seabed, and F_g is the submerged weight of the pipeline with buoyancy taken into account.

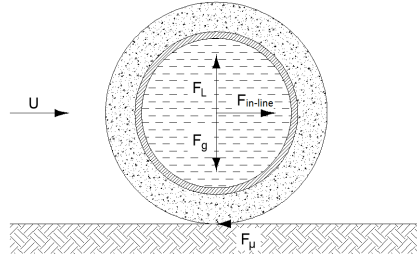


Figure 3.4: Forces acting on the pipeline

The current velocity U_c for the oil-filled pipe with 100 year current is calculated as:

$$U_{c100} = 0.57m/s$$

For the oil-filled pipe with 10 year current, the current velocity is calculated as:

$$U_{c10} = 0.44m/s$$

It should be noted that in PONDUS, the water velocity is defined as the near-bed total effective water velocity, the hydrodynamic force is the in-line force (drag force plus inertia force) and the soil force is the soil resistance force.

3.1.1 Pipelines under combined load of 10-year return currents and 100-year return regular waves

The pipe and environmental data for the pipeline under combined load of 10-year return currents and 100-year return regular waves are shown in table 3.2.

Pipe and environmental data		
Friction coefficient, μ	0.6	-
Int. diameter of pipe, D_{in}	571.8	mm
Concrete coating, t_{con}	55	mm
Wall thickness, t_{wall}	19.1	mm
Corrosion allowance, t_{cal}	1.5	mm
Corrosion coating, t_{cc}	5	mm
Marine growth, t_{mg}	0	m
Pipe roughness, k/D	0.001	-
Wave height, H	14.8	m
Wave period, T	15.9	s
Current velocity, U_{10}	0.44	m/s

Table 3.2: Pipe and environment data for the pipeline under combined load of 10-year return currents and 100-year return regular waves

When the pipe is under combined load of 10-year return currents and 100-year return

regular waves, maximum flow velocity U , which is the sum of current velocity U_{c100} and the near-bed wave velocity U_m , is used in calculation of the Reynolds number. The maximum horizontal velocity is $U_m = 1.04$ m/s and the current velocity is given as $U_{c100} = 0.44$ m/s. The flow velocity is thereby determined as

$$U = U_c + U_m \cdot \sin(\omega t) = 1.48 \text{ m/s}$$

where ω is the circular frequency and t is the time.

Next the Reynolds number for the pipe is calculated to determine the drag and lift force. This number tells which flow regime the pipe is in, describing the water flow around a cylindrical shaped object (figure 3.5). According to Sumer and Fredsøe [13], the Reynolds number and the flow regime can be determined by

$$Re = \frac{UD_4}{\nu} = 1.03 \cdot 10^6 \quad (3.14)$$





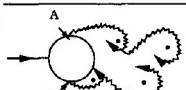
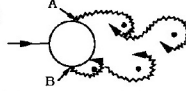
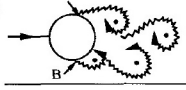


a)		No separation. Creeping flow	$Re < 5$
b)		A fixed pair of symmetric vortices	$5 < Re < 40$
c)		Laminar vortex street	$40 < Re < 200$
d)		Transition to turbulence in the wake	$200 < Re < 300$
e)		Wake completely turbulent. A: Laminar boundary layer separation	$300 < Re < 3 \times 10^5$ Subcritical
f)		A: Laminar boundary layer separation B: Turbulent boundary layer separation; but boundary layer laminar	$3 \times 10^5 < Re < 3.5 \times 10^5$ Critical (Lower transition)
g)		B: Turbulent boundary layer separation; the boundary layer partly laminar partly turbulent	$3.5 \times 10^5 < Re < 1.5 \times 10^6$ Supercritical
h)		C: Boundary layer comple- tely turbulent at one side	$1.5 \times 10^6 < Re < 4 \times 10^6$ Upper transition
i)		C: Boundary layer comple- tely turbulent at two sides	$4 \times 10^6 < Re$ Transcritical

Figure 3.5: Regimes of flow around a smooth, circular cylinder in steady current. Sumer and Fredsøe[13]

The system is dominated by wave judging by the ratio between U_c and U_m as:

$$\frac{U_c}{U_m} = 0.42 \quad (3.15)$$

The drag coefficient and lift coefficient are needed to determine the corresponding hydrodynamic force. The typical development pattern is shown in figure 3.6.

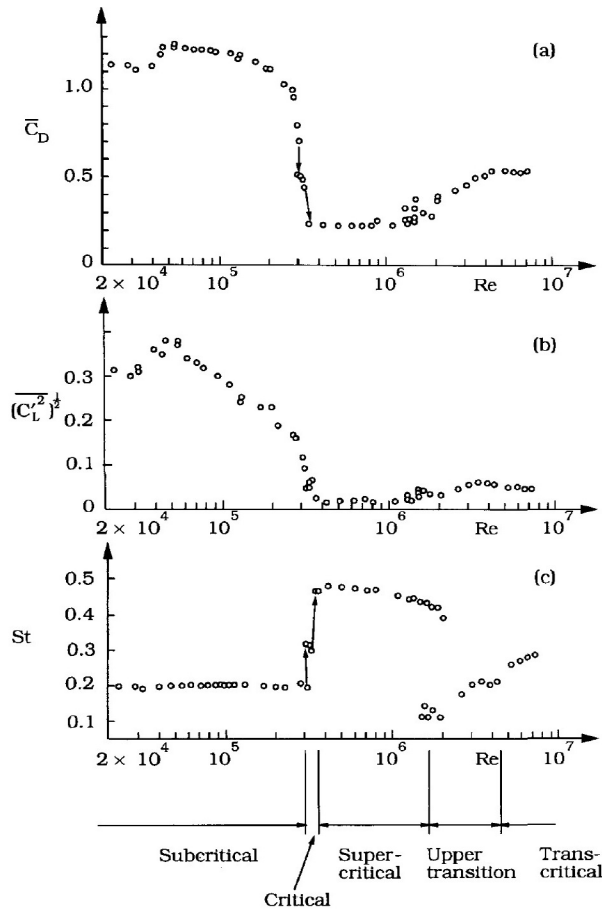


Figure 3.6: Drag coefficient, *r.m.s.* of the lift oscillations and Strouhal number as function of Re for a smooth circular cylinder. Sumer and Fredsøe[13]

The drag coefficient is needed to determine the drag force.

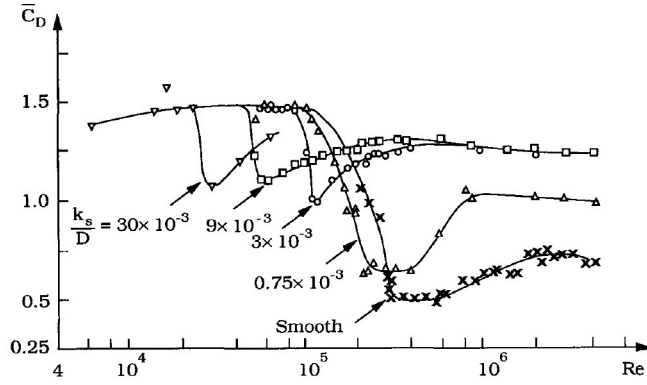


Figure 3.7: Drag coefficient of a circular cylinder at various surface roughness parameters k_s/D . Sumer and Fredsøe[13]

As shown in figure 3.6 and figure 3.7, the drag and lift coefficient will increase along with increasing roughness. By interpolating for the curve with roughness at 0.001, drag coefficient is considered constant when Re is larger than $1 \cdot 10^6$. With $Re = 1.03 \cdot 10^6$ and the given pipe roughness, the mean drag coefficient tends to stay at a constant value. This indicates that for high Re flow regimes, the value of C_D tends to be independent of Re , while it is strongly dependent on the roughness.

As interpolation results corresponds with figure 2.3, the relevant force coefficients are obtained from it.

For on Case 1.1 in table 3.1, the Keulegan-Carpenter number (KC number) is then calculated to determine the drag coefficient and the inertia coefficient.

$$KC = \frac{U_m T_{100}}{D_1} = 22.6 \quad (3.16)$$

For pipes with roughness k/D of $1 \cdot 10^{-3}$ when $KC = 22.6$, the force coefficients are obtained as shown below:

- Drag coefficient $C_D = 1.4$
- Inertia coefficient $C_M = 3.29$
- Lift-force coefficient $C_L = 2.5$

By applying those values as to the parameter input in PONDUS, the results for displacement, near-bed water velocity, water acceleration and related forces are presented as follows.

According to figure 3.8 and figure 3.9, the maximum displacement is $2.3m$. The stability criteria for dynamic analysis in DNV-OS-F101[3] is fulfilled as the maximum displacement is smaller than $L_{10} = 7.3m$.

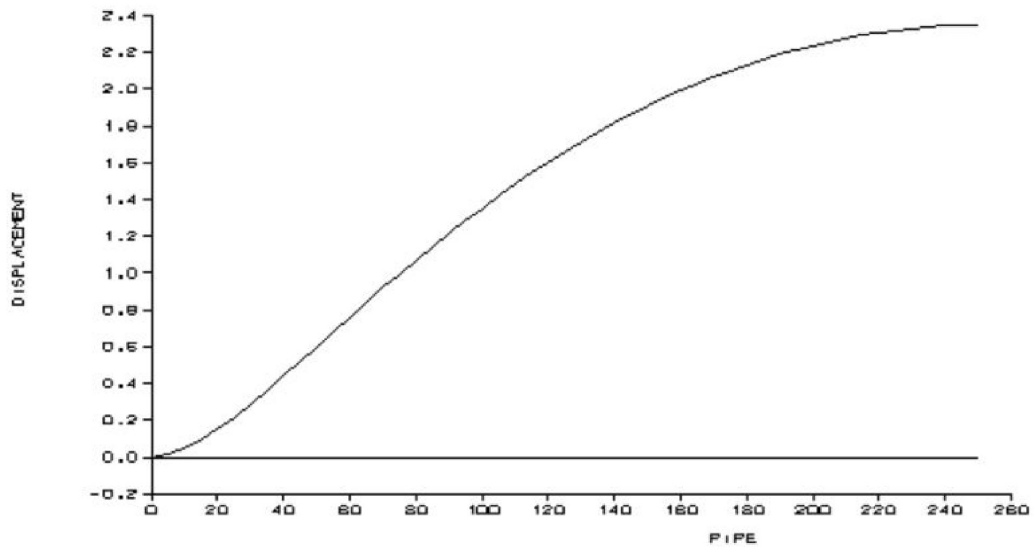


Figure 3.8: Displacement vs length for an oil-filled pipeline under combined load of 10-year return currents and 100-year return regular waves

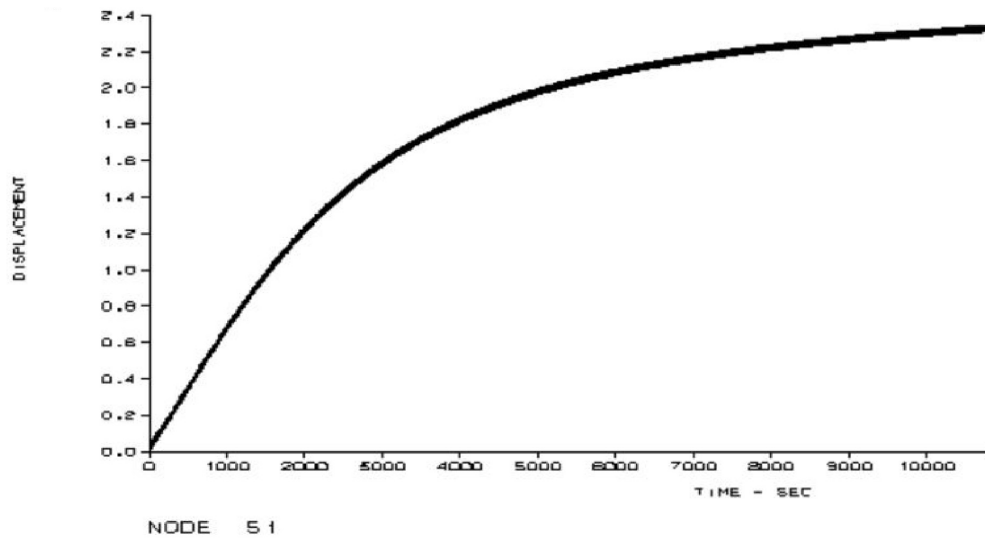


Figure 3.9: Nodal displacement vs time for an oil-filled pipeline under combined load of 10-year return currents and 100-year return regular waves

A more detailed presentation of figure 3.9 in 0 – 100s is shown in figure 3.10

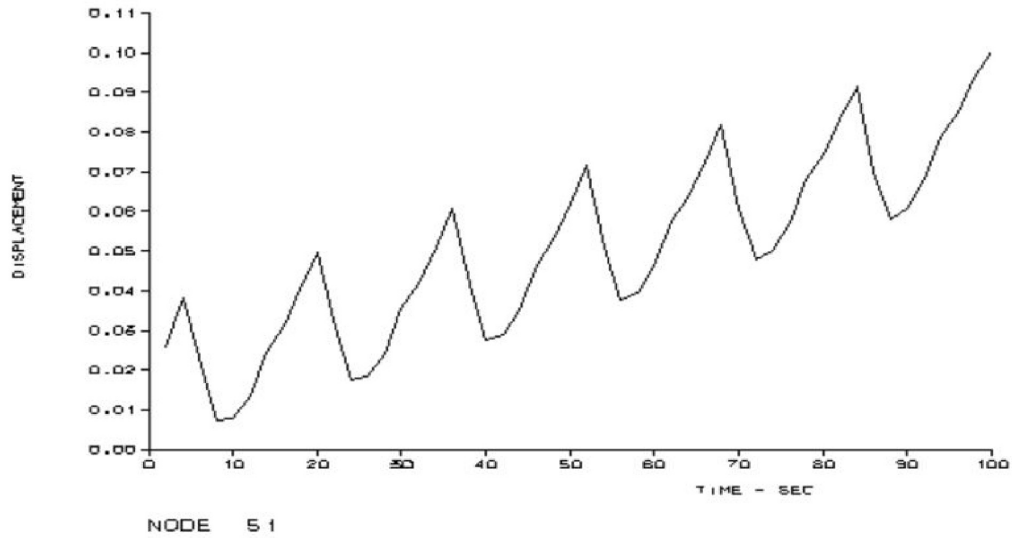


Figure 3.10: Nodal displacement vs time (0-100s) for an oil-filled pipeline under combined load of 10-year return currents and 100-year return regular waves

The simulation results of water velocity, hydrodynamic force, lift force and soil force are presented in figure 3.11, figure 3.12, figure 3.13 and figure 3.14. As it shows in these figures, the water velocity and those 3 forces are all oscillating with their own amplitude when the pipe is exposed in combined 100-year return regular waves and 10-year return current.

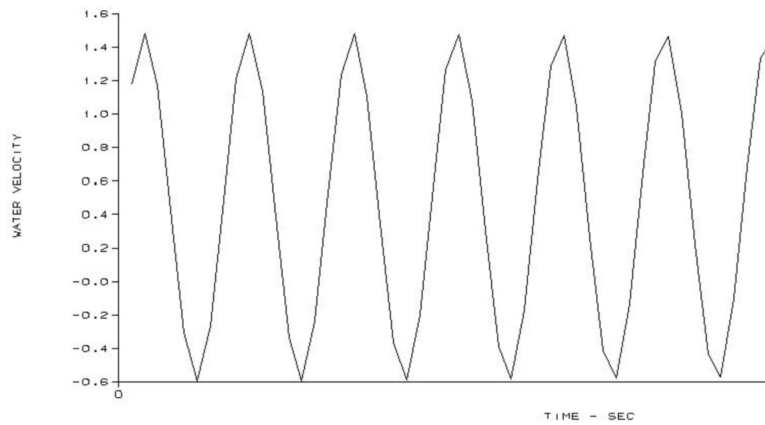


Figure 3.11: Water velocity by time acting on an oil-filled pipeline under combined load of 10-year return currents and 100-year return regular waves

The maximum water velocity is 1.5 m/s.

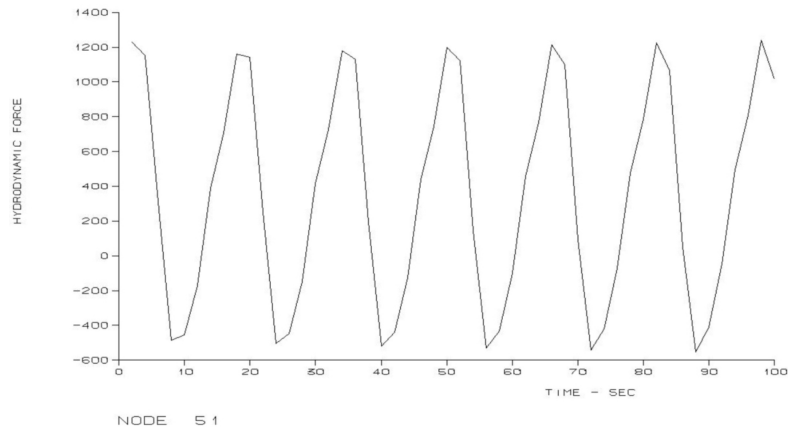


Figure 3.12: Hydrodynamic force by 100 seconds acting an oil-filled pipeline under combined load of 10-year return currents and 100-year return regular waves

The maximum inertia force is 1300 KN.

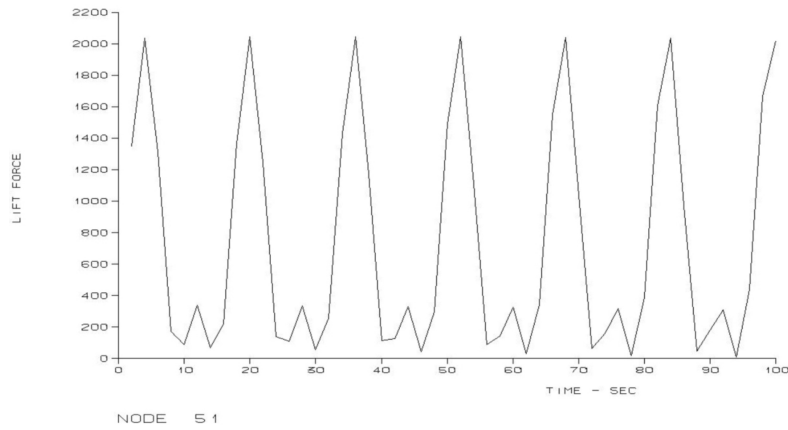


Figure 3.13: Lift force by 100 seconds acting an oil-filled pipeline under combined load of 10-year return currents and 100-year return regular waves

The maximum lift force is 2100 KN.

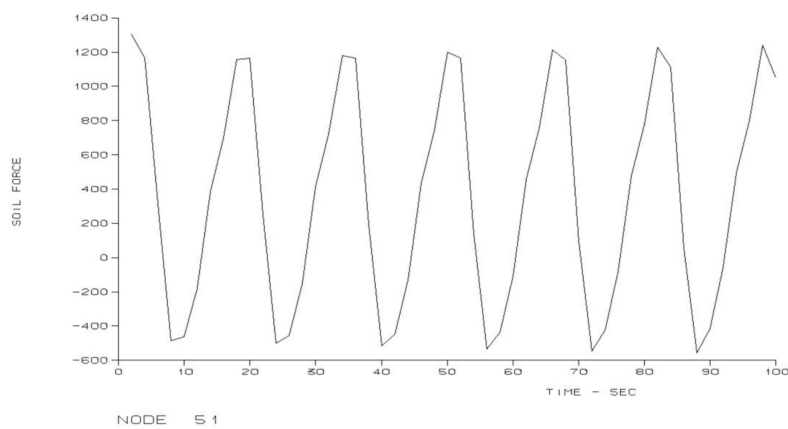


Figure 3.14: Soil force by 100 seconds acting an oil-filled pipeline under combined load of 10-year return currents and 100-year return regular waves

The maximum soil force is 1350 KN.

The same simulation will be conducted for the pipeline under the combination of 100-year return currents and 10-year return regular waves in the following section. The same types of results will be compared with the pipeline under the combination of 10-year return currents and 100year return regular waves.

3.1.2 Pipelines under combined load of 100-year return currents and 10-year return regular waves

The pipe and environmental data for the pipeline under combined load of 100-year return currents and 10-year return regular waves are shown in table 3.3.

Pipe and environmental data		
Friction coefficient, μ	0.6	-
Int. diameter of pipe, D_{in}	571.8	mm
Concrete coating, t_{con}	55	mm
Wall thickness, t_{wall}	19.1	mm
Corrosion allowance, t_{cal}	1.5	mm
Corrosion coating, t_{cc}	5	mm
Marine growth, t_{mg}	0	m
Pipe roughness, k/D	0.001	-
Wave height, H	12.6	m
Wave period, T	14.7	s
Current velocity, U_{100}	0.57	m/s

Table 3.3: Pipe and environment data for the pipeline under combined load of 100-year return currents and 10-year return regular waves

When the pipe is under combined load of 100-year return currents and 10-year return waves, maximum flow velocity U , which is the sum of the current velocity U_{c100} and the wave induced near-bed velocity U_m , is used in calculation of the Reynolds number.

The maximum horizontal velocity is $U_m = 0.74$ m/s and the current velocity is given as $U_{c100} = 0.57$ m/s. The flow velocity with respect to time is thereby determined as

$$U_{max} = U_c + U_m \cdot \sin(\omega t) = 1.31\text{m/s}$$

where ω is the circular frequency and t is the time.

Next the Reynolds number is calculated by

$$Re = \frac{UD_4}{\nu} = 9.11 \cdot 10^5 \quad (3.17)$$

Keulegan-Carpenter number (KC number) is determined as

$$KC = \frac{U_m T}{D_1} = 14.8 \quad (3.18)$$

By evaluating the ratio between U_c and U_m , the dominating impact can be found.

$$\frac{U_c}{U_m} = 0.77 \quad (3.19)$$

This value indicates that wave is dominating the system.

As it is proceeded in section 3.1.1, the relevant force coefficients are read from figure 2.3 according to Sumer and Fredsøe[13], for pipes with roughness of $1 \cdot 10^{-3}$ when $KC = 14.8$, the force coefficients are obtained as shown below:

- Drag coefficient $C_D = 1.5$
- Inertia coefficient $C_M = 3.29$
- Lift coefficient $C_L = 2.5$

Using the values as input in PONDUS input, the displacement results are presented. The maximum value of displacement at 40m from the initial point is $0.024m$ according to figure 3.15, which is rather smaller than $L_{1/2} = 0.365m$. According to the stability criteria for dynamic analysis in DNV-OS-F101[3], the pipe is considered virtually stable.

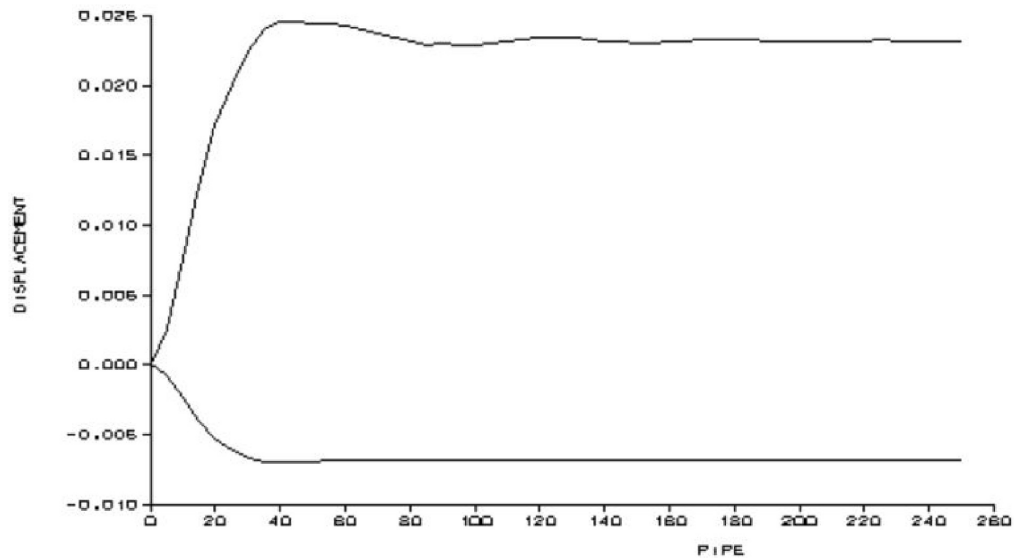


Figure 3.15: Displacement - length of an oil-filled pipeline under combined load of 100-year return currents and 10-year return regular waves

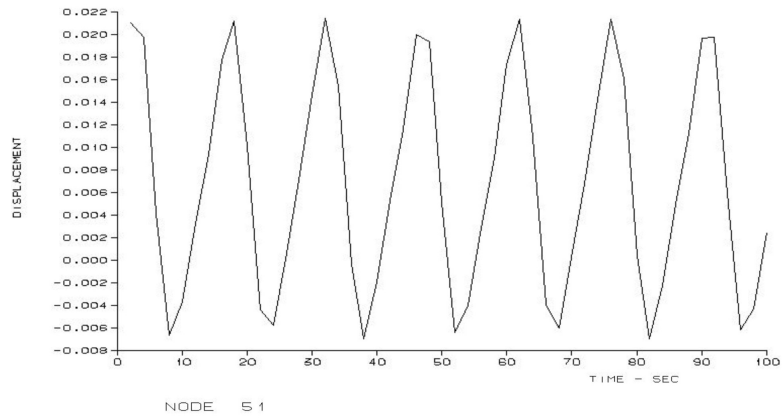


Figure 3.16: Displacement - time of an oil-filled pipeline under combined load of 100-year return currents and 10-year return regular waves

The simulation results of water velocity, hydrodynamic force, lift force and soil force are presented in figure 3.17, figure 3.18, figure 3.19 and figure 3.20.

Same as in the case for the oil-filled pipe under combined load of 10-year return currents and 100-year return waves, those 3 forces are all oscillating with their own amplitudes when the pipe is exposed in combined 100-year return regular waves and 10-year return current.

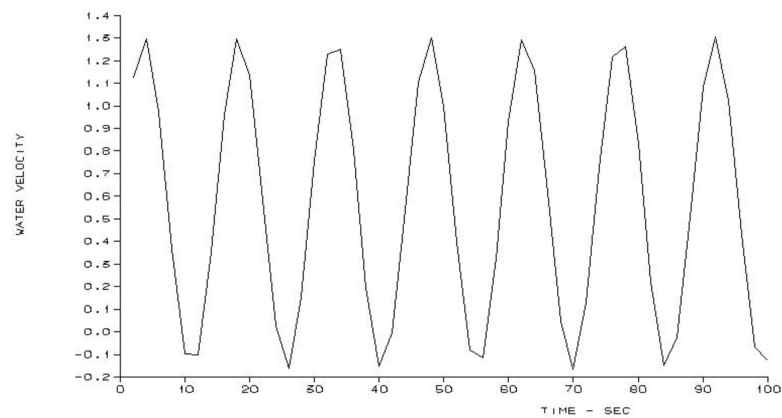


Figure 3.17: Water velocity by time acting an oil-filled pipeline under combined load of 100-year return currents and 10-year return regular waves

The maximum water velocity is 1.3 m/s.

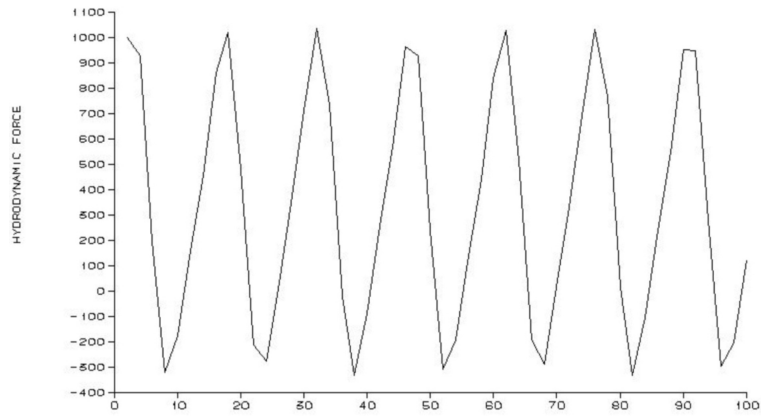


Figure 3.18: Hydrodynamic force acting an oil-filled pipeline under combined load of 100-year return currents and 10-year return regular waves

The maximum hydrodynamic force is 1050 KN.

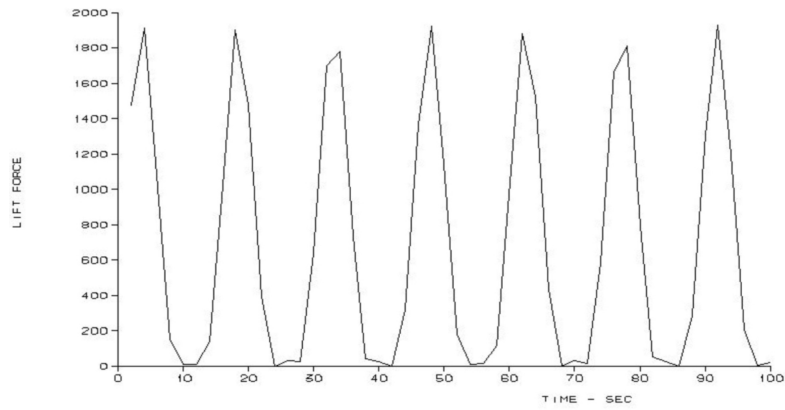


Figure 3.19: Lift force by 100 seconds acting an oil-filled pipeline under combined load of 100-year return currents and 10-year return regular waves

The maximum lift force is 1900 KN.

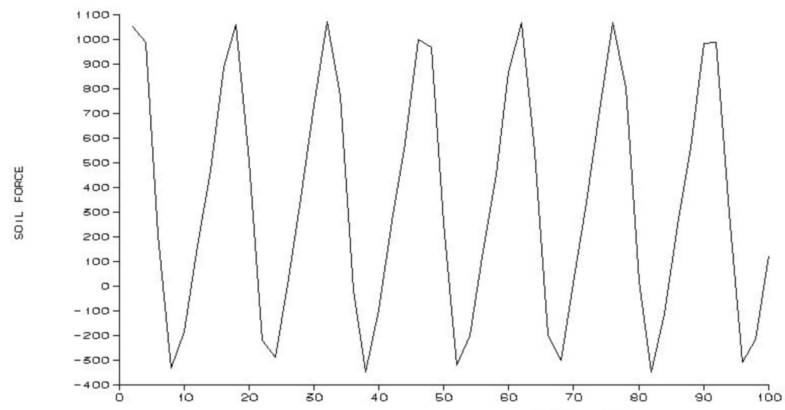


Figure 3.20: Soil force by 100 seconds acting an oil-filled pipeline under combined load of 100-year return currents and 10-year return regular waves

The maximum soil force is 1100 KN.

A summary of the results in the two load combinations investigated in this section is presented as in table 3.4. As shown in the table, Case 1.1, where the pipeline is exposed to 10-year return currents and 100-year return regular waves appears to be the most critical case, as the displacement is considerably larger than that in Case 1.2.

Result overview for combined regular waves and current									
Case No.	Description	H [m]	T [s]	Uc [m/s]	U [m/s]	Disp [m]	F _D [N]	F _L [N]	F _μ [N]
1.1	Combined 10 year curren 100 year regular waves	14.8	15.9	0.44	1.5	2.3	1300	2100	1350
1.2	Combined 100 year curren 10 year regular waves	12.6	14.7	0.57	1.3	0.02	1050	1900	1100

Table 3.4: Summary of results from Case 1.1 and Case 1.2

While in a real sea state, waves will not appear to be regular at any point and this irregularity will to a certain extent impact the forces on the pipeline. According to table 3.1, the regular waves in Case 1.1 and 1.2 will be substituted with irregular waves to study the on-bottom stability of the pipeline in a more realistic environmental context.

3.2 Combined irregular waves plus currents

Most of the studies on irregular waves done in the past, Sumer and Fredsøe [13] took the actual wave conditions into consideration. Experiments were designed to be conducted in water tunnels or simulated by the motion of a carriage in an otherwise still water. The results were grouped for each data cycle and processed by the least-squares fit of the force time series (The detailed mathematical process is described according to Sumer and Fredsøe[13] Section 4.1.4).

In the study of irregular waves, the characteristic parameters in the description of sea state are redefined based on the environment with regular waves. Following definitions are taken from the Coastal Engineering Manual (CEM)[14].

- Regular waves:
 - Wave height H : The vertical distance between crest and trough. Wave height is limited by both depth and wavelength. For a given water depth and wave period, there is a maximum height limit above which a wave becomes unstable and breaks. In deep water this upper limit of wave height, called breaking wave height, is a function of the wavelength.
 - Wave period T : The horizontal distance between successive crests or troughs.
- Irregular waves

- Significant wave height H_s : The mean of the highest 1/3 of the waves in a time-series of waves representing a certain sea state. This corresponds well with the average height of the highest waves in a wave group. H_s computed on the basis of a spectrum, is referred to as H_{m0} .
- Peak wave period T_p : The wave period with the highest energy. The analysis of the distribution of the wave energy as a function of wave frequency for a time-series of individual waves is referred to as a spectral analysis. Wind wave periods (frequencies) often follow the so-called JONSWAP and Pierson-Moskowitz spectra. The peak wave period T_p is extracted from the spectra. As a rule of thumb the following relation can be used: $T_p \sim 5.3\sqrt{H_{m0}}$.

Based on the different definition for the characteristic values that describe the sea state environment, it appears that the wave height value with irregular waves is larger than it is with regular waves, as the wave data is processed with different statistical methods.

The significant near-bed water velocity U_s is measured based on the significant wave height, therefore also a realization of the average of the highest one-third (33%) velocity of the significant wave height (measured from trough to crest) that occur in a given period. U_s is applied mostly in irregular waves, while the maximum flow velocity U_m is considered in regular waves. It indicates also that the statistical realization of U_s is based on a higher maximum flow velocity than it is for regular waves.

3.2.1 Pipelines under combined load of 10-year return currents and 100-year return irregular waves

As it is introduced in 2.5.1, *WAVESIM* and *PREPONDUS* are applied in the analysis for the environment simulation of irregular waves.

The pipe and environmental data for the pipeline under combined load of 10-year return currents and 100-year return irregular waves are shown in table 3.2.

Pipe and environment data		
Friction coefficient, μ	0.6	-
Int. diameter of pipe, D_{in}	571.8	mm
Concrete coating, t_{con}	55	mm
Wall thickness, t_{wall}	19.1	mm
Corrosion allowance, t_{cal}	1.5	mm
Corrosion coating, t_{cc}	5	mm
Marine growth, t_{mg}	0	m
Pipe roughness, k/D	0.001	-
Significant wave height, H_s	14.8	m
Peak wave period, T_p	15.9	s
Current velocity, U_{10}	0.44	m/s

Table 3.5: Pipe and environment data for the pipeline under combined load of 10-year return currents and 100-year return irregular waves

Typical PONDUS input files of this case are given in Appendix A. With the given input values of parameters, the displacement results are shown in figure 3.21 and figure 3.22. The displacement is increasing up to 5.6m, which indicates that the structure of the pipe is sufficient according to the $L_{stable} < L_{10}$ criteria in DNV-RP-F109[5].

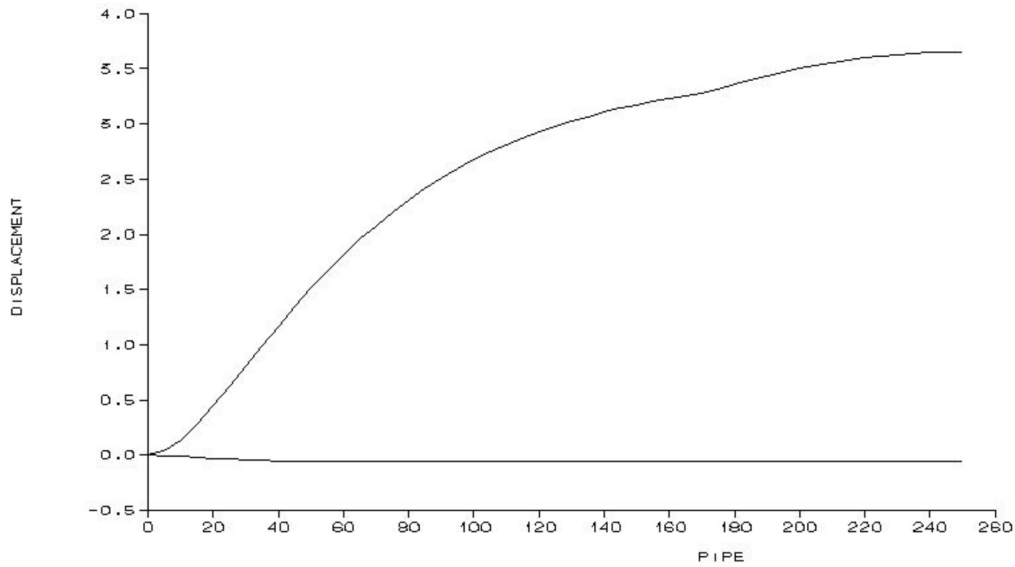


Figure 3.21: Displacement - length of an oil-filled pipeline under combined load of 10-year return currents and 100-year return irregular waves

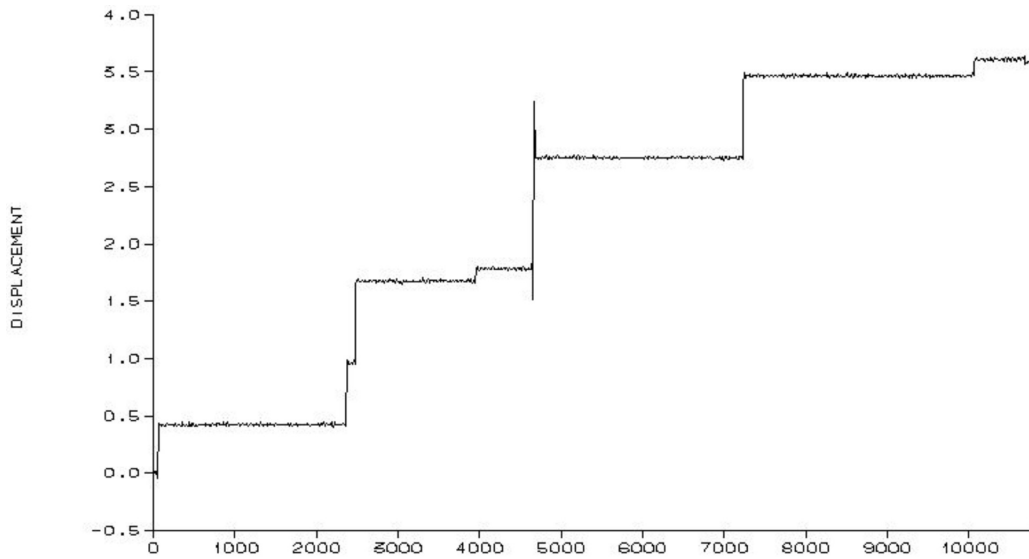


Figure 3.22: Displacement - time of an oil-filled pipeline under combined load of 10-year return currents and 100-year return irregular waves

The simulation results of the water velocity, hydrodynamic force, lift force and soil force are presented in figure 3.23, figure 3.24, figure 3.25 and figure 3.26 respectively.

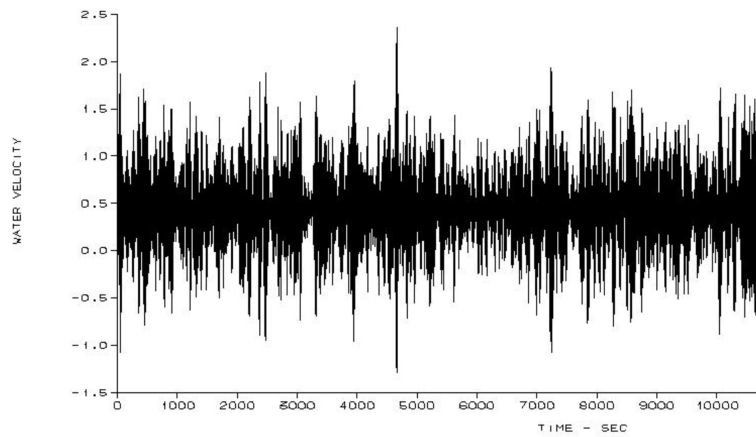


Figure 3.23: Water velocity by time acting an oil-filled pipeline under combined load of 10-year return currents and 100-year return irregular waves

The maximum water velocity is 2.4 m/s.

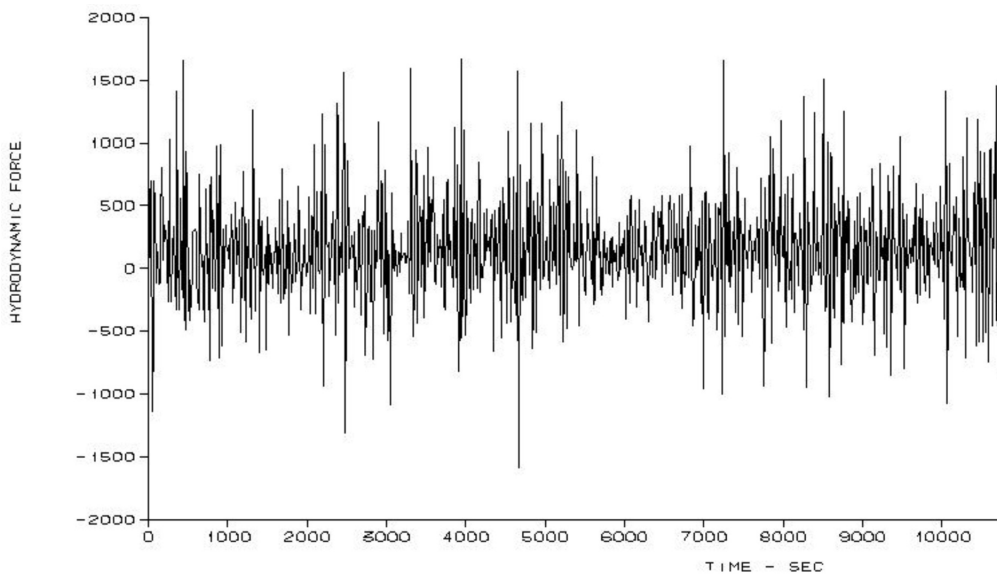


Figure 3.24: Hydrodynamic force by time acting an oil-filled pipeline under combined load of 10-year return currents and 100-year return irregular waves

The maximum hydrodynamic force is 1600 KN.

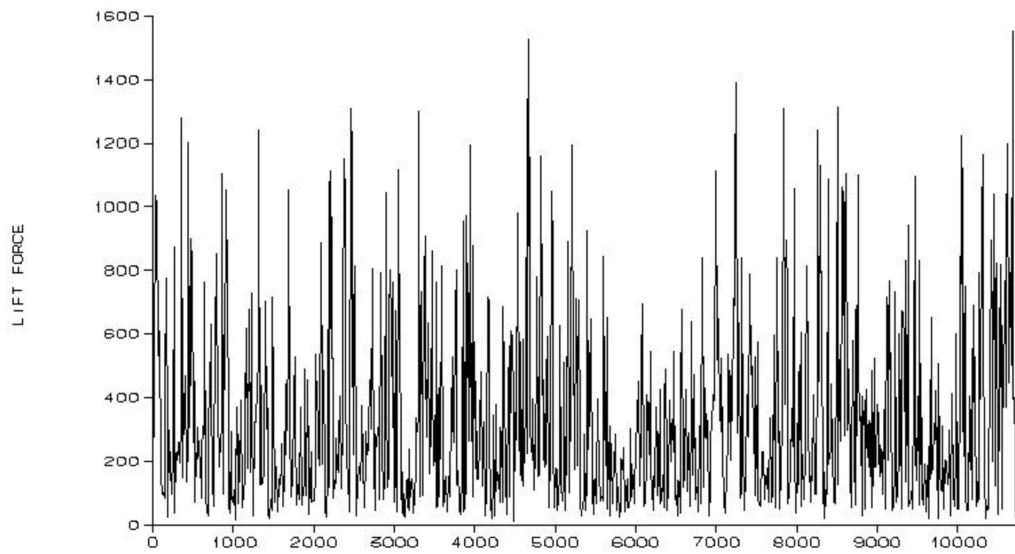


Figure 3.25: Lift force by time seconds acting an oil-filled pipeline under combined load of 10-year return currents and 100-year return irregular waves

The maximum lift force is 1550 KN.

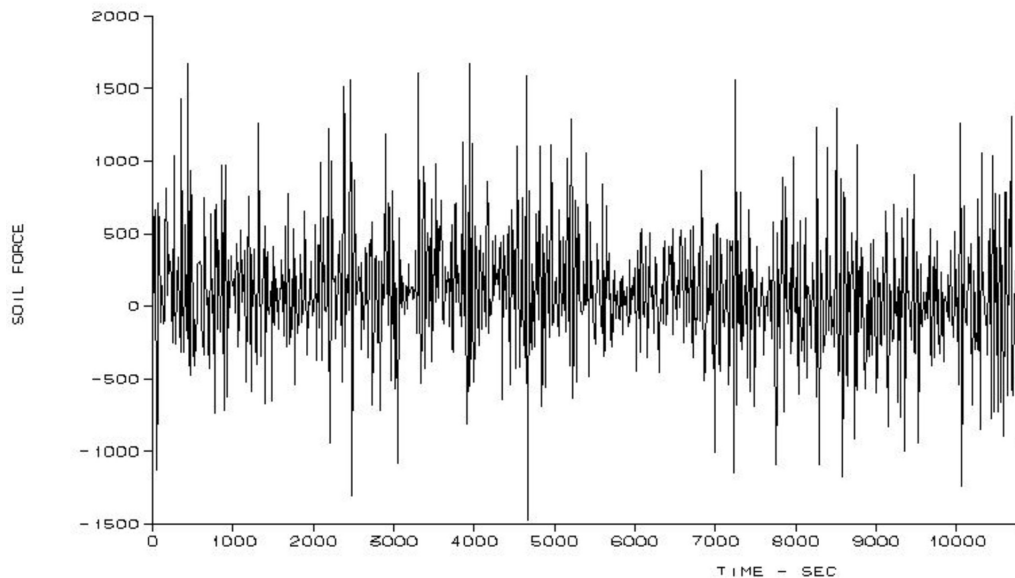


Figure 3.26: Soil force by time acting an oil-filled pipeline under combined load of 10-year return currents and 100-year return irregular waves

The maximum soil force is 1650 KN.

As it can be seen from the figures above, those 3 forces are all oscillating irregularly when the pipe is exposed in combined 100-year return irregular waves and 10-year return current. The same simulation will be conducted for the pipeline under the combination of 100-year return currents and 10-year return irregular waves in the following section. The same types of results will be compared with the pipeline under the combination of

10-year return currents and 100 year return irregular waves.

3.2.2 Pipelines under combined load of 100-year return currents and 10-year return irregular waves

Pipe and environment data		
Friction coefficient, μ	0.6	-
Int. diameter of pipe, D_{in}	571.8	mm
Concrete coating, t_{con}	55	mm
Wall thickness, t_{wall}	19.1	mm
Corrosion allowance, t_{cal}	1.5	mm
Corrosion coating, t_{cc}	5	mm
Marine growth, t_{mg}	0	m
Pipe roughness, k/D	0.001	-
Significant wave height, H_s	12.6	m
Peak wave period, T_p	14.7	s
Current velocity, U_{100}	0.57	m/s

Table 3.6: Pipe and environment data for the pipeline under combined load of 100-year return currents and 10-year return irregular waves

The same pipe properties in 3.1.2 are applied to the case with the combination of 100-year return currents and 10-year return irregular waves.

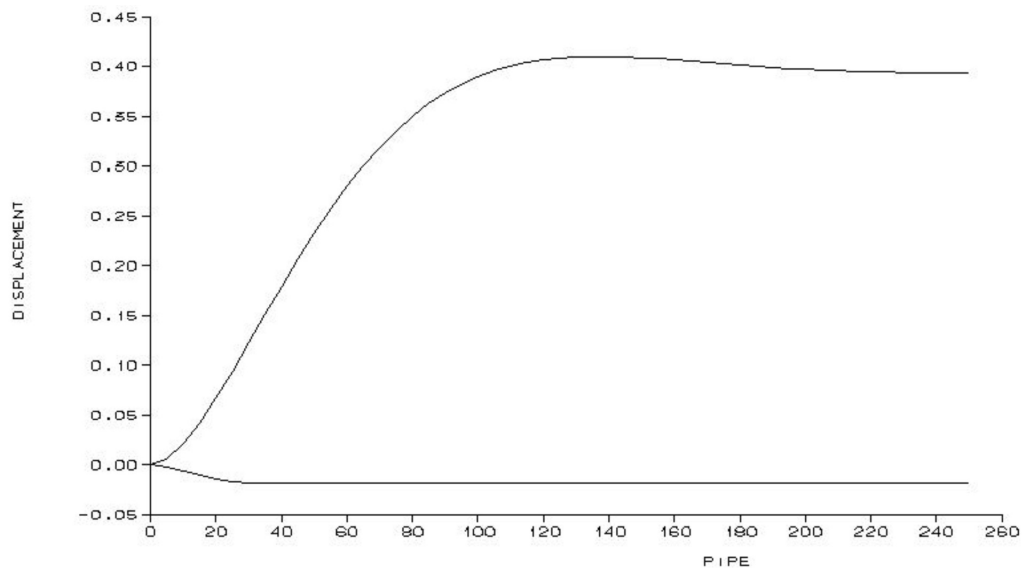


Figure 3.27: Displacement - length of an oil-filled pipeline under combined load of 100-year return currents and 10-year return irregular waves

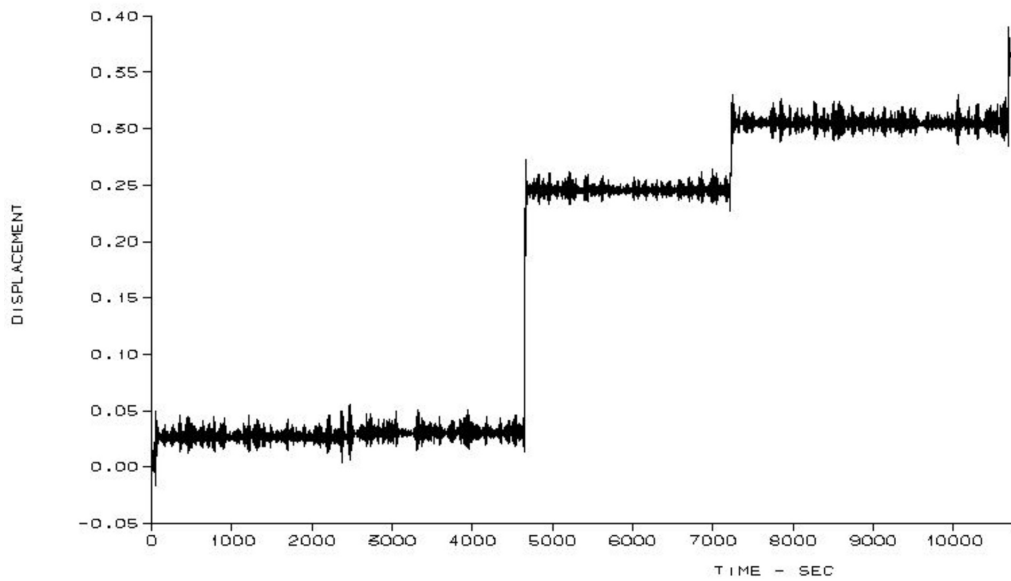


Figure 3.28: Displacement - time of an oil-filled pipeline under combined load of 100-year return currents and 10-year return irregular waves

The maximum value of displacement is at $0.4m$ according to figure 3.27 and figure 3.28, which satisfies the L_{10} criteria referring to DNV-RP-F109[5], therefore the pipe is considered acceptable.

The simulation results of hydrodynamic force, lift force and soil force are presented in figure 3.29, figure 3.30, figure 3.31 and figure 3.32.

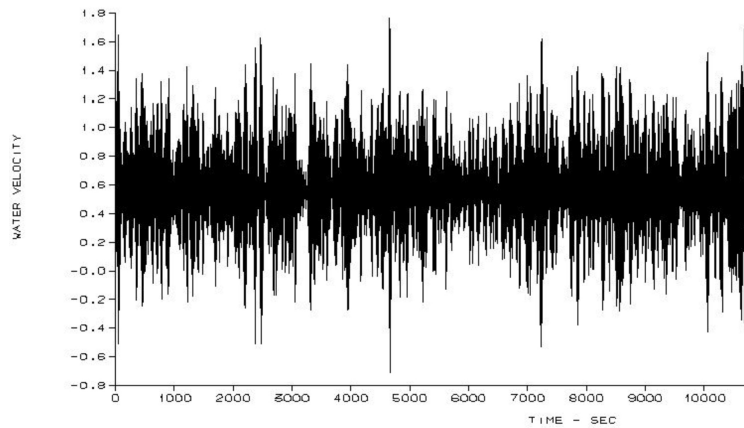


Figure 3.29: Water velocity by time acting an oil-filled pipeline under combined load of 10-year return currents and 100-year return irregular waves

The maximum water velocity is 1.8 m/s .

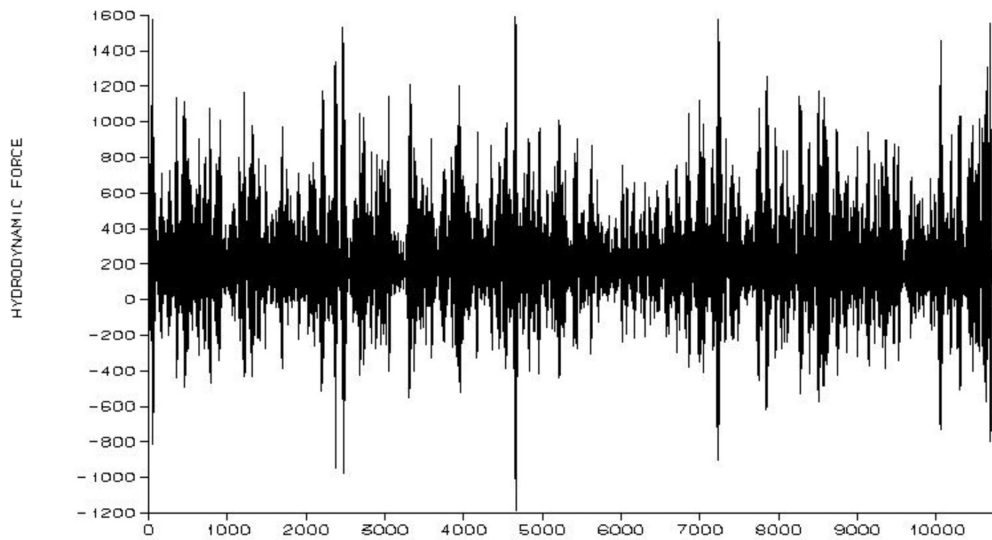


Figure 3.30: Hydrodynamic force by time acting an oil-filled pipeline under combined load of 100-year return currents and 10-year return irregular waves

The maximum hydrodynamic force is 1600 KN.

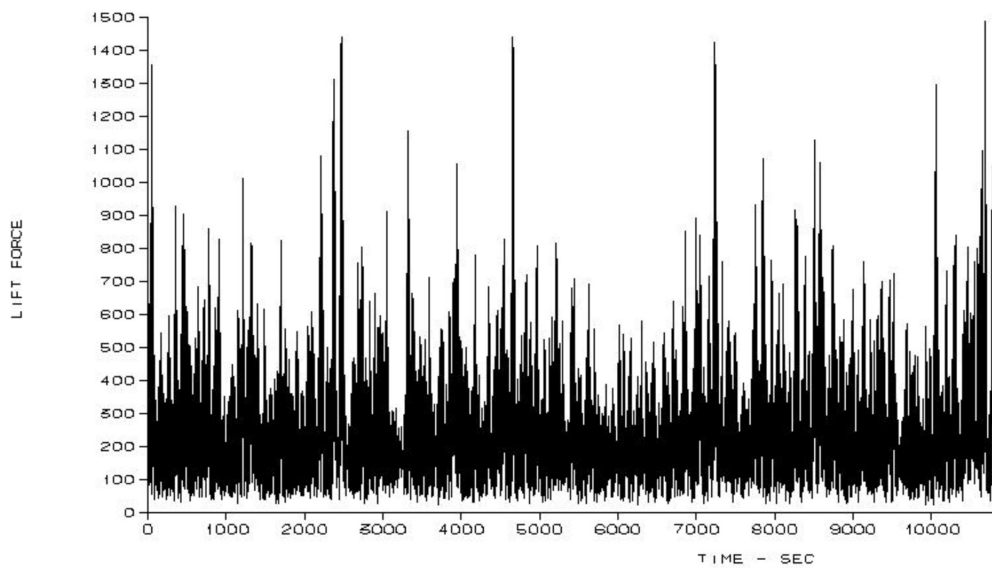


Figure 3.31: Lift force by time seconds acting an oil-filled pipeline under combined load of 100-year return currents and 10-year return irregular waves

The maximum lift force is 1500 KN.

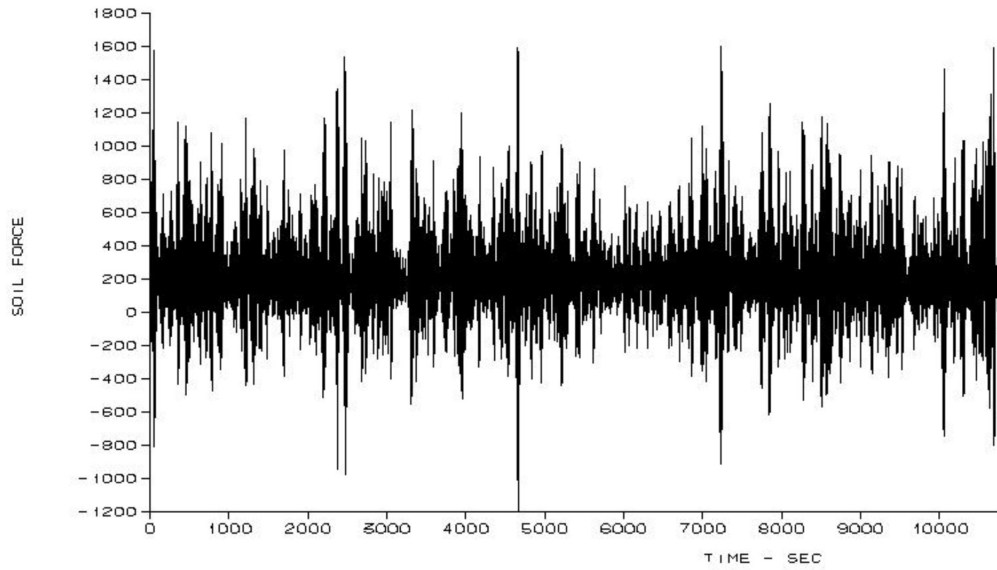


Figure 3.32: Soil force by time acting on an oil-filled pipeline under combined load of 100-year return currents and 10-year return irregular waves

The maximum soil force is 1600 KN.

As it can be seen from the figures above, those 3 forces are all oscillating irregularly when the pipe is exposed in combined 100-year return irregular waves and 10-year return current.

A summary of the results in the two load combinations investigated in this section is presented as in table 3.7. As shown in the table, Case 1.3, where the pipeline is exposed to 10-year return currents and 100-year return irregular waves appears to be the most critical case, as the displacement is considerably larger than that are in Case 1.4.

Result overview for combined irregular waves and current									
Case No.	Description	Hs [m]	Tp [s]	U [m/s]	Disp [m]	F _D [N]	F _L [N]	F _μ [N]	F _g [N]
1.3	Combined 10 year curren 100 year irregular waves	14.8	15.9	2.4	3.6	1600	1550	1650	3985
1.4	Combined 100 year curren 10 year irregular waves	12.6	14.7	1.8	0.4	1600	1500	1600	3985

Table 3.7: Summary of results from Case 1.3 and Case 1.4

Comparison will be made in the following section. A more realistic environmental condition will be suggested after the discussion on the differences between all the 4 cases in different wave-current combinations.

3.3 Comparison of the pipeline with combined regular waves and currents versus combined irregular waves and currents

A summary in table 3.8 is made for the important results for all the 4 cases in table 3.1.

Result overview for combined regular/irregular waves and currents									
Case No.	Description	H [m]	T [s]	Uc [m/s]	U [m/s]	Disp [m]	F _D [N]	F _L [N]	F _μ [N]
1.1	Combined 10 year curren 100 year regular waves	14.8	15.9	0.44	1.5	2.3	1300	2100	1350
1.2	Combined 100 year curren 10 year regular waves	12.6	14.7	0.57	1.3	0.024	1050	1900	1100
Case No.	Description	Hs [m]	Tp [s]	Uc [m/s]	U [m/s]	Disp [m]	F _D [N]	F _L [N]	F _μ [N]
1.3	Combined 10 year curren 100 year irregular waves	14.8	15.9	0.44	2.4	3.6	1600	1550	1650
1.4	Combined 100 year curren 10 year irregular waves	12.6	14.7	0.57	1.8	0.4	1600	1500	1600

Table 3.8: Summary of results for Case 1.1 to Case 1.4

The displacement in Case 1.3 appears to be larger than it is in Case 1.1, which indicates that irregular waves will generate larger hydrodynamic forces acting on the pipe. Furthermore, it suggests that the most critical environmental condition is 10-year return currents and 100-year return irregular waves, and this condition should be considered when designing the pipeline.

The impact of irregular/regular waves on forces is compared for the pipe with the original outer diameter $D = 0.73m$. The diagrammatic results from different wave-current-combinations with regular/irregular waves are compared on displacement, soil resistance force, lift force and hydrodynamic force respectively, and results in the characteristic time-interval (4500s-4800s) are demonstrated for a better observation.

The comparison of the pipe in irregular and regular waves begins with the displacement, as this is the most explicit indication for the stability requirement.

3.3.1 10-year return currents and 100-year return waves

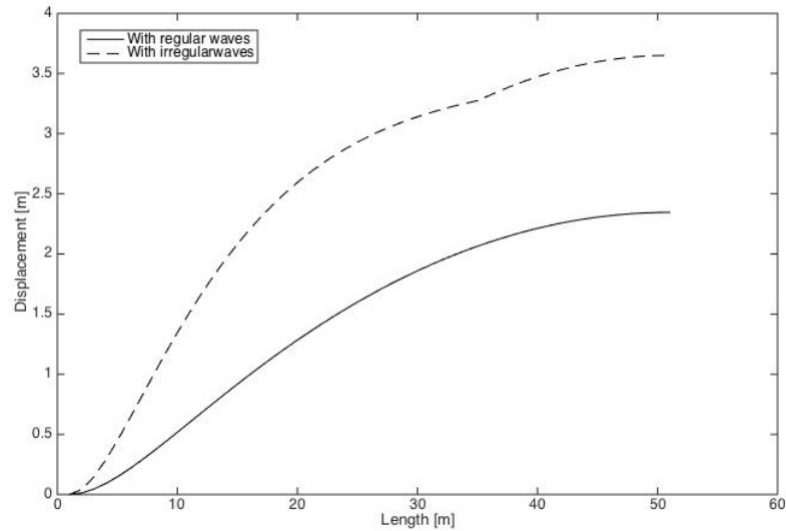


Figure 3.33: Displacement - length for the pipe under combined load of 10-year return currents and 100-year return waves

As it shows in figure 3.33, the maximum displacement occurs at the right end node for both cases. Therefore, further investigations on nodal displacement and forces are conducted for node 51 specifically for the combination of 10-year return currents and 100-year return waves.

According to figure 3.33, the displacement is larger with irregular waves than that in regular waves, and the hydrodynamic force and soil resistance force in figure 3.37 and figure 3.39 shows the same pattern with higher extreme values in irregular waves than in regular waves. While the lift force displays an opposite pattern, as in larger with regular waves than in irregular waves. It further proves that the water velocity contributes directly to the hydrodynamic force, which is also a driving force for the motion of the pipe. In irregular waves, when the significant wave height and significant water velocity is an average value of a 1/3 realization, the actual maximum wave height and flow velocity is much higher than it is in regular waves, therefore the maximum displacement tends to be more critical in irregular waves.

Diagrammatic comparisons on nodal displacement, water acceleration, water velocity and related forces are presented as follow.

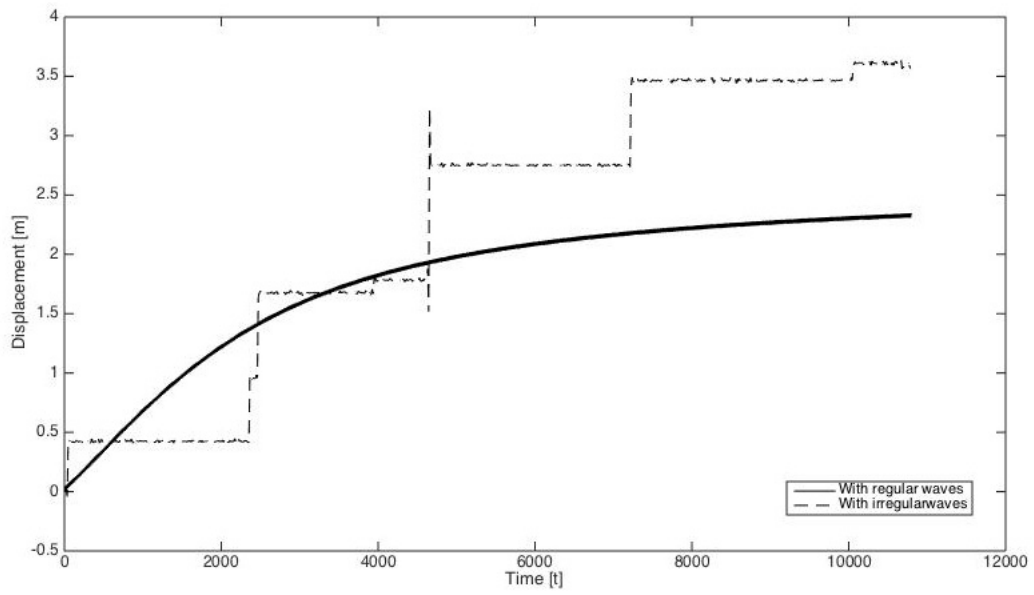


Figure 3.34: Displacement - time at node 51 for the pipe under combined load of 10-year return currents and 100-year return waves

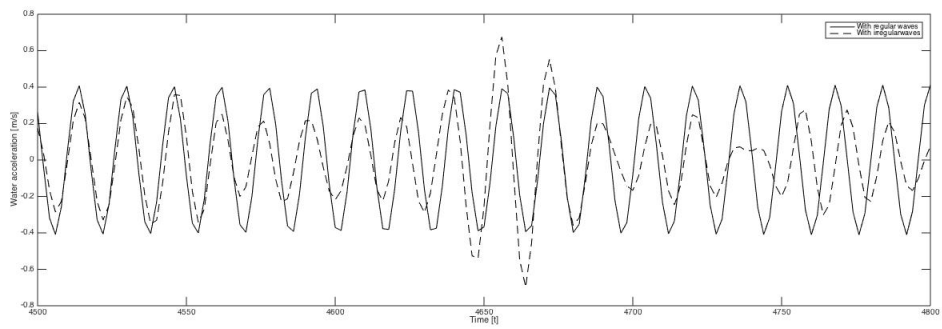


Figure 3.35: Water acceleration at node 51 for the pipe under combined load of 10-year return currents and 100-year return waves

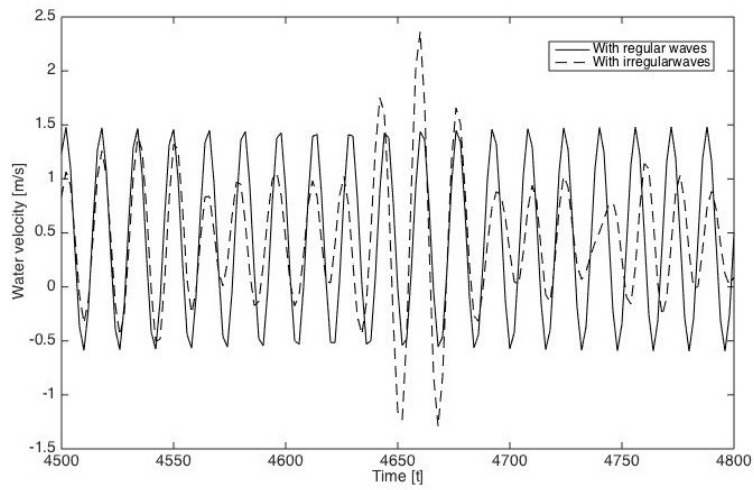


Figure 3.36: Water velocity at node 51 for the pipe under combined load of 10-year return currents and 100-year return waves

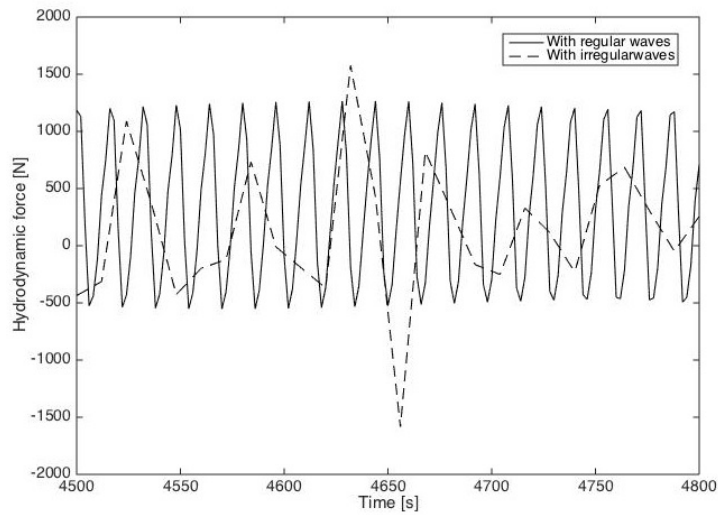


Figure 3.37: Hydrodynamic force at node 51 for the pipe under combined load of 10-year return currents and 100-year return waves

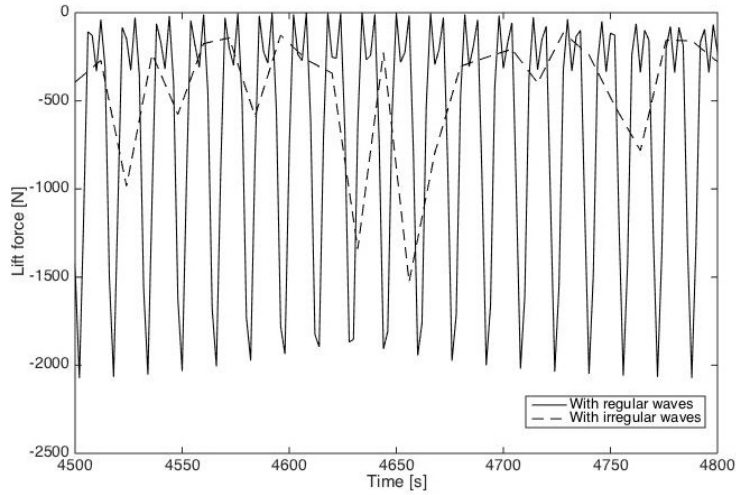


Figure 3.38: Lift force by time at node 51 for the pipe under combined load of 10-year return currents and 100-year return waves

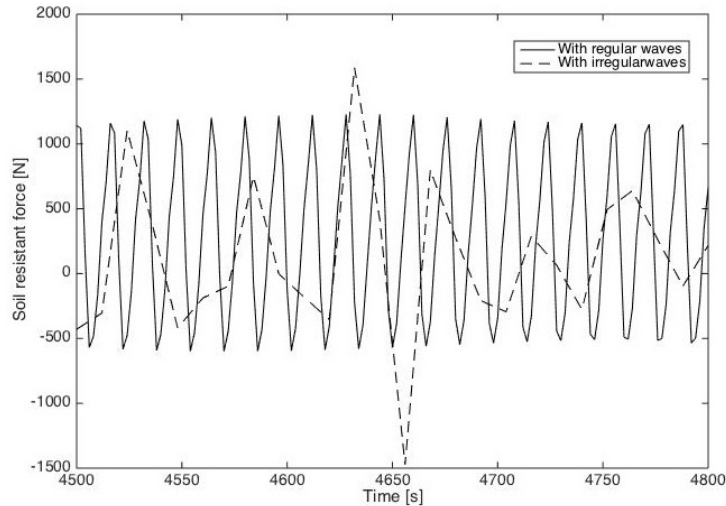


Figure 3.39: Soil resistance force by time at node 51 for the pipe under combined load of 10-year return currents and 100-year return waves

More discussion on the differences will be made with the comparison for cases with 100-year current and 10-year return waves in the following section.

3.3.2 100-year return currents and 10-year return waves

Figure 3.40 indicates that the maximum displacement for the pipe under 100-year return currents and 10-year return waves occurs from node 20 to node 30, thus the forces and transient displacement on this node will be investigated further.

According to figure 3.34 and figure 3.41, the nodal displacements in both load combinations are developing with constant oscillations in the combination with regular waves and current, while when irregular waves plus current are applied, the displacement ap-

pears to climb stair-like with several oscillations of different amplitudes.

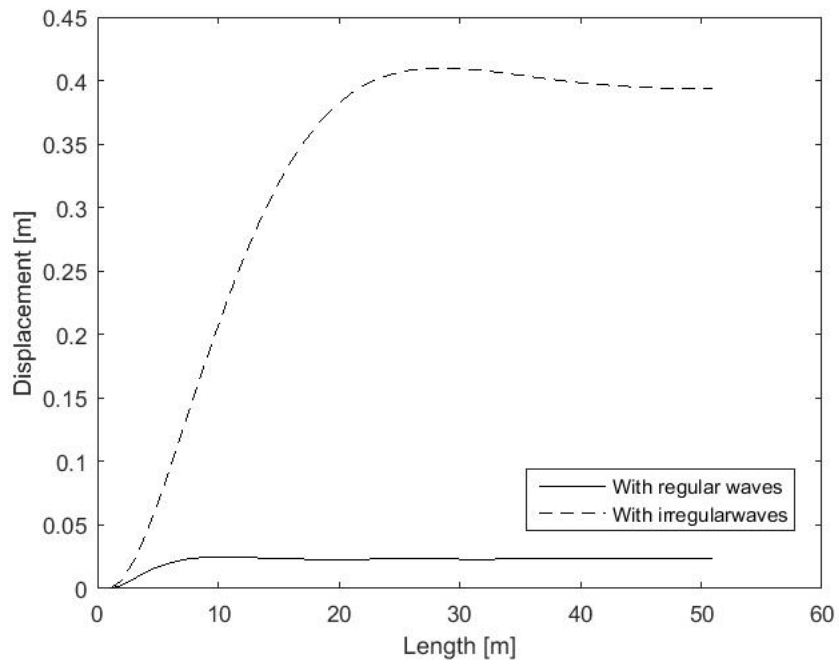


Figure 3.40: Displacement - length for the pipe under combined load of 100-year return currents and 10-year return waves

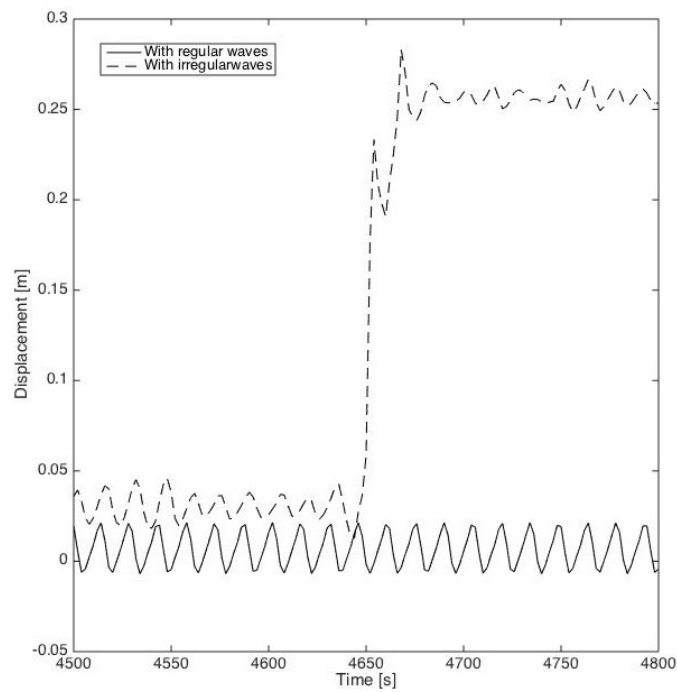


Figure 3.41: Displacement - time at node 30 for the pipe under combined load of 100-year return currents and 10-year return waves

In general, the displacement development with respect to length for both cases suggests that the pipe will have larger movement under irregular waves than under regular waves. Further discussions will be made for the comparisons of forces (figure 3.37 to figure 3.46), water acceleration (figure 3.42) and water velocity (figure 3.43).

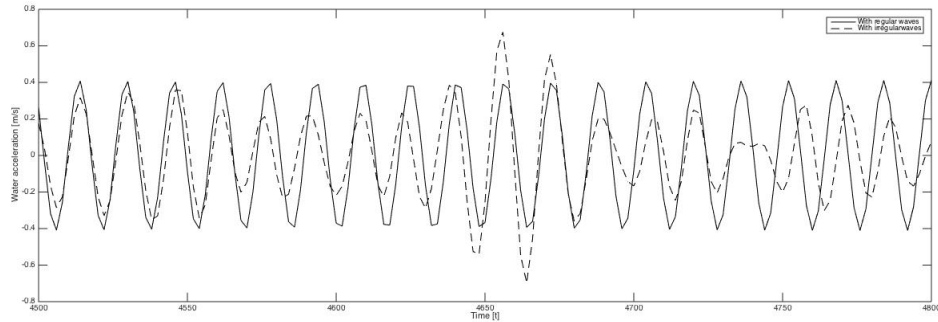


Figure 3.42: Water acceleration at node 30 for the pipe under combined load of 100-year return currents and 10-year return waves

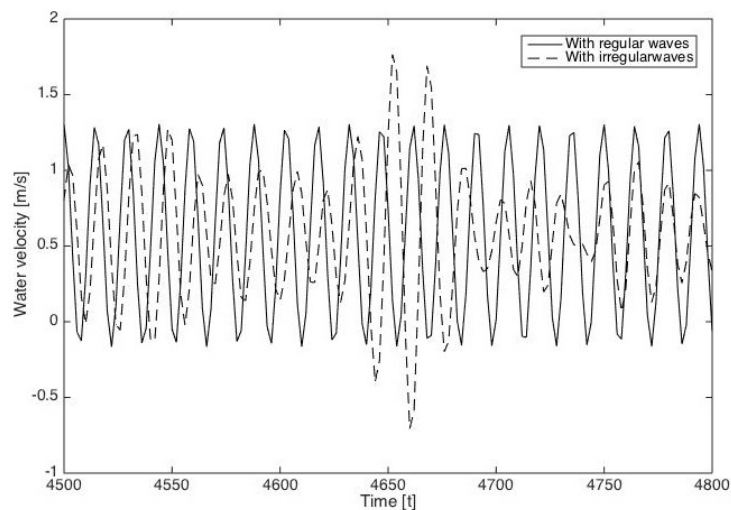


Figure 3.43: Water velocity at node 30 for the pipe under combined load of 100-year return currents and 10-year return waves

Figure 3.37-3.46 present the development of related forces at the significant nodes for each load combinations with irregular waves and regular waves respectively. A rather shorter time-series (4500-4800s) that characterizes the development is defined for a better observation. The forces tends to have a constant amplitude of oscillation in regular waves, while it appears to be relatively non-harmonic with irregular waves.

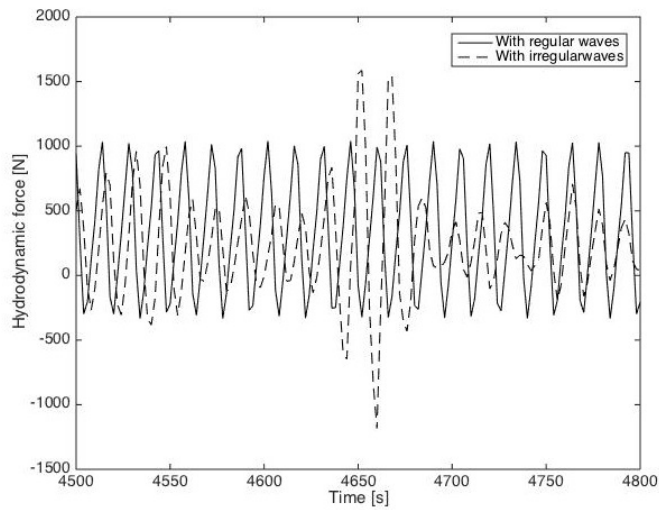


Figure 3.44: Hydrodynamic force at node 30 for the pipe under combined load of 100-year return currents and 10-year return waves

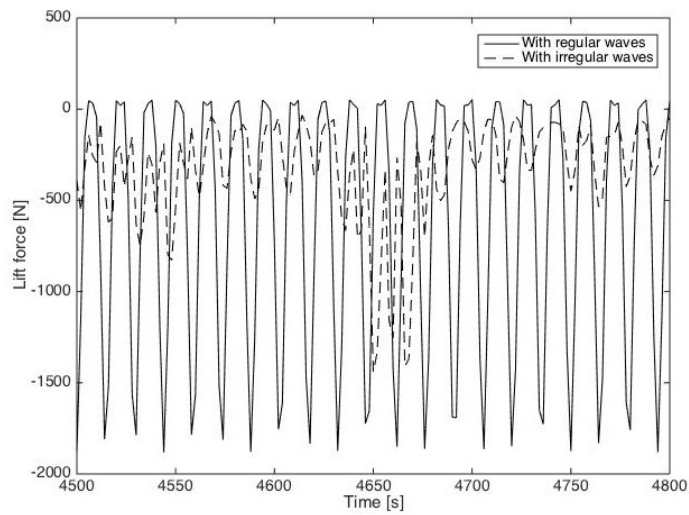


Figure 3.45: Lift force by time at node 30 for the pipe under combined load of 100-year return currents and 10-year return waves

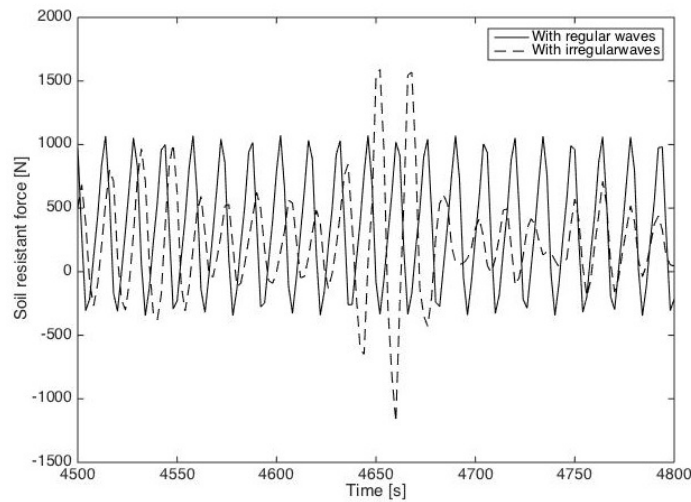


Figure 3.46: Lift force by time at node 30 for the pipe under combined load of 100-year return currents and 10-year return waves

Referring to Chapter 3.1 and Chapter 3.2, it appears that the displacement of pipe with regular waves tend to have a oscillatory pattern by time. While the displacement develops stair-like with partial oscillatory behaviour in cases where irregular waves are applied.

For both cases, the displacement is rather larger with irregular waves than it is with regular waves, and the hydrodynamic force and soil resistance force in figure 3.37 and figure 3.39 shows the same pattern with higher extreme values in irregular waves than in regular waves. While the lift force displays an opposite pattern, and is larger with regular waves than with regular waves.

Studies and experiments have provided some explanations on the differences of forces according to Sumer and Fredsøe[13] and Longoria et al.[14]. The vortex-flow regime is classified as shown in table 3.9.

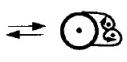
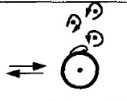
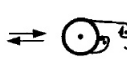
Regime of vortex motion	Pattern	KC range
Vortex pair		$0(1) < KC \leq 7$
Transverse vortex street		$7 < KC \leq 15$
Vortex street		$KC > 15$

Table 3.9: Classification of vortex-flow regimes in regular sinusoidal oscillatory flow. Sumer and Fredsøe[13]

Experiments by Longoria et al(1995)[14] indicate that a regular vortex-flow regime for $KC > 7$ (i.e. the transverse vortex street) is actually a product of regular, repeatable

interactions between vortices of two successive half periods in sinusoidal flows. When KC is within the range of $10 - 25$, which applies to Case 1.1 to Case 1.4, the drag coefficient and the inertia coefficient appear to be smaller in regular waves than in irregular waves. According to the Morrison equation in equation 3.3, the hydrodynamic force consists of two parts, namely the drag force and the inertia force, the varying extreme values in both regular and irregular waves are caused by the interaction that is partially or at times nearly completely prevented, which is the result of the randomly changing successive half periods of the motion. This would accordingly leads to the disruption of the regular vortex regimes, and over lapping of different magnitudes for the drag coefficient and the inertia coefficient.

Figure 3.47 and figure 3.48 present the results of this typical test along with the results obtained in a sinusoidally oscillating flow under corresponding conditions in the same oscillatory water tunnel.

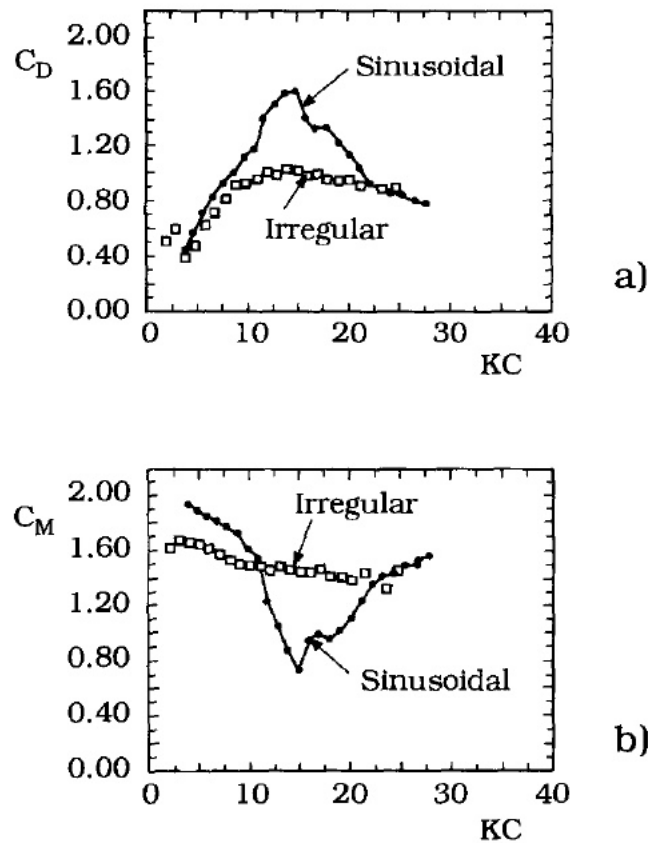


Figure 3.47: Inertia and drag coefficients measured under sinusoidal and irregular(random) oscillatory flow conditions. Sumer and Fredsøe[13]

According to figure 3.38 and figure 3.48, the lift force tends to have higher extreme values in regular waves than in irregular waves. As the lift force is directly related to the lift coefficient shown in equation 3.5, this difference in regular waves and irregular waves can presumably be explained by the experiment results from Longoria et al [14].

As shown in figure 3.48[14], the lift force coefficients differ significantly under sinus-

oidal and irregular wave conditions. This is attributed to the tremendous changes in the vortex-flow regimes in the case of random oscillatory flow. The lift coefficient in irregular waves appears too be smaller than in regular waves with KC number in the range of 10 to 25, which further leads to the smaller lift force in irregular waves than in regular waves.

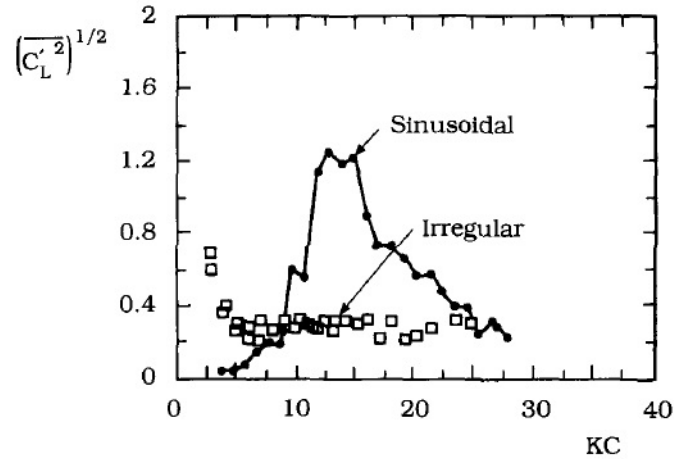


Figure 3.48: Root-mean-square lift force coefficient measured under random flow conditions compared with that obtained in the case of corresponding sinusoidal flow. Sumer and Fredsøe[13]

According to the Morrison equations described in equation 3.3, figure 3.36 to figure 3.46 verify that with regular waves:

- Drag force is proportional to flow velocity
- Inertia force is proportional to acceleration
- Lift force is proportional to flow velocity, always upwards(the downward direction is defined as positive in PONDUS).

While for cases with irregular waves, the proportional effect becomes uncertain, which is likely due to the simulation is based on one single seed. Random wave trains are represented by a user-defined number of component waves whose amplitudes and periods are selected to give a sea state having the specified spectrum. However the phase shifts and locations of extreme values appear to be at the same points, which indicates the correlations described in *Morrison* formulation is still applicable for irregular waves.

This is likely due to the higher water velocity in irregular waves according to figure 3.36 and figure 3.43, which again proves that the water velocity contributes directly to the hydrodynamic force, which is also a driving force for the motion of the pipe. And with irregular waves, when the significant wave height and significant water velocity is an average value of a highest 1/3 realization, the actual maximum wave height and flow velocity is much higher than it is in regular waves, therefore the maximum displacement tends to be more critical in irregular waves than in regular waves.

The results also indicate that there are likely a certain sets of overlapped wave amplitudes in irregular waves, as irregular waves consists of multiple sets of regular waves

with different amplitudes theoretically. The stairs-steps in each displacement figures for irregular waves correspond with the time-steps where the peak values for the oscillating hydrodynamic force, lift force and soil resistance force are situated. It indicates that the peak values for force components, which are built up by overlapped amplitudes of multiple regular waves, will contribute directly to the increment of displacement. It suggests that a irregular waves simulation model gives more realistic estimations on the on-bottom stability of the pipe.

4 Study on soil coefficients

Apart from the structural capacity and the external hydrodynamic environment, the stability of a pipeline is affected by the soil properties as well. Various kinds of failure or defect modes like pipeline walking and lateral buckling are considerably sensitive to the pipe-soil interaction. In this study, the pipe-soil interaction is investigated with different combinations and arrangements of two types of soil, namely sand and clay. This investigation is intended to achieve a better understanding of pipe-soil interaction. Displacement, soil force and penetration will be investigated and compared with the default soil database and algorithm in PONDUS.

In order to achieve a better understanding for the sensitivity of the soil parameters, a lighter pipe should be studied in order to exclude the self-weight-dominating effect. Referring to Case 1.3 in table 2.4 the original pipe with combined load of 10-year current and 100-year random waves is selected for further investigations. The material and structure data of the pipe is listed out in table 4.1 and the PONDUS model in figure 3.3 will be applied.

Int. diameter of pipe, D_{in}	571.8	mm
Concrete coating, t_{con}	55	mm
Wall thickness, t_{wall}	19.1	mm
Corrosion allowance, t_{cal}	1.5	mm
Corrosion coating, t_{cc}	5	mm
Marine growth, t_{mg}	0	m
Pipe roughness, k/D	0.001	-

Table 4.1: Pipe property

The lateral soil interaction has been modelled in the past (Verley and Lund [9][10]) based on the Coulomb model with a simple friction coefficient. As the soil force exhibits a non-linearity behaviour in reality, this model is too simplified and proven to be unrealistic for the pipe-soil interaction. The model developed by Verley [10] and SAFEBUCK Joint Industry Program (SAFEBUCK JIP) [2] became most applicable in researches. While Verley's model is utilized in PONDUS simulation.

The applied lateral soil model consists of two main components, namely Coulomb friction force and passive soil force. Verley and Sot[10] developed the soil model for sand while Verley and Lund[9] developed the soil model for clay.

The calculation principle in PONDUS is that the response of the pipe is non-linear due to non-linear hydrodynamic forces and non-linear interaction between the pipe and the soil. According to [8], the FEM model of soil force are sorted into several types as follows:

- Simple Coulomb friction model
- Pipe - Clay Model
- Pipe - Sand Model

The simple Coulomb friction model is applied in Chapter 3 for comparison of random and regular waves. Here in this section, the pipe-clay model and the pipe-sand model will be introduced with different combinations. As it is listed in table 4.2, there will be 5 cases designed based on the assumption that the soil properties may vary along the pipe, and the soil force in pipe axis direction is not considered.

Case no.	Case description
2.1	Pipe-clay model
2.2	Pipe-sand model
2.3	50% sand and 50% clay
2.4	30% sand + 40% clay + 30% sand
2.5	30% clay + 40% sand + 30% clay

Table 4.2: Case design for pipe-soil interaction

As it is seen from the case description, the pipe-soil model is sectioned by defined ratios of sand/clay distribution. The intention of this strategical design is to look into the sensitivity level and structural impact of soil parameters.

Modified friction coefficients will also be tested to study the sensitivity of parameters. Many studies and experiments have been conducted on the friction coefficient μ for different soil types [10] [9]. The range for the friction coefficient of clay lies between 0.2 and 0.6, while it is between 0.4 and 0.8 for sand. Therefore 3 cases will be investigated for the pipe-clay model with the friction coefficient selected as 0.2, 0.4 and 0.6. The friction coefficients are defined as 0.4, 0.6 and 0.8 for the pipe-sand model.

The total lateral displacement y is resulted by both elastic and plastic reactions as in equation 4.1

$$y = y_e + y_p \quad (4.1)$$

where y_e is the elastic displacement while y_p is the plastic displacement.

The soil force in the elastic phase is defined in equation 4.2.

$$F_s = k_s x_e \quad (4.2)$$

where k_s is the elastic stiffness of the soil.

Meanwhile the plastic soil resistance is defined as:

$$F_s = F_f + F_r \quad (4.3)$$

where F_f is the pure friction component (Coulomb friction force) and F_r is the passive resistance, which is a function of soil penetration, lift force, and displacement of the soil. The force formulars are elaborated as follows:

$$F_f = \mu(w_{sub} - F_L) * sgn(\dot{y}) \quad (4.4)$$

$$F_r = D_s * sgn(\dot{y}) \quad (4.5)$$

where

F_L : the lift force
 F_S : the plastic soil force
 w_{sub} : is the submerged weight of the pipe
 μ : the constant friction coefficient
 D_s : the remaining force function

There are generally 4 phases of the passive resistance of the force according to [5]

1. An elastic region where the lateral displacement is less than typically 2% of the diameter. The upper limit of the passive resistance in this stage is denoted as F_{r1} .
2. A region where significant lateral displacement may be experienced, up to half the pipe diameter for sand and clay soils in which the pipe-soil interaction causes an increase in the penetration and thus in the pipe-soil resistance. The upper limit of soil passive resistance is called breakout resistance F_{r3} .
3. After breakout, the resistance and penetration decrease.
4. When displacement exceeds typically one diameter, the passive resistance and penetration may be assumed constant. The soil resistance at this stage is denoted as F_{r3} .

The relationship of those 4 stages is presented in figure 4.1

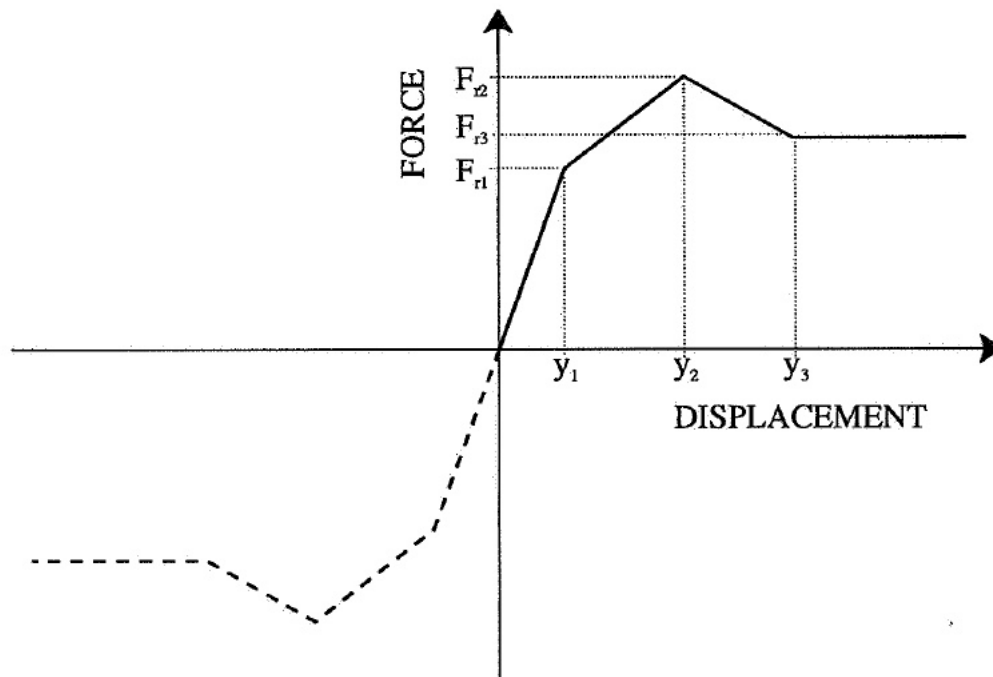


Figure 4.1: Passive resistance model[8]

For movements within 0 and y_1 , the resistance is linearly elastic and no work is done. The pipe penetration does not change nor does the origin move. The distance y_1 is determined as a function of pipe outer diameter. The increasing penetration will also cause the force

level F_{r3} to increase.

For displacements $y > y_2$, the origin is translated a distance $(y - y_2)$ and the penetration decreases until $(y = y_3)$, after which it remains constant.

If the pipe section continues to move in the same direction after break-out, due to a mound of soil being pushed ahead of the pipe, there will be a horizontal resistance in addition to the direction . The residual force F_{r3} will have an effect on how far a pipe section will move after break-out whilst pipe motion is still in the same direction.

Through the expression for F_{r3} , F_{r3} is expressed as an equivalent penetration after break-out. The transition from the elastic to plastic regime can be expressed as

$$|k_s y_e| = (\mu(w_s - F_L) + D_s) \quad (4.6)$$

In the plastic regime, the elastic displacement can be derived from the relationship shown in equation 4.7 and figure 4.2 as follows

$$y_e = F_s k_s \quad (4.7)$$

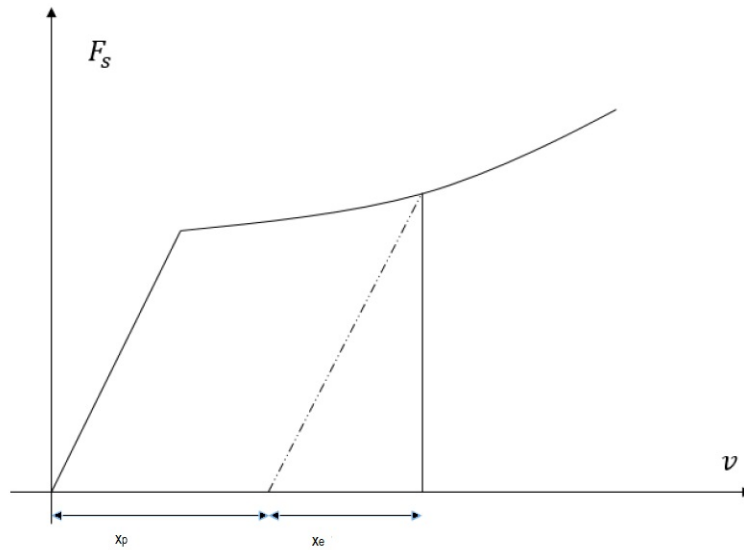


Figure 4.2: Elastic and plastic displacement by soil force

For the pipe-sand model, following expressions are presented by [5] for the break-out resistance

$$\frac{F_R}{F_C} = \begin{cases} (5.0k_s - 0.15k_s^2)\left(\frac{z_p}{D}\right)^{1.25} & \text{for } k_s \leq 26.7 \\ k_s\left(\frac{z_p}{D}\right)^{1.25} & \text{for } k_s > 26.7 \end{cases}$$

where

$$k_s = \frac{\gamma D^2}{w_{sub} - F_L} = \frac{\gamma D^2}{F_C}, F_C = w_{sub} - F_L \quad (4.9)$$

where

F_R : Passive resistance
 F_C : Contact pressure between pipe and soil
 F_L : Lift force
 w_{sub} : Pipe submerged weight
 D : Pipe diameter
 z_p : Pipe penetration
 γ_s : Sand submerged weight

The initial penetration on sand can be taken as

$$z_i/D = 0.037k_s^{-0.67} \quad (4.10)$$

Assume that the initial passive soil resistance is linear elastic and there is no work done. The assumed pipe penetration remains constant, while the initial penetration due to the self-weight of the pipe for the pipe-clay model is defined as follows:

$$\frac{z_i}{D} = 0.0071\left(\frac{G^{0.3}}{K_c}\right)^{3.2} + 0.062\left(\frac{G^{0.3}}{K_c}\right)^{0.7} \quad (4.11)$$

$$G = \frac{s_u}{D\gamma_s} \quad (4.12)$$

$$K_C = \frac{s_u D}{w_{sub} - F_L} \quad (4.13)$$

where

D : Contact pressure between pipe and soil
 F_L : Lift force
 w_{sub} : Pipe submerged weight

Referring to figure 4.1, F_{r1} is denoted as the upper boundary of the passive resistance, it can be expressed as

$$F_{r1} = \frac{4.1K_c(w_{sub} - F_L)}{G^{0.392}} \left(\frac{z_i}{D}\right)^{1.31} \quad (4.14)$$

The expression for a pipe-clay interaction is defined by DNV according to [5]

$$\frac{F_R}{F_C} = \frac{4.1k_c}{G^{0.39}} \left(\frac{z_p}{D}\right)^{1.31} \quad (4.15)$$

where

$$\begin{aligned}
 G &= \frac{s_u}{D\gamma_s} \\
 k_c &= \frac{s_u D}{F_C} \\
 F_C &= s_u - F_L
 \end{aligned}$$

Here

s_u : Clay undrained shear strength
 γ_s : Clay dry unit weight

Here z_i is the initial soil penetration of the pipe. Moreover, the upper limit for the lateral displacement in the elastic regime of the pipe is defined as 2% of the outer diameter of the pipe[5], while in PONDUS a ratio of $(F_{r1} + F_f)/k_s$ is applied.

The elastic soil resistance can therefore be found as

$$F_R = k_s x \quad (4.16)$$

The elastic stiffness for clay is defined as $2000MPa$, and a default value for the initial penetration $Z_{R0} = Z_{penetr}/D$ is calculated by the program. The submerged pipe weight W_{sub} , lift force F_L and vertical soil contact force $F_v = W_{sub} - F_L$ is calculated automatically based on the material and environment data given in prior context.

Referring to figure 4.1, the passive soil resistance will enter the plastic region with a increasing lateral displacement for the clay soil. While the soil penetration increases along with a cumulative energy caused by the lateral displacement. The work done within the plastic region is

$$E = \int_0^t F_R ds \quad (4.17)$$

The total soil penetration, here defined as z_{tot} , can be obtained as

$$\frac{z_{tot}}{D} = [0.12S^{0.037}\xi^{0.32}\left(\frac{a}{D}\right)^{-0.25}] \quad (4.18)$$

where $\frac{a}{D} \leq 0.05$, and

$$\xi = \frac{E}{s_u D_2} \quad (4.19)$$

where a is the oscillation amplitude of the pipe in translational direction.

The soil penetration in the plastic regime is restricted in the ranges as follows:

$$\left(\frac{z_2}{D}\right)_{max} = 1.1SG^{0.54}\left(\frac{a}{D}\right)^{0.17}\frac{z_2}{D} \leq 0.3\frac{a}{D} \geq 0.05 \quad (4.20)$$

The upper boundary of the soil penetration in Verley's model is defined as

$$z_{2,max} = 0.3D \quad (4.21)$$

While the maximum soil resistance in this region F_{r2} is

$$F_{r2} = \frac{4.13K_c(w_{sub} - F_L)}{G^{0.392}}\left(\frac{z_2}{D}\right)^{1.31} \quad (4.22)$$

Deducted from equation 4.22 and equation 4.21 that the maximum strength capacity before a breakout varies due to the lateral displacement. Here the maximum value of lateral displacement is denoted as x_2 and it occurs when it exceeds $D/2$ according to [4].

The soil stiffness in the plastic regime is then defined as a function of soil penetration

$$k_{z2} = \frac{F_{r2} - F_{r1}}{x_2 - x_1} \quad (4.23)$$

Based on equation 4.23 and equation 4.22, it appears that the soil stiffness it not a constant and changes by the increasing soil penetration in plastic region. This indicates that the passive soil resistance will still be non-linear due to the varying breakout strength in lateral motion, even if the a linearly behaviour is assumed.

4.1 Pipe-soil interaction with uniform soil types

4.1.1 Pipe-clay model

The material and environment data with pipe-clay model for the pipe under combined load of 10-year currents and 100-year return irregular waves in table 4.3 will be applied to the simulation in PONDUS.

Steel yielding stress	415	MPa
Clay shear strength	2000	N/m ²
Elastic Stiffness	65 000	N/m ²
Depth	104	m
Current	0.374	m/s
Peak period	14.5	s
Significant wave height	12.5	m
Simulation time	3	hours
Time increment	0.01	s(1080000 time steps)

Table 4.3: Pipe and environment property for the pipe-clay model

Based on the researches and studies from the past [10][9], the lower limit of the friction coefficient for clay is 0.2 while the upper limit is 0.6, therefore the variation of friction coefficient in this study is defined to be 0.2, 0.4 and 0.6 respectively to test the sensitivity of the friction coefficient for the pipe-clay interaction. As the default value for the friction coefficient for clay in PONDUS is defined as $\mu = 0.2$, solid line style refers to this initial case with $\mu = 0.2$ in comparison figures.

The simulation results are as follows.

Displacement

As it shows from 4.3, the displacement in general decreases as the friction coefficient increases. Moreover, there is a steep increase before node 15 and then it becomes relatively stable afterwards. Based on the development of the displacement curves, the end node, node 51 is selected to be investigated further as a significant node.

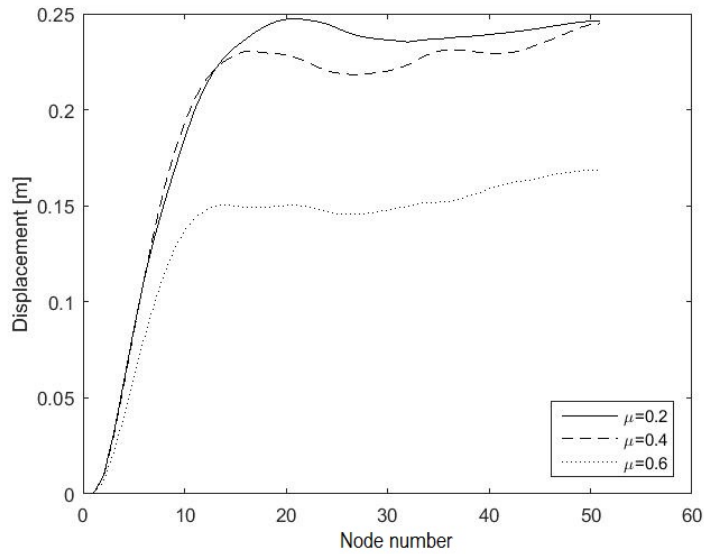


Figure 4.3: Displacement by length of pipe-clay model with different friction coefficients

The displacement develops in a stair-like pattern according to figure 4.4, this is considered as a typical form of oscillation in random waves. The drastic vibrations occurs at the same steps despite of different friction coefficients. The significant time intervals 2300s-2500s and 4600-4700s will be looked into respectively.

As it is shown in 4.4, figure 4.5 and figure 4.6, there is a very drastic change of amplitudes along those two important time intervals. But the nodal results of displacement do not always correspond with the different friction coefficients proportionally as it is in figure 4.6. This is possibly due to the change of neutral positions in every cycle of the force-displacement that runs through the simulation.

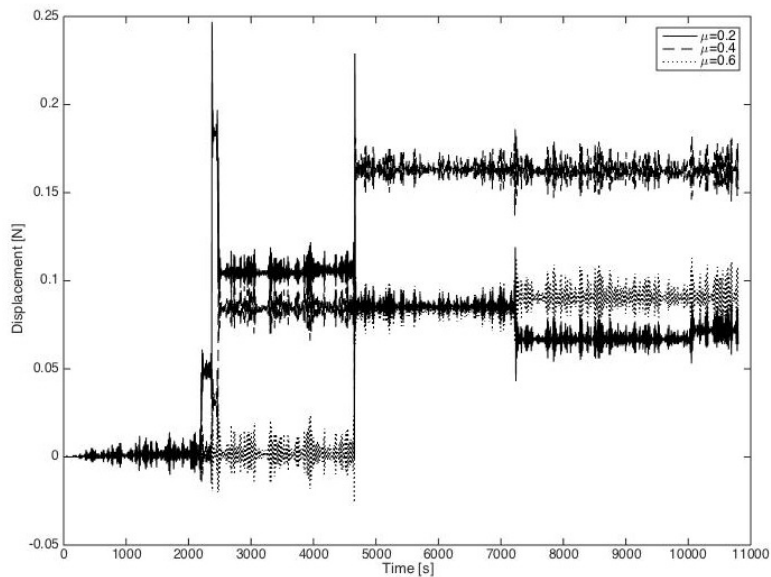


Figure 4.4: Displacement by time at node 51 of pipe-clay model with different friction coefficients

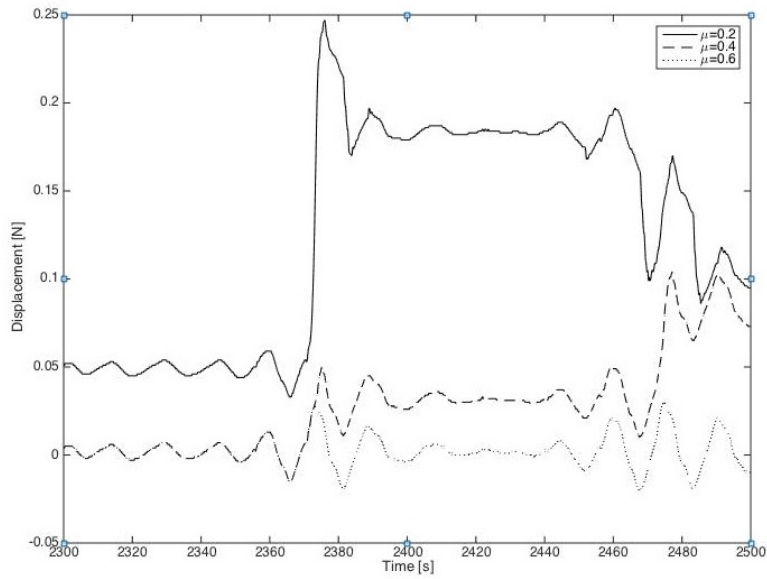


Figure 4.5: Displacement by time at node 51 of pipe-clay model with different friction coefficients in 2300s-2500s

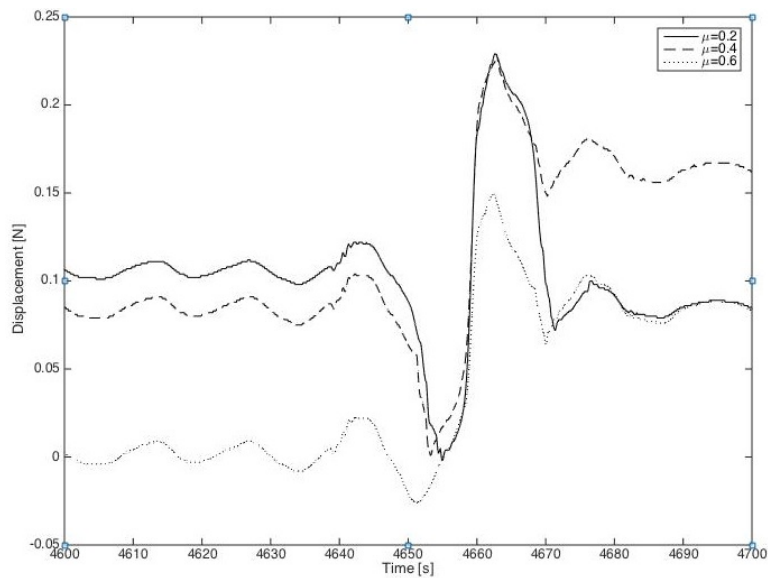


Figure 4.6: Displacement by time at node 51 of pipe-clay model with different friction coefficients in 4600s-4700s

The force in figure 4.7 refers to the soil resistance force. During simulation, the model may go through many force-displacement cycles of different amplitude. Figure 4.7 indicates a cycle of amplitude greater than y_2 causing both force level F_{r2} (therefore F_{r1} and F_{r3}) to decrease and the origin to move.

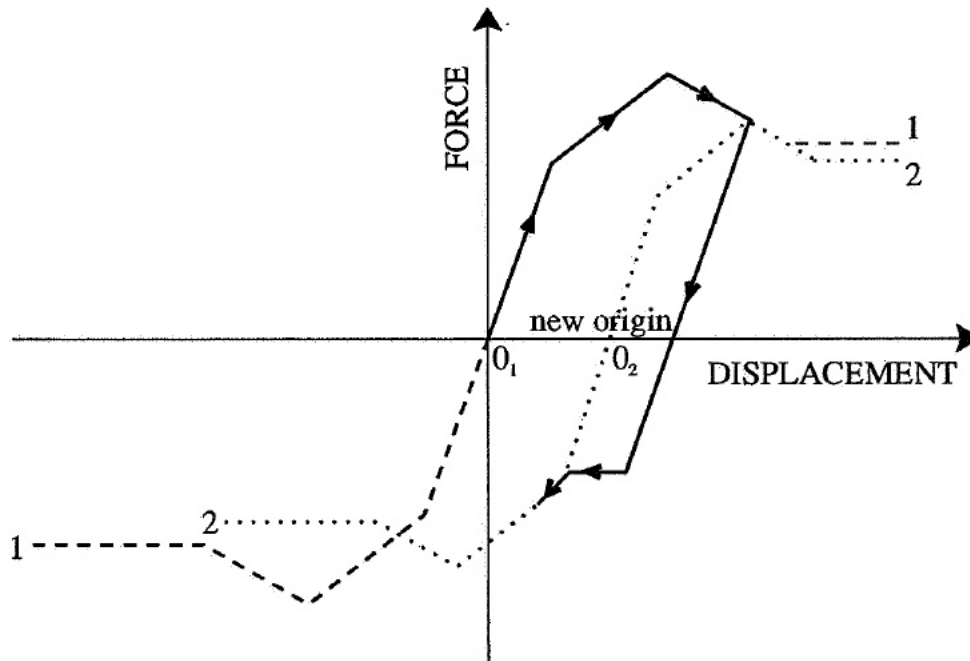


Figure 4.7: Force displacement model. 1 cycle with amplitude $> y_2$ [8]

As the displacement is generated by all the forces acting on the pipe, the hydrodynamic force, lift force and soil resistance force will be looked into to find out the reason for this significant difference for the three cases. The relative velocity between water particle and pipeline is different at time instance when pipeline has significant movement namely at 2300s-2500s and 4500-4700s.

Based on equation 4.5, and equation 3.9, the friction force, relative velocity between pipe and water particle and penetration will interact with each other. As the friction coefficient directly affects the soil resistance force, there will be changes at the initial time when the pipe line starts to move in lateral direction, and the time history of displacement of pipeline is changed for different friction coefficients. The penetration is related to the accumulated displacement of pipeline as well. The larger the soil friction coefficient is, the smaller the displacement of the pipeline will be, as the pipeline penetrates the soil deeper and creates a kind of soil berm. The accumulated displacement is defined as the sum of displacement from neutral position, and the neutral position is varying by time as shown in figure 4.7.

Hydrodynamic force

Referring to figure 4.8 to figure 4.13, the drastic change of magnitude for the hydrodynamic force and lift force occurs at the same time steps as it is for displacement. According to equation 3.9, both the relative drag and inertia force in the horizontal direction and the lift force in vertical direction are proportional to the effective/relative

velocity. It indicates also that this node is experiencing a significant large wave at those time intervals that generates the corresponding increase of the horizontal and vertical forces, which further leads to the drastic increase of magnitude for the nodal displacement. The effective velocity will therefore consequentially demonstrate the same drastic change of magnitude in those two characteristic time intervals as shown in figure 4.14, figure 4.15 and figure 4.16

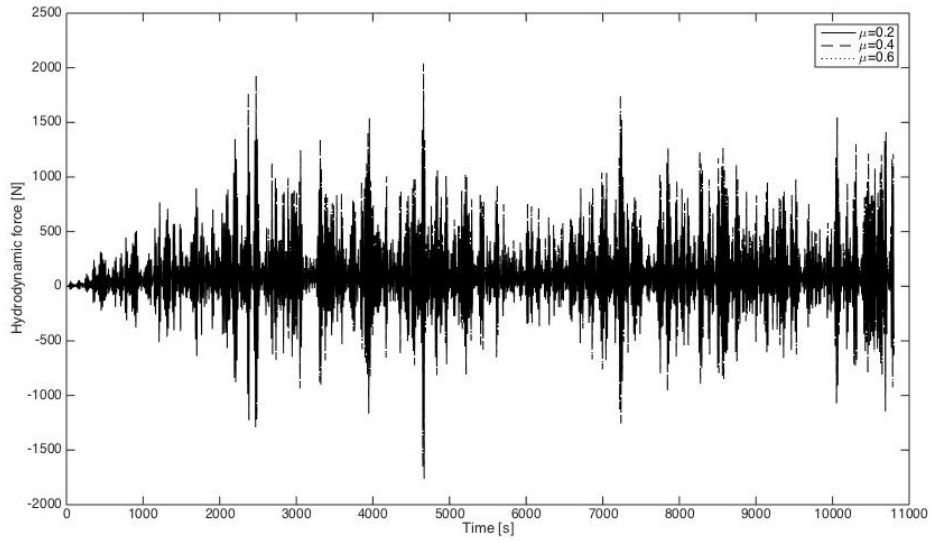


Figure 4.8: Hydrodynamic force by time at node 51 of pipe-clay model with different friction coefficients

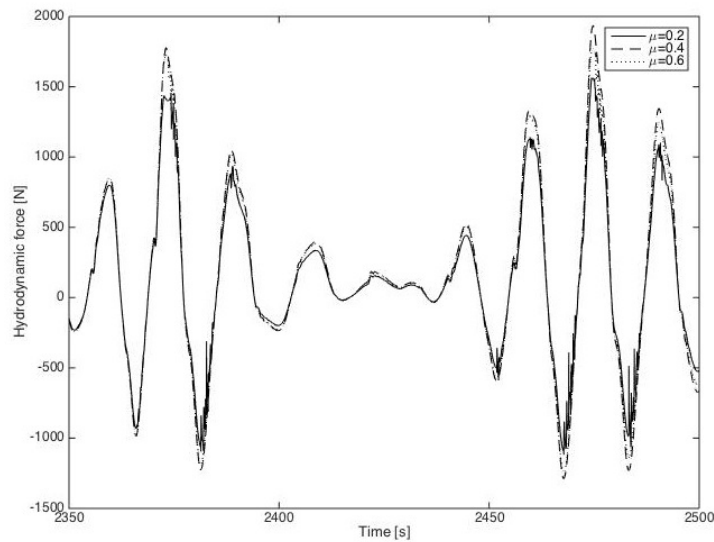


Figure 4.9: Hydrodynamic force by time at node 51 of pipe-clay model with different friction coefficients in 2450s-2500s

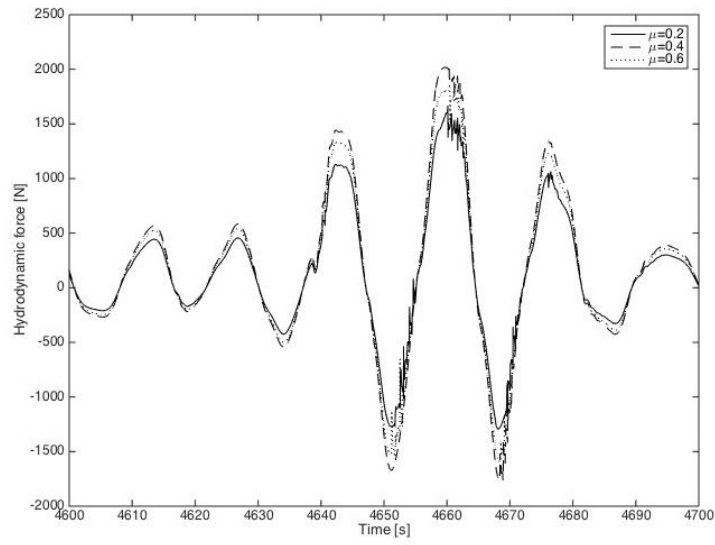


Figure 4.10: Hydrodynamic force by time at node 51 of pipe-clay model with different friction coefficients in 4600s-4700s

Lift force

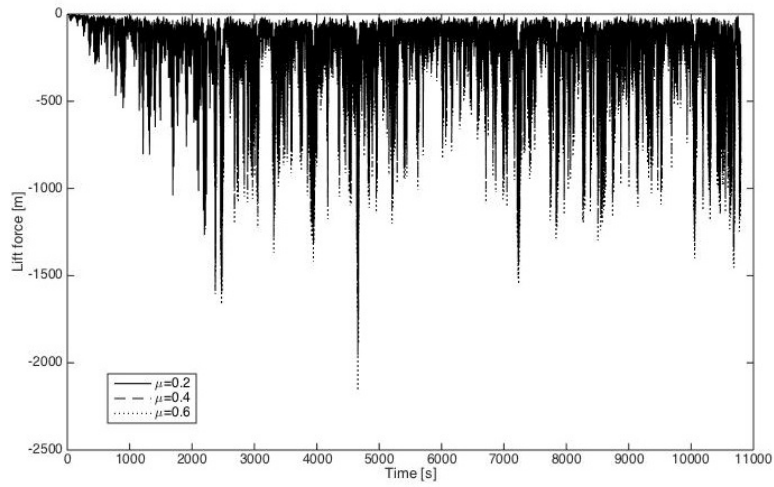


Figure 4.11: Lift force by time at node 51 of pipe-clay model with different friction coefficients

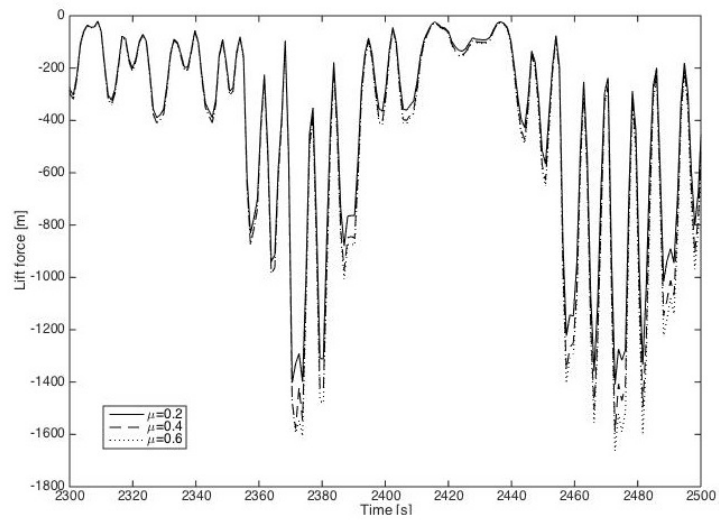


Figure 4.12: Lift force by time at node 51 of pipe-clay model with different friction coefficients in 2300s-2500s

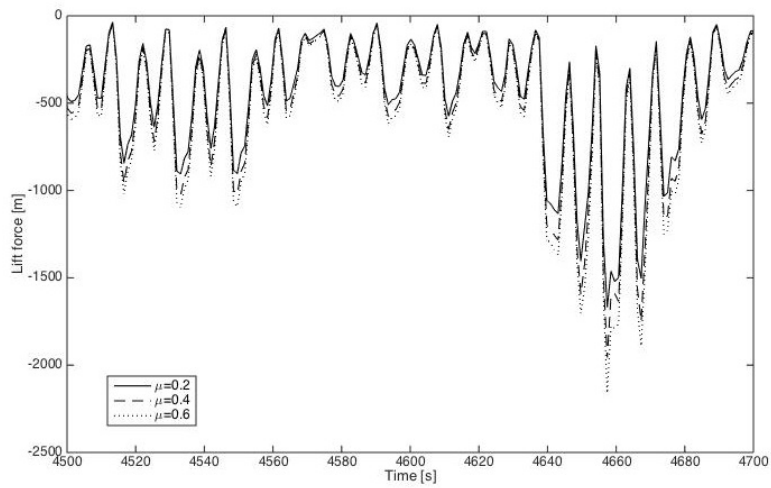


Figure 4.13: Lift force by time at node 51 of pipe-clay model with different friction coefficients in 4500s-4700s

Relative velocity

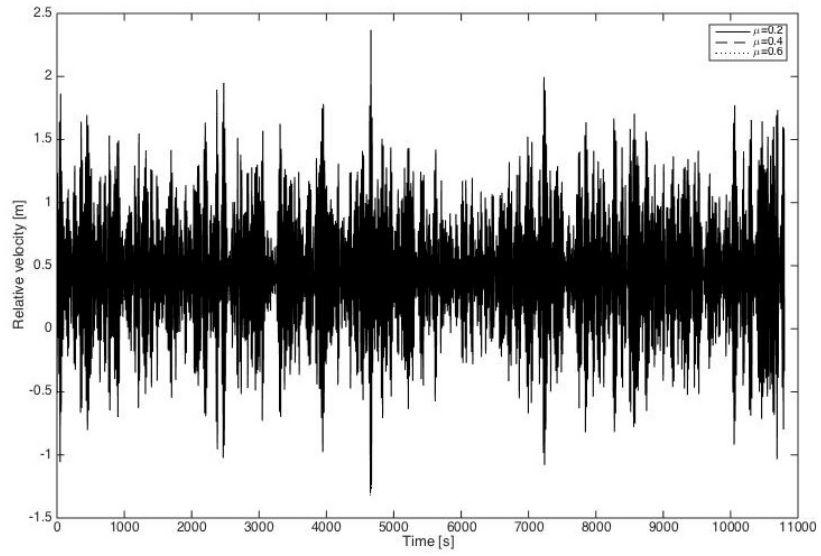


Figure 4.14: Relative velocity by time at node 51 of pipe-clay model with different friction coefficients

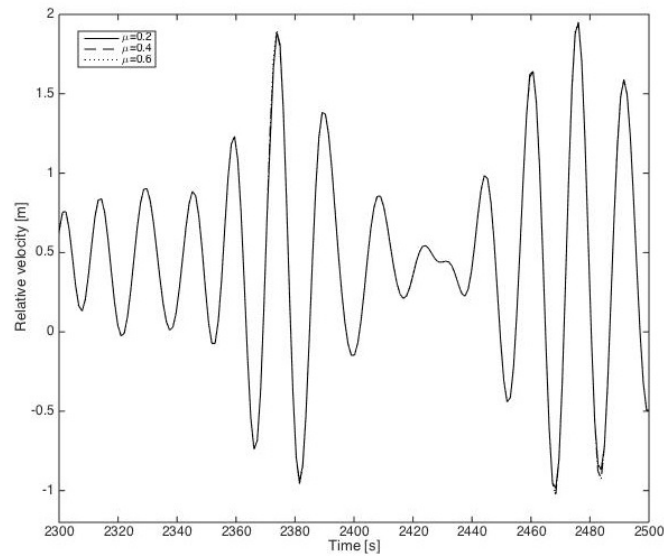


Figure 4.15: Relative velocity by time at node 51 of pipe-clay model with different friction coefficients in 2300s-2500s

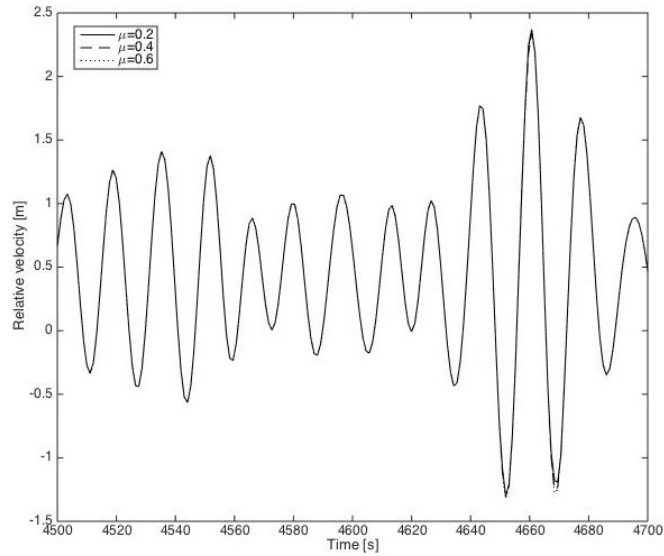


Figure 4.16: Relative velocity by time at node 51 of pipe-clay model with different friction coefficients in 4500s-4700s

Soil resistance force

According to figure 4.17, the soil resistance force for each case oscillates with very small deviations, except for one period namely from approximately 4500s to 7500s. As the oscillation waves for $\mu = 0.2$ stays in the middle of the other two, it indicates that this case tends to have a more stable development. It should also be noticed that the peak points are located at the same time steps for each case as well. Referring to figure 4.4 and figure 4.7, the shift of magnitudes further confirms that the neutral position of displacement is changing and the development of force-displacement appears to develop with the same pattern shown in figure 4.7.

Moreover, the penetration is also related to the accumulated displacement of pipeline which is reduced for large friction coefficient.

The simulation results for the soil resistance force are presented as follows.

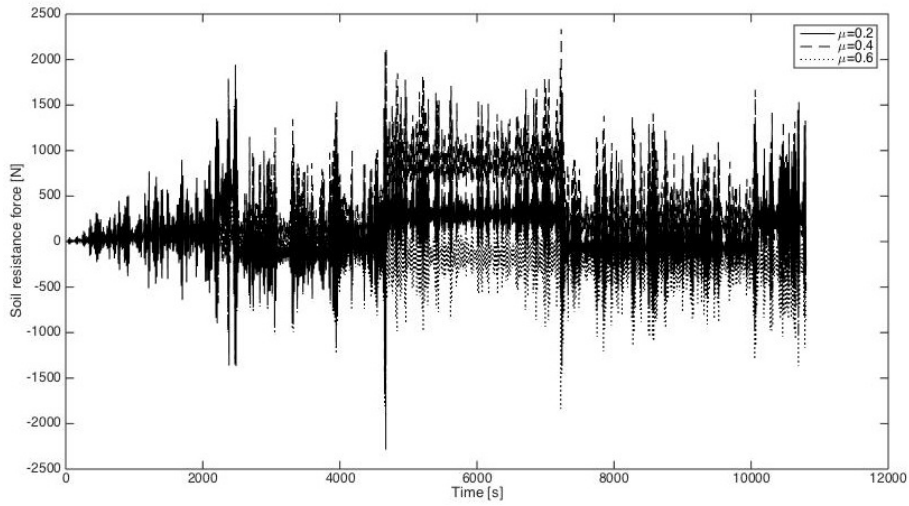


Figure 4.17: Soil resistance force by time at node 51 of pipe-clay model with different friction coefficients

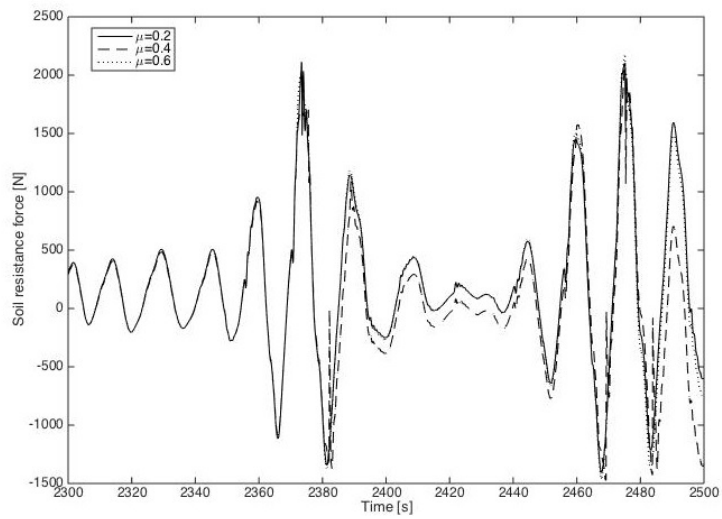


Figure 4.18: Soil resistance force by time at node 51 of pipe-clay model with different friction coefficients in 2300s.2500s

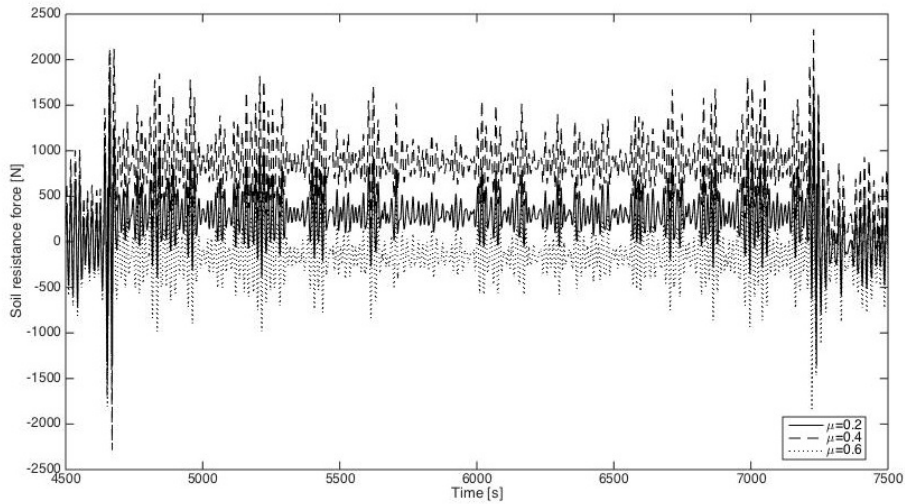


Figure 4.19: Soil resistance force by time at node 51 of pipe-clay model with different friction coefficients in 4500s-7500s

Relative penetration

The relative penetration climbs in a stair-like manner as shown in figure 4.20, and this indicates that the relative penetration is not stable for any cases.

Referring to figure 4.4, figure 4.5 and figure 4.6, with the same relative penetration, the smaller the friction is, the earlier the pipe starts to move with a larger magnitude. Although from 4500s where the penetration of the three cases deviates largely from each other, the development of nodal displacement does not correspond explicitly to the different friction coefficients. However, the relative penetration still increases as the friction coefficient decreases when considering the accumulated displacement in figure 4.3.

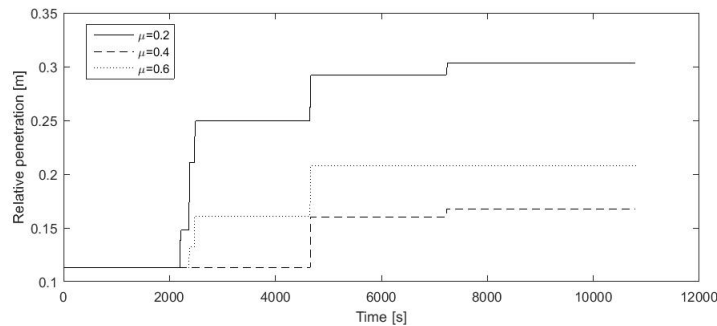


Figure 4.20: Relative penetration by time at node 51 of pipe-clay model with different friction coefficients

4.1.2 Pipe-sand model

Material and environment data listed below is for the pipe under combined load of 10 year currents and 100 year return irregular waves with pipe-sand model.

Steel yielding stress	415	MPa
Sand density	1863.	kg/m ³
Elastic Stiffness	65000	N/m ²
Depth	104	m
Current	0.374	m/s
Peak period	14.5	s
Significant wave height	12.5	m
Simulation time	3	hours
Time increment	0.01	s(1080000 time steps)

Table 4.4: Pipe and environment property for the pipe-sand model

Same as in subsection 4.1.1, a default value for the initial embedment $Z_{R0} = Z_{penetr}/D$ is calculated by the program. The submerged pipe weight W_{sub} , lift force F_L and vertical soil contact force $F_v = W_{sub} - F_L$ is calculated automatically based on the material and environment data given in prior input. The submerged unit weight of sand $\gamma_s = (\rho_s - \rho_w)g$ is calculated to be $8203N$.

Displacement

As it shows from 4.21, the displacement decreases as the the friction coefficient increases. Moreover, it becomes relatively stable after a steep increment from node 20. Based on the development of the displacement curves, node 15, node 30 and node 32 is selected to be the significant node for $\mu = 0.6, \mu = 0.4$ and $\mu = 0.8$. The drastic vibrations occurs at the same steps despite of different friction coefficients. The significant time intervals 2300s-2500s and 4600-4700s will be looked into respectively.

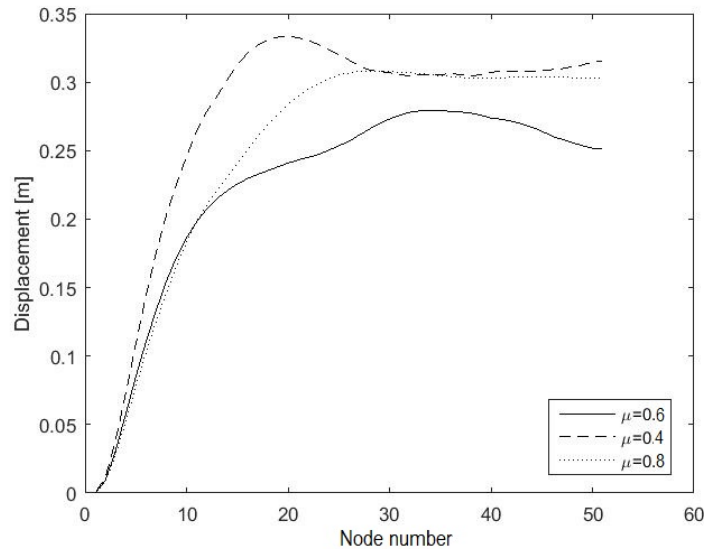


Figure 4.21: Displacement by length of pipe-sand model with different friction coefficients

As shown in figure 4.22, the displacement for each case oscillates with overlapped amp-

litudes approximately in the first 2200s. While it starts to deviate from each other until about 4700s. The waves for $\mu = 0.4$ and $\mu = 0.8$ begin to oscillate at amplitudes of very small deviation. Moreover, the oscillation waves with $\mu = 0.6$ has the smallest gradient comparing to the two others, which suggests that the displacement tends to have a rather stable development with the default value for the friction coefficient in PONDUS. According to figure 4.22, there is a very drastic change of amplitudes along the two important intervals namely 2300s-2500s and 4600-4700s.

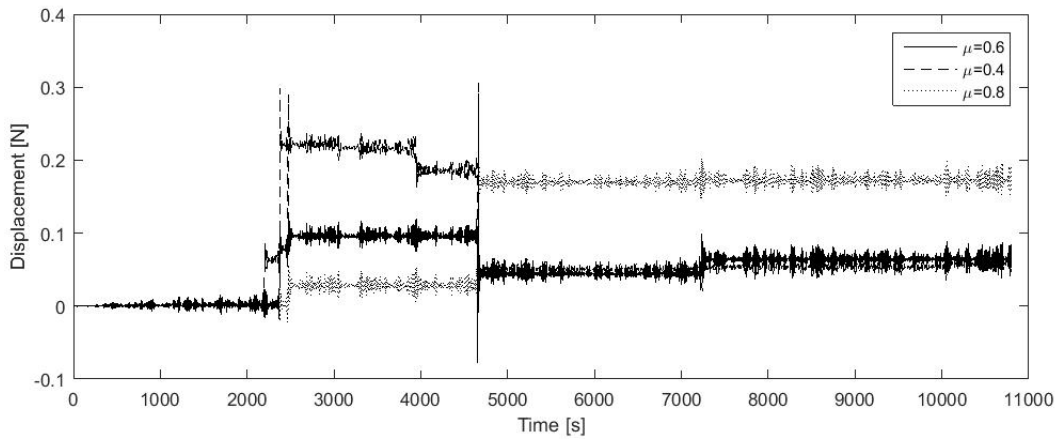


Figure 4.22: Displacement by time at significant nodes for pipe-sand model with different friction coefficients

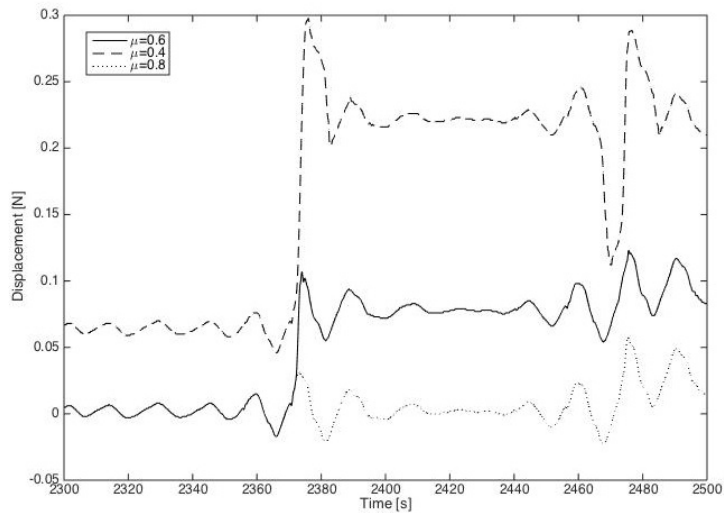


Figure 4.23: Displacement by time at significant nodes for pipe-sand model with different friction coefficients in 2300s-2500s

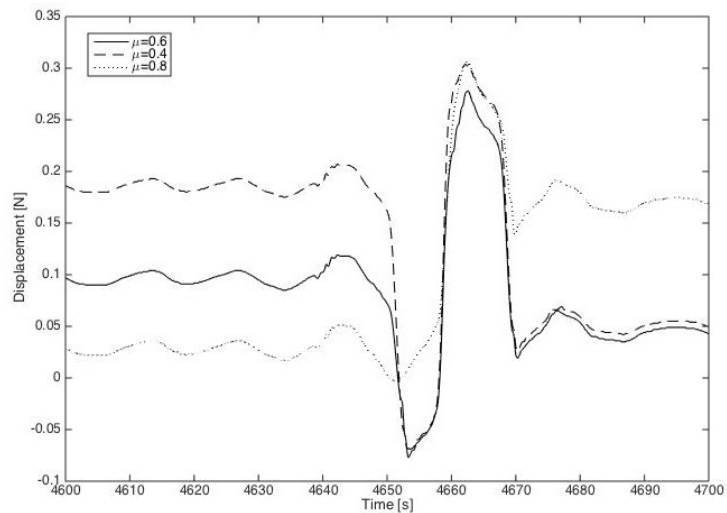


Figure 4.24: Displacement by time at significant nodes for pipe-sand model with different friction coefficients in 4600s-4700s

The maximum displacement shows very different magnitudes, and it increases as the value of friction coefficient decreases. the related hydrodynamic forces will be further looked into accordingly.

Hydrodynamic force

Referring to figures 4.25 to 4.30, the drastic change of magnitude for the hydrodynamic force and lift force occurs at the same time steps as it is for displacement. Same as it is for the pipe-clay model, both the relative drag and inertia force in the horizontal direction and the lift force in vertical direction are proportional to the effective/relative velocity. It indicates also that this node is experiencing a significant large wave at those time intervals that generates the corresponding increase of the horizontal and vertical forces, which further leads to the drastic increase of magnitude for the nodal displacement. The effective velocity will therefore consequentially demonstrate the same drastic change of magnitude as shown in figure 4.31 to figure 4.34.

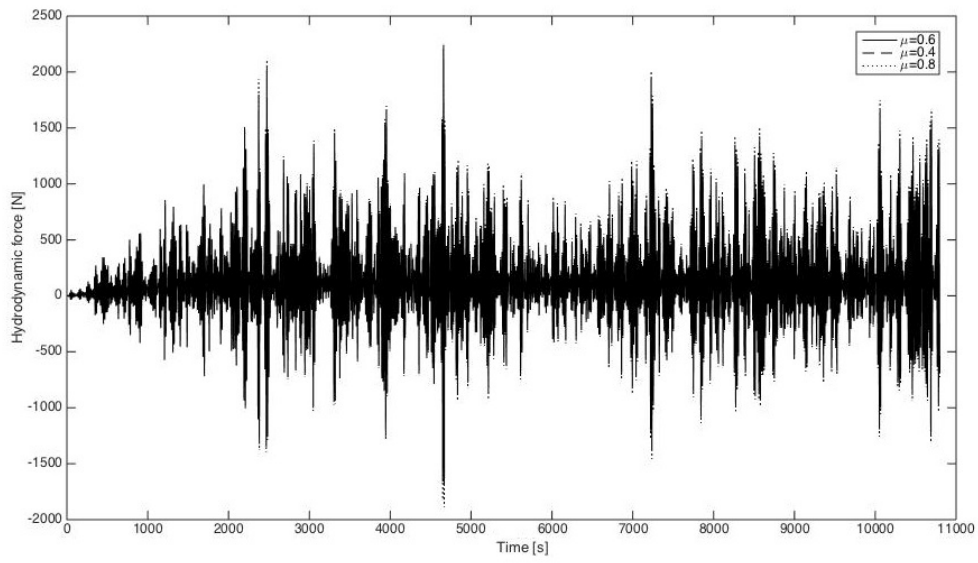


Figure 4.25: Hydrodynamic force by time at significant nodes of pipe-sand model with different friction coefficients

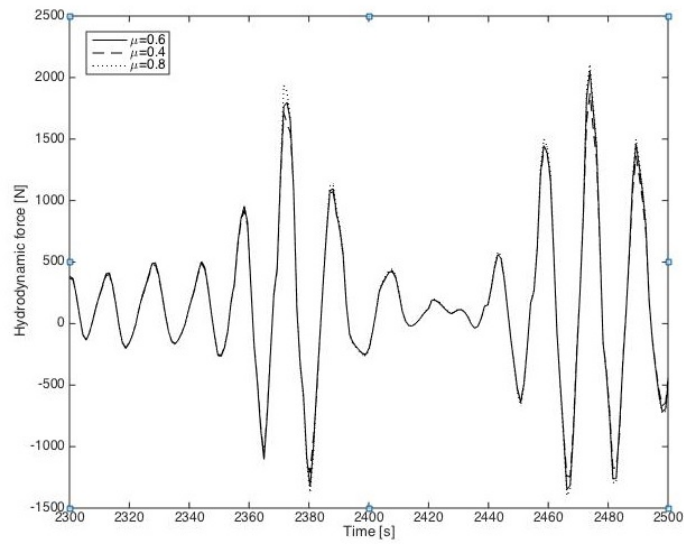


Figure 4.26: Hydrodynamic force by time at significant nodes of pipe-sand model with different friction coefficients in 2450s-2500s

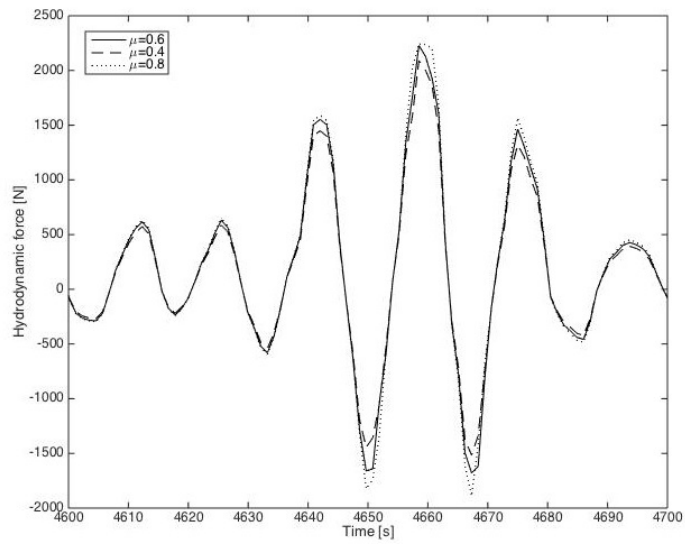


Figure 4.27: Hydrodynamic force by time at significant nodes of pipe-sand model with different friction coefficients in 4600s-4700s

Lift force

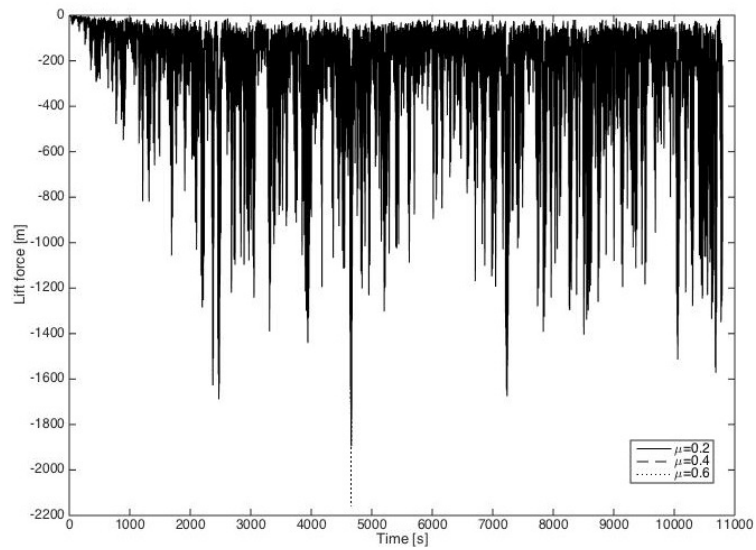


Figure 4.28: Lift force by time at significant nodes of pipe-sand model with different friction coefficients

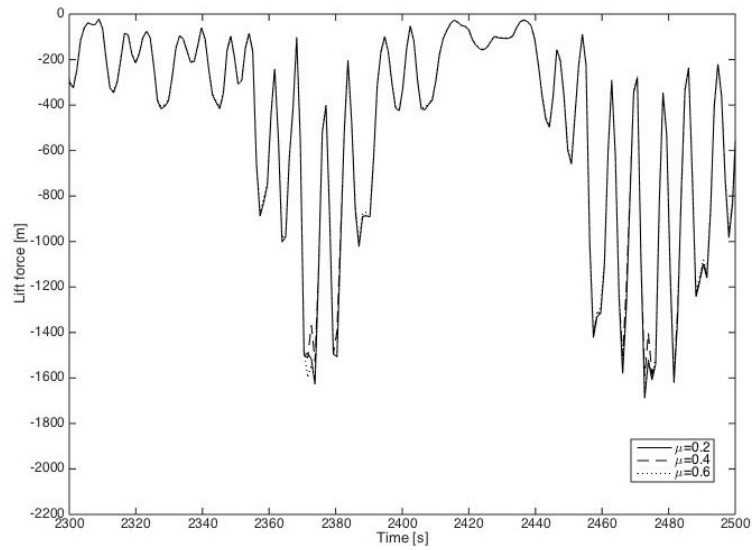


Figure 4.29: Lift force by time at significant nodes of pipe-sand model with different friction coefficients in 2300s-2500s

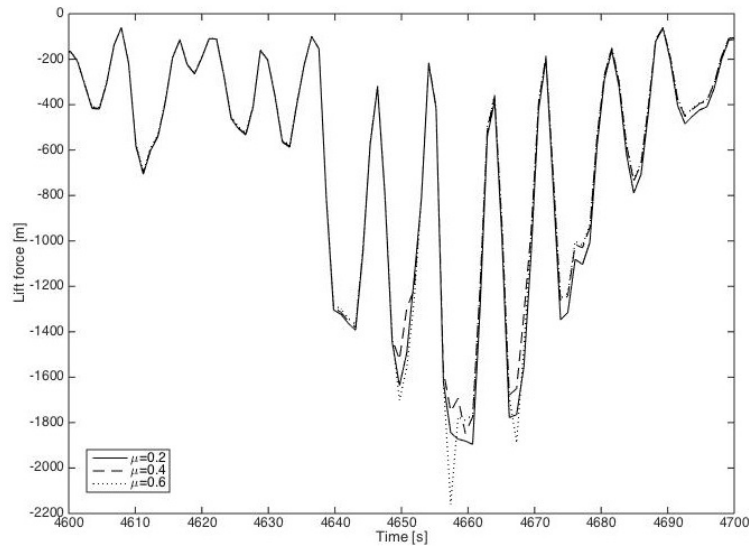


Figure 4.30: Lift force by time at significant nodes of pipe-sand model with different friction coefficients in 4600s-4700s

Relative velocity

The relative velocity between water particle and pipeline is different at time instance when pipeline has significant movement as shown in the following figures.

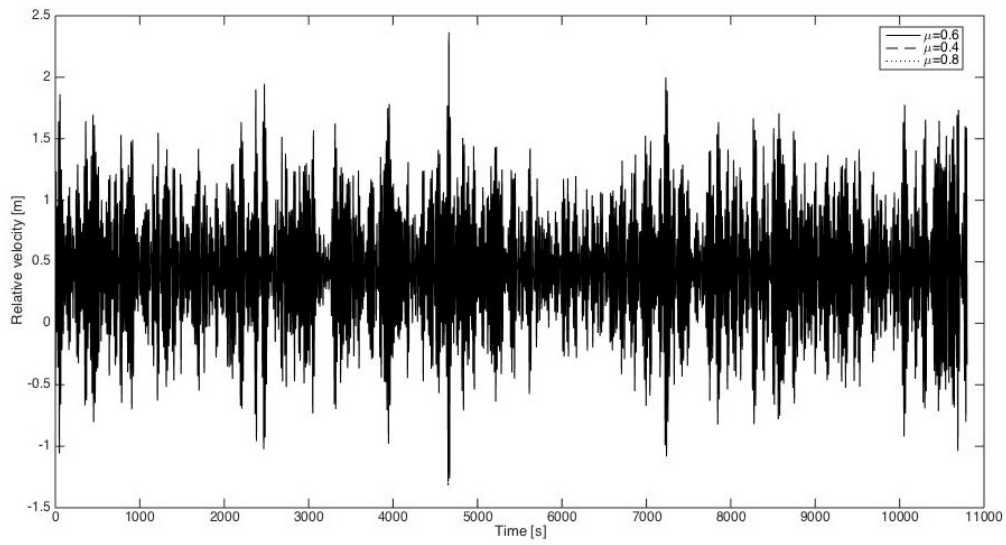


Figure 4.31: Relative velocity by time at significant nodes of pipe-sand model with different friction coefficients

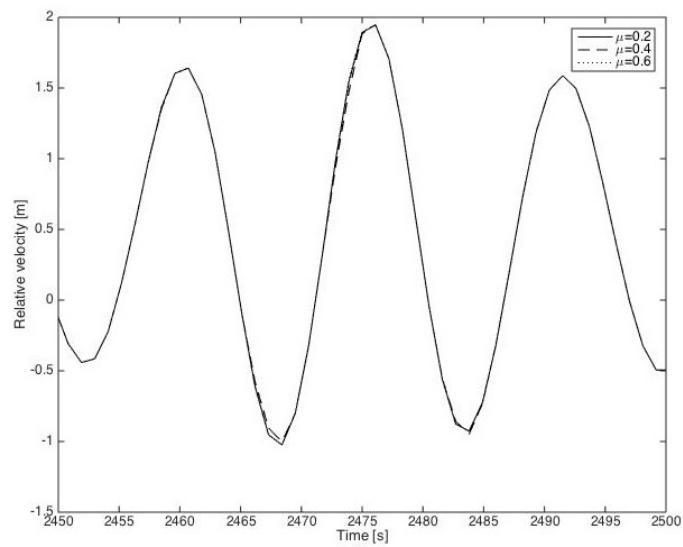


Figure 4.32: Relative velocity by time at significant nodes of pipe-sand model with different friction coefficients in 2300s-2500s

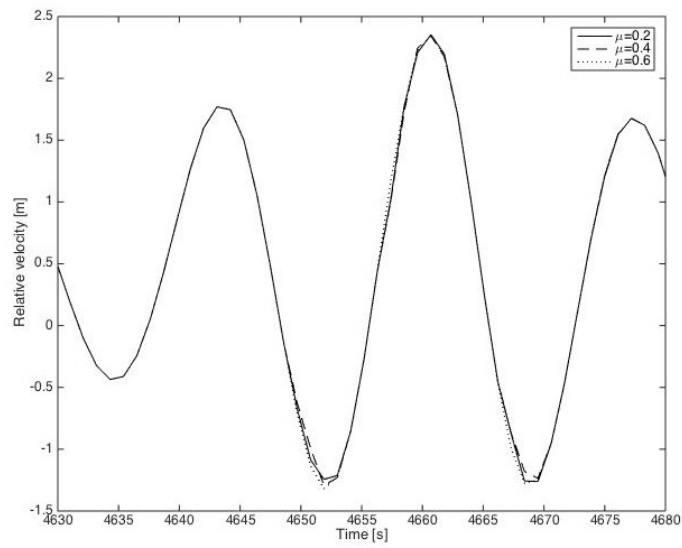


Figure 4.33: Relative velocity by time at significant nodes of pipe-sand model with different friction coefficients in 4600s-4700s

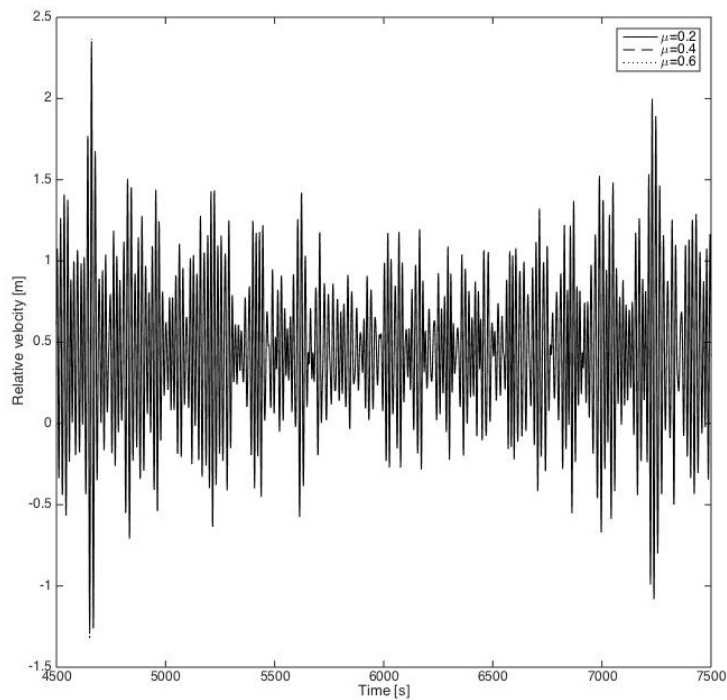


Figure 4.34: Relative velocity by time at significant nodes of pipe-sand model with different friction coefficients in 4500s-7500s

Based on equation 4.5, and equation 3.9, the friction force, relative velocity between pipe and water particle and penetration will interact with each other. As the friction coefficient directly affects the soil resistance force, there will be changes at the initial time when the pipeline starts to move in the lateral direction, and the time history of displacement of pipeline is changed for different friction coefficients. The penetration is related to the accumulated displacement of the pipeline as well. The larger the soil friction coefficient

is, the smaller the displacement of the pipeline will be, as the pipeline penetrates the soil deeper and creates a kind of soil berm. The accumulated displacement is defined as the sum of displacement from neutral position. The neutral position is varying by time as shown in figure 4.7.

Soil resistance force

As shown in figure 4.35, the oscillation waves for $\mu = 0.6$ stays in the middle of the other two, it indicates that this case tends to have a more stable development. Referring to figure 4.35 to figure 4.37 and figure 4.7, the constant shift of magnitudes for the soil resistance force further confirms that the neutral position of displacement is changing and the development of force-displacement appears to be constantly cycling with the pattern shown in figure 4.7.

Moreover, the penetration is related to the accumulated displacement of pipeline as well. The larger the soil friction coefficient is, the smaller the displacement of the pipeline will be, as the pipeline penetrates the soil deeper and creates a kind of soil berm.

The simulation results for the soil resistance force are presented as follows.

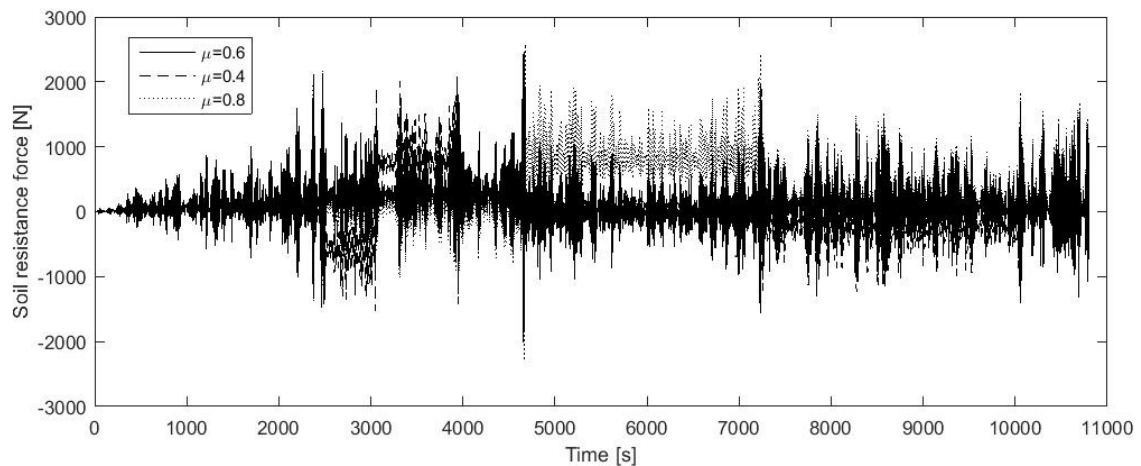


Figure 4.35: Soil resistance force by time at significant nodes for pipe-sand model with different friction coefficients

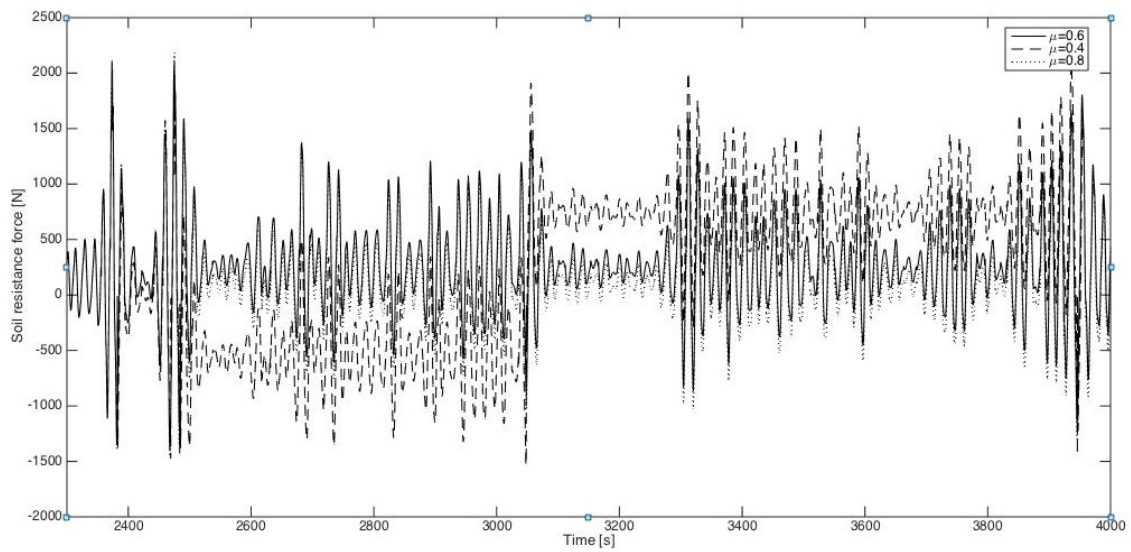


Figure 4.36: Soil resistance force by time at significant nodes for pipe-sand model with different friction coefficients in 2350s-2500s

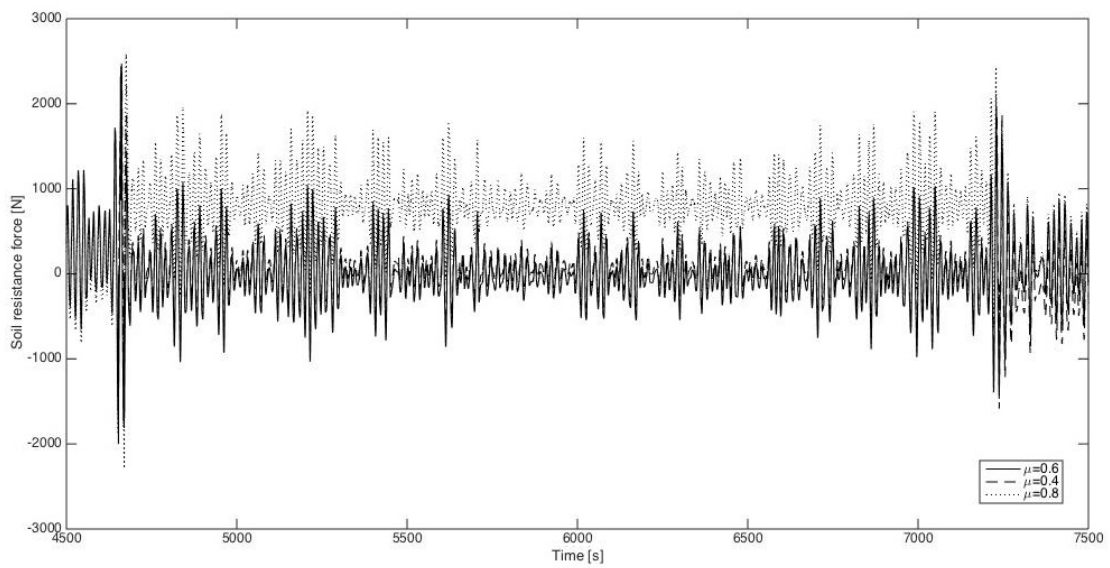


Figure 4.37: Soil resistance force by time at significant nodes for pipe-sand model with different friction coefficients n 4500s-7500s

Relative penetration

The relative penetration is not stable in this case with any friction coefficient, it suggests also that the relative penetration climbs in a stair-like manner as shown in figure 4.20.

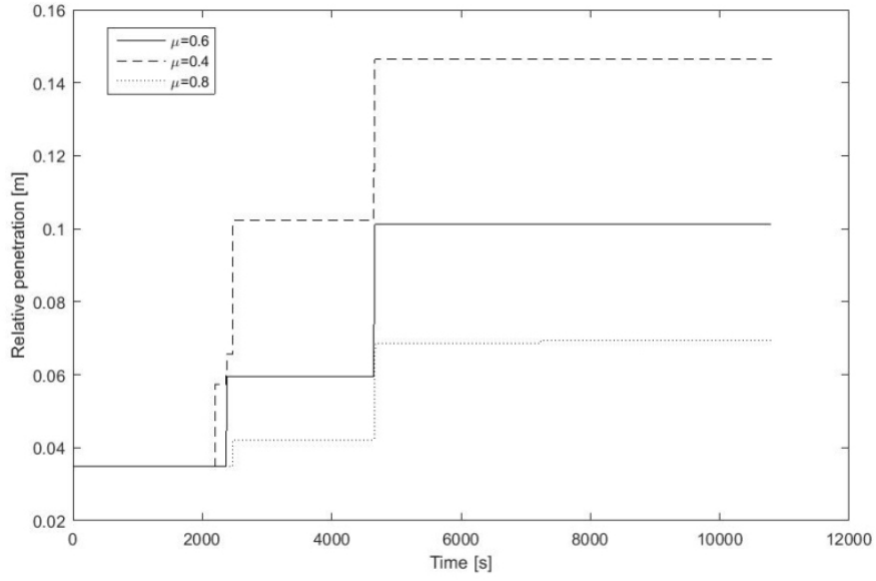


Figure 4.38: Relative penetration by time at significant nodes for pipe-sand model with different friction coefficients

4.2 Summary for pipe-soil interaction with uniform soil types

Table 4.5 is created based on PONDUS output results and presents the characteristic values for the single-modelled pipe-soil interaction with different friction coefficients.

Case no.	Case description	Max.displacement [m]		Max.soil resistance force [N]	Max.relative penetration [m]
		$\mu = 0.2$	$\mu = 0.4$		
1	Pipe-clay model	$\mu = 0.2$	0.25	1600	0.30
		$\mu = 0.4$	0.24	1650	0.16
		$\mu = 0.6$	0.17	1700	0.21
2	Pipe-sand model	$\mu = 0.6$	0.28	2300	0.11
		$\mu = 0.4$	0.34	2500	0.15
		$\mu = 0.8$	0.31	2400	0.07

Table 4.5: Summary of characteristic values for the single-modeled pipe-soil interaction with different friction coefficients

It should be noted that the significant time intervals(2300s-2500s and 4600-4700s) are the same for all iterations in Case 2.1 and Case 2.2. This is possibly due to the same environmental condition is applied, which gives the pipeline one particular pattern of nodal behaviour.

According to figures 4.3 to 4.38 and table 4.5, which are expressed based on equation 4.8 to 4.15 for the pipe-clay model, the maximum displacement seems to decrease as the friction coefficient increases. The friction coefficient and the relative velocity between the pipe and the water particles, and the penetration will interact with each other. While for

the pipe-sand model, the different friction coefficients do not seem to affect the displacement in the same way as it is for the pipe-clay model. This is likely due to the varying residual force F_{r3} described in figure 4.1, which interacts differently and further leads to a different interaction between the soil resistance force, the relative penetration and the displacement. It appears that the displacement and friction coefficient does not interact with each other in any explicit pattern. But in general, the penetration and accumulated displacement tends to grow larger as the friction coefficient decreases.

It appears that there are few shared features for both the pipe-clay and pipe-sand model:

- The friction coefficient will affect the soil resistance force, and further changes the initial time when the pipe line starts to move in lateral direction. The time history of displacement for the pipeline is changed for different friction coefficients.
- The relative velocity between water particle and pipeline is different at time instance when pipeline has significant movement
- The penetration is related to the accumulated displacement of pipeline which is reduced for large friction coefficient.
- The penetration and accumulated displacement tends to grow larger as the friction coefficient decreases.

The simulation results for both clay and sand soil further prove that the soil reaction is a non-linear behaviour, and the relative penetration contributes in a non-linear way to the stability of the pipe by inducing a trench-like surrounding under the pipe, which reduces the movement of the pipe and diffuses the soil resistance force to shear forces along the circumference of the trench. As sand soil is more stiff and less permeable than clay soil, the penetration depth is subsequently larger for the pipe-clay model than it is for the pipe-sand soil.

Considering the length of a pipeline and the complicity of the seabed environment in practice, a combined soil model with multiple soil types in different sequence will be simulated in the following section.

4.3 Pipe-soil interaction with multiple soil types

4.3.1 Mixed soil types of 50% sand and 50% clay

With the same material and environment data as presented in table 4.1, a simulation is conducted with the soil distribution sectioned by 50%-50% under the pipe.

The soil distribution is defined as in figure 4.39. The pipe and environment data are given in table 4.6.

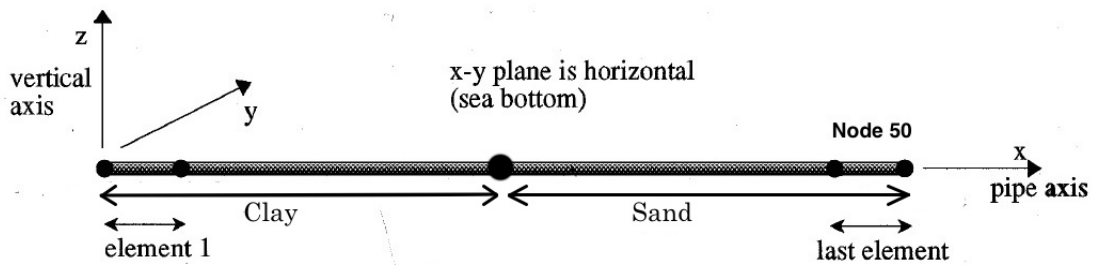


Figure 4.39: Soil distribution of the pipe with 50%sand-50%clay model

Pipe and soil data		
Friction coefficient for sand soil, μ	0.6	-
Friction coefficient for clay soil, μ	0.2	-
Int. diameter of pipe, D_{in}	571.8	mm
Concrete coating, t_{con}	55	mm
Wall thickness, t_{wall}	19.1	mm
Corrosion allowance, t_{cal}	1.5	mm
Corrosion coating, t_{cc}	5	mm
Marine growth, t_{mg}	0	m
Pipe roughness, k/D	0.001	-
Significant wave height, H_s	14.8	m
Significant wave period, T_p	15.9	s
Current velocity, U_0	0.51	m/s

Table 4.6: Pipe and environment data for the pipeline with mixed soil types under combined load of 10-year return currents and 100-year return irregular waves

Displacement

As it shows in figure 4.40, the maximum displacement is 0.24m for the sand section and 0.33m for the clay section. The global maximum displacement is therefore located in the clay section. It should also be noted that transitional node 26, where the soil type is changed from sand to clay, the increment of the displacement is very steep while it develops rather mildly within the single-modelled sections.

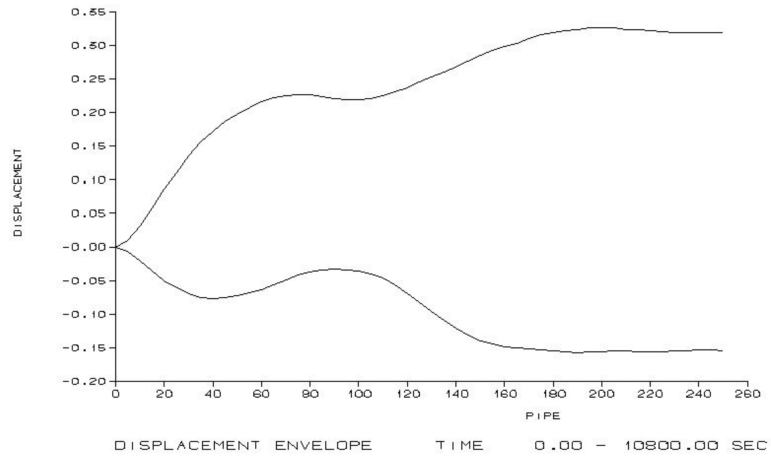


Figure 4.40: Displacement by length of the pipe with 50% sand-50% clay model

Soil resistance force

The soil resistance force oscillates with maximum amplitudes at 1700N and 2600N for the sand section and clay section respectively, which corresponds with the smaller displacement in the sand section and the larger displacement for clay section.

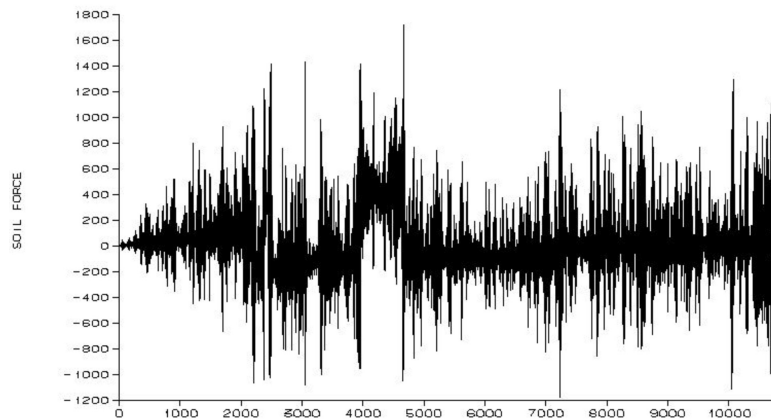


Figure 4.41: Soil force at node 26 by time of the pipe with 50% sand-50% clay model

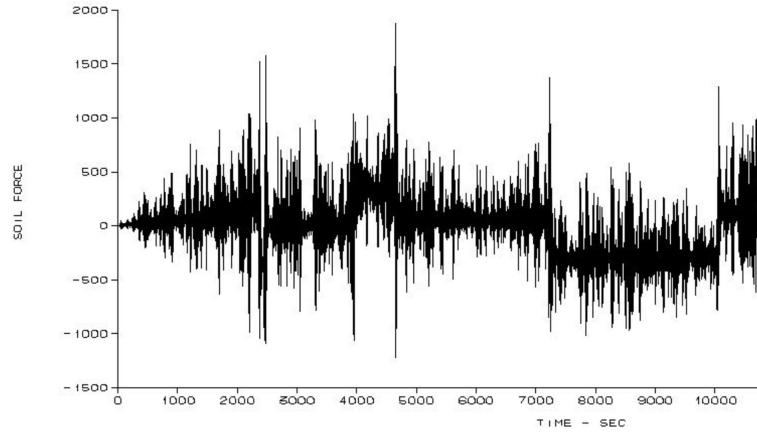


Figure 4.42: Soil force at node 40 by time of the pipe with 50% sand-50% clay model

Relative penetration

Based on the location of the occurrence for the maximum displacement, the investigation of the relative penetration will be started from node 7 instead of node 8. This is to create a better context for the variation of the relative penetration along the pipe.

As it is shown in figure 4.43, the relative penetrations are not stable in both sections and develop in a stair-like way. Moreover, the maximum relative penetration in the sand section is smaller than the one in the clay section. This difference along with the different displacement for clay/sand sections will be discussed further in the end of this section.

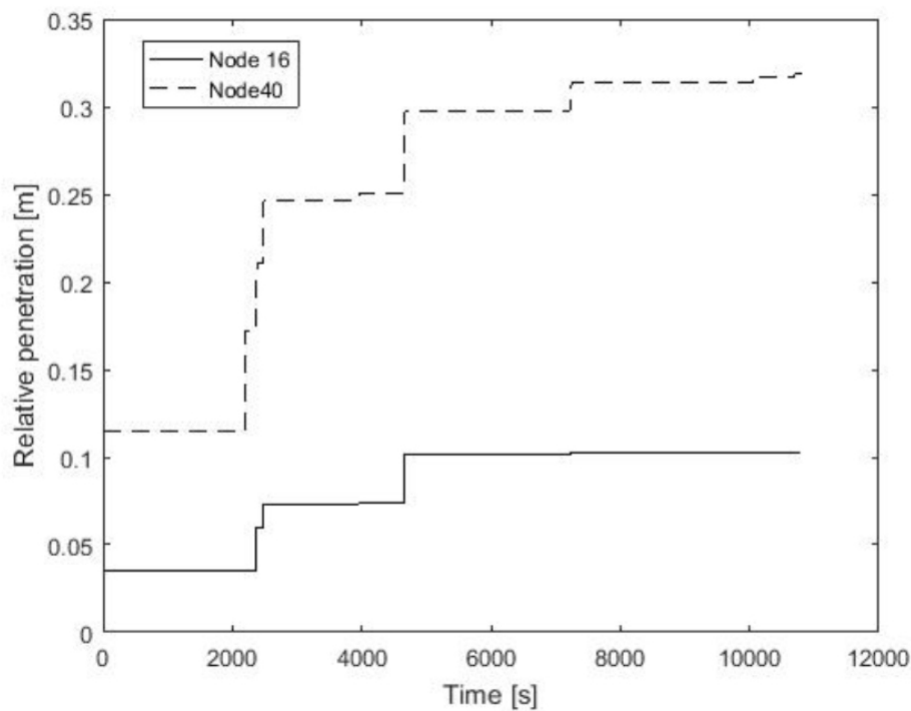


Figure 4.43: Relative penetration at node 26 and node 40 by time of the pipe with 50% sand-50% clay model

4.3.2 Mixed soil-types case

A complex-soil model is referred to a tri-sectional soil model in this study. However it can be interpreted as any pipe-soil model with more than three sections of different soil types.

With the same material and environment data as presented in table 4.1, a simulation is conducted with the soil distribution sectioned by 30% sand-40% clay-30% sand and 30% clay-40% sand-30% clay under the pipe as shown in figure 4.44 and figure 4.45 respectively. Those two models will be referred as S30C40S30 and C30S40C30. The transition of soil type occurs at node 16 (80m) and node 36 (180m). The pipe and material data are shown in table 4.7

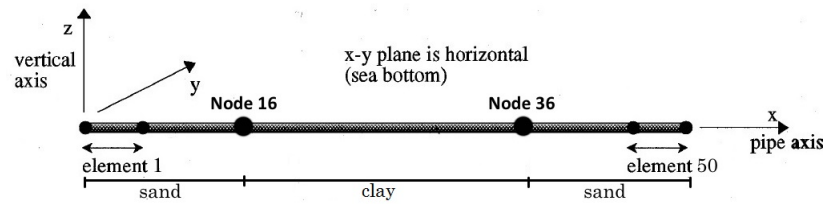


Figure 4.44: Pipe-soil model S30C40S30 with 30% sand-40% clay-30% sand

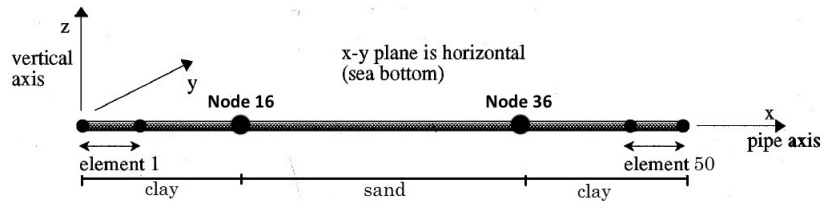


Figure 4.45: Pipe-soil model C30S40C30 with 30% clay-40% sand-30% clay

Pipe and soil data	
Friction coefficient for sand soil, μ	0.6 -
Friction coefficient for clay soil, μ	0.2 -
Int. diameter of pipe, D_{in}	571.8 mm
Concrete coating, t_{con}	55 mm
Wall thickness, t_{wall}	19.1 mm
Corrosion allowance, t_{cal}	1.5 mm
Corrosion coating, t_{cc}	5 mm
Marine growth, t_{mg}	0 m
Pipe roughness, k/D	0.001 -
Significant wave height, H_s	14.8 m
Significant wave period, T_p	15.9 s
Current velocity, U_0	0.51 m/s

Table 4.7: Pipe and environment data for the pipeline with mixed soil types under combined load of 10-year return currents and 100-year return irregular waves

Displacement

As it shows in figure 4.46, the maximum displacement at node 5 for S30C40S30, while the clay section in C30S40C30 is subjected to a maximum displacement at a relatively constant value. Moreover, the displacement develops in a rather symmetric manner for C30S40C30. Based on the location of the sectional maximum displacement, node 8, node 18 and node 51 will be considered as significant nodes, where more detailed nodal results regarding transient displacement and forces will be studied and discussed.

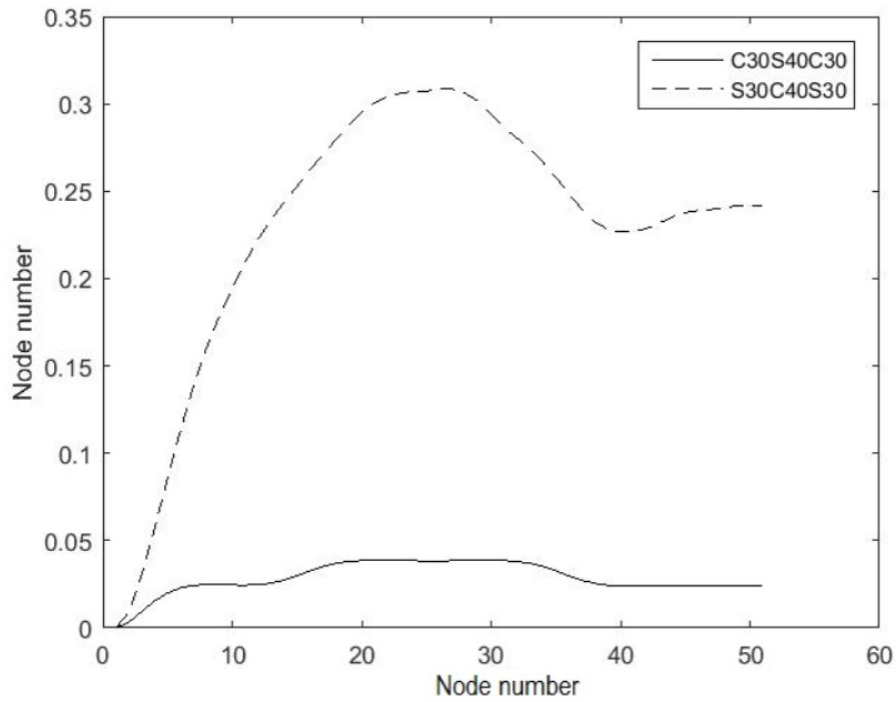


Figure 4.46: Displacement by length of the pipe with tri-sectional model

The nodal displacements for node 8, node 18 and node 51 are presented in figure 4.47-4.49. These nodal results shows explicitly that the pipe tends to have a quite stable oscillatory movement at a stable and constant amplitude of displacement for C30S40C30.

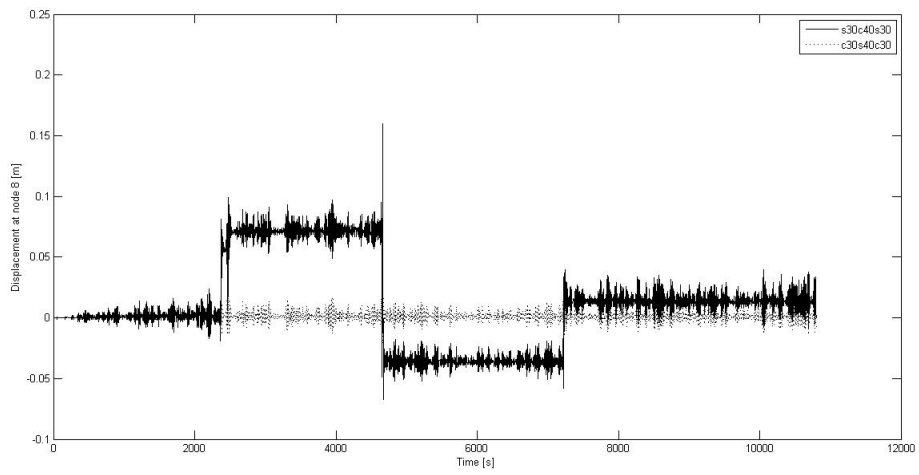


Figure 4.47: Displacement at node 8 by time of the pipe with tri-sectional model

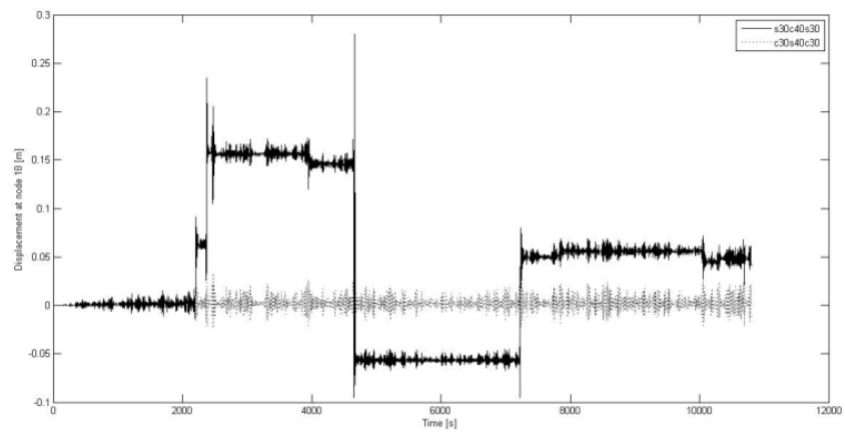


Figure 4.48: Displacement at node 18 by time of the pipe with tri-sectional model

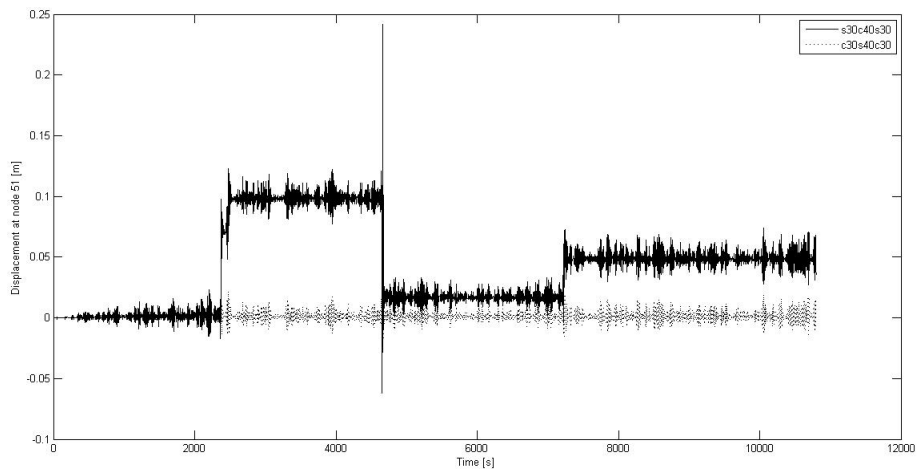


Figure 4.49: Displacement at the node 51 by time of the pipe with tri-sectional model

Soil resistance force

According to figure 4.50 to figure 4.52, the soil resistance force for S30C40S30 seems to be larger in average at node 18, where displacement approaches the maximum for both cases. This is likely caused by the global maximum displacement is larger for S39C40S30 than it is for C30S40C30, and further indicates a positive correlation between the displacement and soil resistance force in this case.

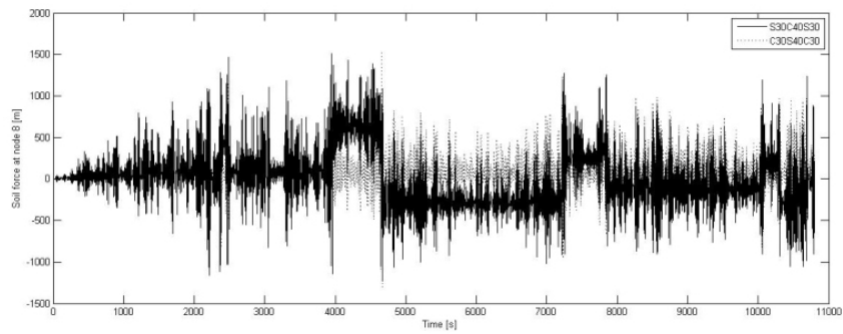


Figure 4.50: Soil force at node 8 by time of the pipe with tri-sectional model

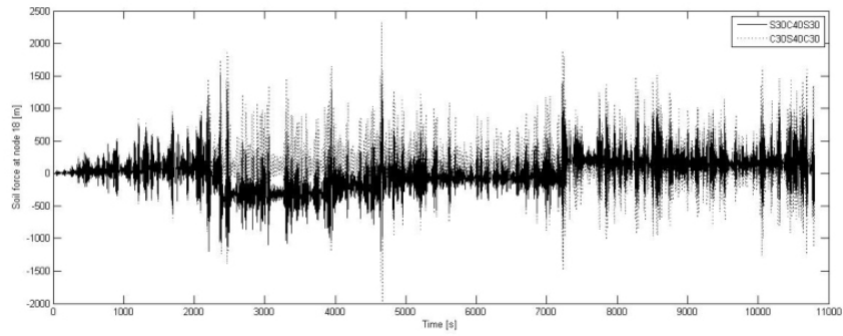


Figure 4.51: Soil force at node 18 by time of the pipe with tri-sectional model

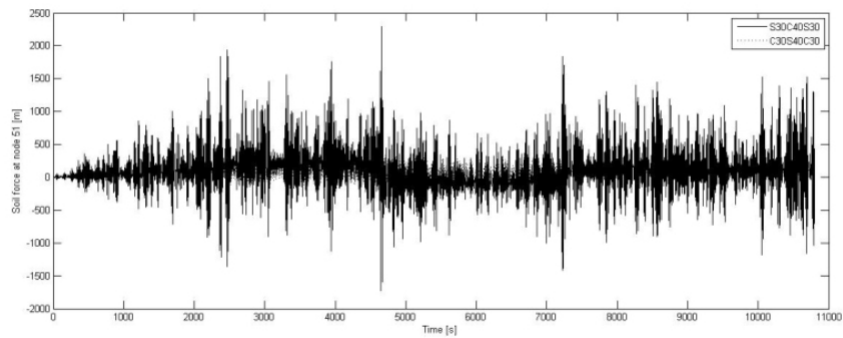


Figure 4.52: Soil force at node 51 by time of the pipe with tri-sectional model

Relative penetration

With the same procedures as in the previous section, the investigation of the relative penetration will be conducted at the significant nodes as in node 8, node 18 and node 51.

According to figure 4.53-4.55. the relative penetration develops with exactly the same pattern for node 8 and node 51, which are characteristic nodes for the initial and end section. While for node 18 where the displacement is approaching its maximum value for each case, the relative penetration for C30S40C30 remains constant while it still appears to be instable by climbing stair-likely for S30C40S30. This is likely due to the higher soil strength in the sand-section which provides larger resistance against the pipe to sink.

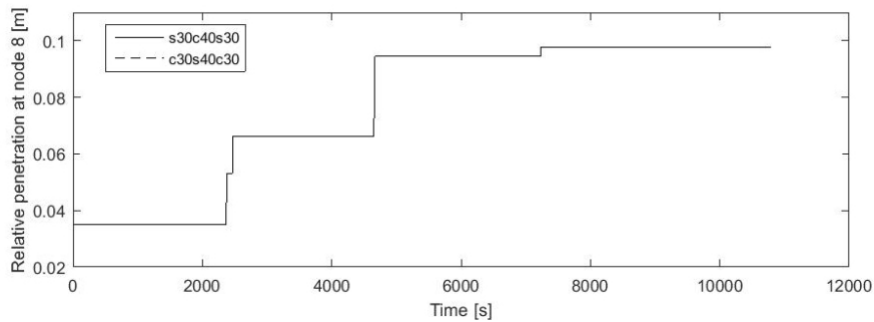


Figure 4.53: Relative penetration at node 8 by time of the pipe with tri-sectional model

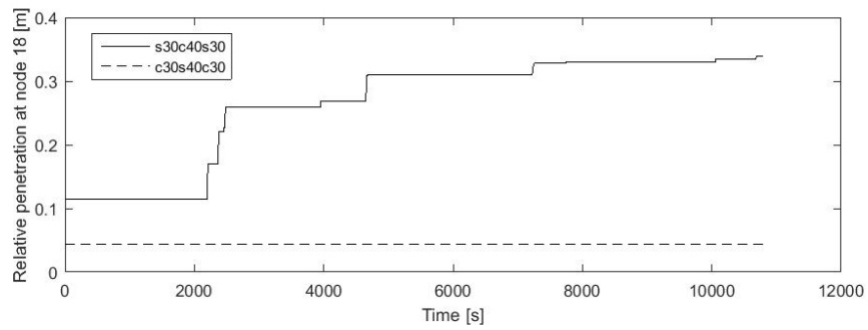


Figure 4.54: Relative penetration at node 18 by time of the pipe with tri-sectional model

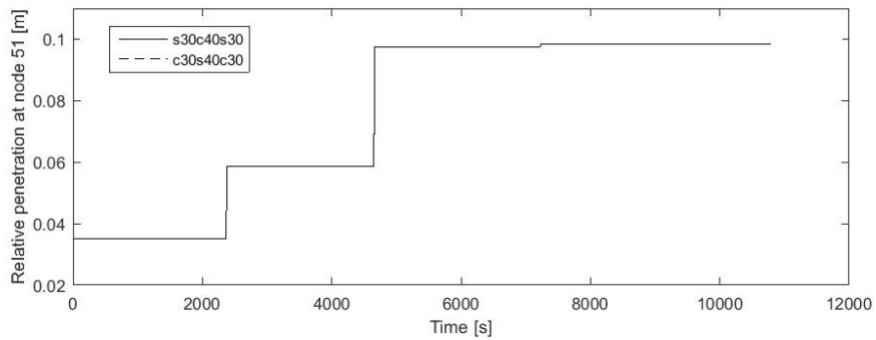


Figure 4.55: Relative penetration at node 51 by time of the pipe with tri-sectional model

It should be noticed that at node 8 and node 51, the developments of the relative penetration depth for S30C40S30 and C30S40C30 are the same.

4.4 Summary for pipe-soil interaction with multiple soil types

The relative penetration at node 51 by time of the pipe with tri-sectional model in figure 4.56 is made based on figure 4.40 and figure 4.46.

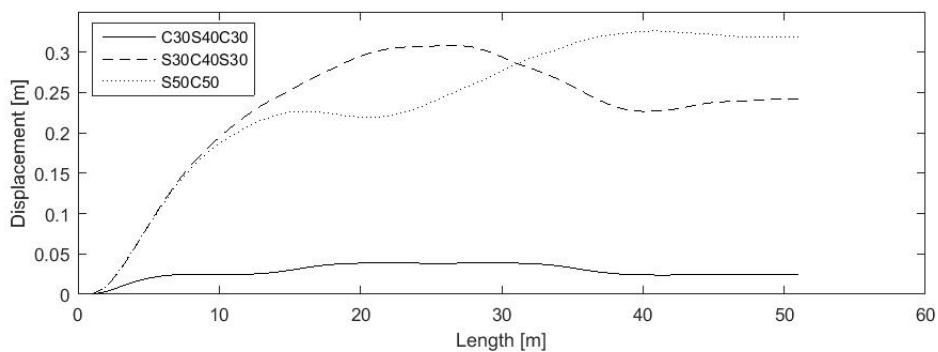


Figure 4.56: Relative penetration at node 51 by time of the pipe with tri-sectional model

It indicates that the movement of pipe tends to have significant increase when there is sand under the end node or the end section. Moreover, figure 4.40 to 4.55 with the com-

plex soil environments shows that when sand is the dominant soil type, the maximum displacement tends to remain the same for any soil combinations. However when the percentage of clay increases, the maximum displacement will be reduced considerably, not only for the whole pipe but for the local sections as well. Furthermore, nodal displacement, soil force and relative penetration appears to be quite stable and oscillates with a constant amplitude in C30S40C30. This is probably due to the relatively small movement at the end nodes as the clay soil provides a trench-like environment and therefore more resistance against and movement in the surroundings. It makes the end nodes kept in a fixed boundary condition.

These results indicate that the maximum displacement is mostly dependent on the soil type at end nodes, and when there is clay under the both ends of the pipe, the maximum displacement will be reduced substantially.

5 Comparison on different procedures

As the on-bottom stability is a highly non-linear phenomenon, it is important to consider waves with large periods and large values of current to wave ratios. A real sea state is likely to experience storms and thus it is more critical to maintain the on-bottom stability during storm.

Apart from the hydrodynamic environment, the pip-soil interaction will also have major impacts on the on-bottom stability. The passive resistance force depends on the soil penetration depth of the pipe, soil types such as stiff clay or rock will present more critical environments for the on-bottom stability, as they provide less pronounced soil penetration capacity. The simulation with different soil properties are described in Chapter 4. The initial penetration is also an important parameter for the on-bottom stability. Therefore it is important to find the stabilized penetration depth for the pre-storm situation.

3 approaches will be compared in this study.

1. Standard 3-hour simulation procedure with default initial penetration calculated by PONDUS
2. Procedure recommended by the PONDUS user manual[8]
3. Procedure recommended by DNV-RP-F109[5]

Referring to table 2.4, Case 1.3 is most critical to the on-bottom stability analysis, and is therefore selected to investigate the effects of different procedures with modified soil properties.

Pipe on stiff clay		
Friction coefficient, μ	0.6	-
Int. diameter of pipe, D_{in}	571.8	mm
Concrete coating, t_{con}	55	mm
Wall thickness, t_{wall}	19.1	mm
Corrosion allowance, t_{cal}	1.5	mm
Corrosion coating, t_{cc}	5	mm
Marine growth, t_{mg}	0	m
Pipe roughness, k/D	0.001	-
Significant wave height, H_s	14.8	m
Peak wave period, T_p	15.9	s
Current velocity, U_0	0.51	m/s

Table 5.1: Pipe and environment data for the pipeline under combined load of 10-year return currents and 100-year return irregular waves with increase layer

5.1 Standard 3-hour simulation procedure with default initial penetration calculated by PONDUS

The soil property for Case 1.3 in table 2.4 is modified to stiff-clay soil type. The initial penetration is calculated to be 0 according to equation 5.1[5].

$$\frac{z_i}{D} = 0.0071\left(\frac{G^{0.3}}{K_c}\right)^{3.2} + 0.062\left(\frac{G^{0.3}}{K_c}\right)^{0.7} \quad (5.1)$$

$$G = \frac{s_u}{D\gamma_s} \quad (5.2)$$

$$K_C = \frac{s_u D}{w_{sub} - F_L} \quad (5.3)$$

where

z_i : Initial penetration depth

s_u : Clay undrained shear strength

γ_s : Clay dry unit weight

D : Contact pressure between pipe and soil

F_L : Lift force

w_{sub} : Pipe submerged weight

A 3-hour simulation is performed for a design storm condition. The simulation results are shown as follows.

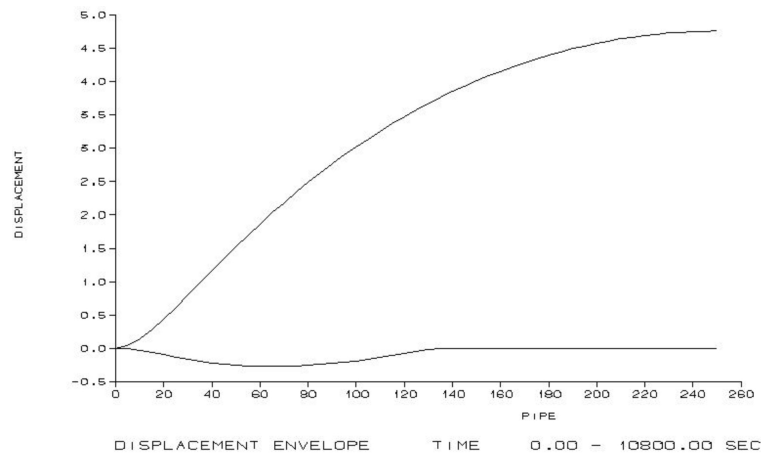


Figure 5.1: Displacement envelop along the pipe for the stiff-clay model

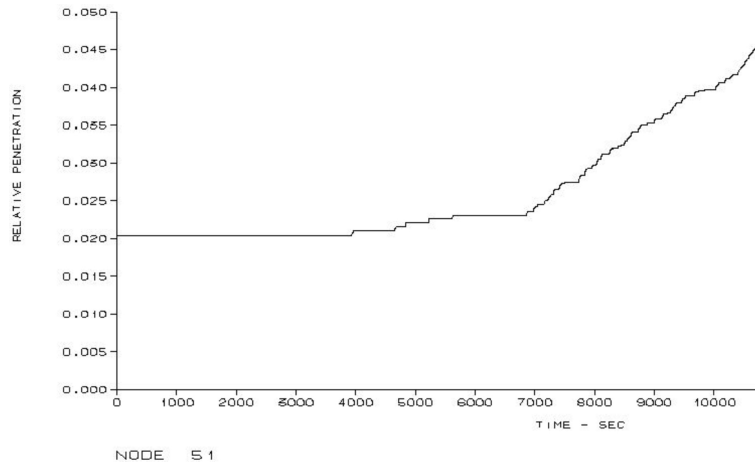


Figure 5.2: Relative penetration at node 51 for the pipe with the stiff-clay model

The maximum displacement is about 5m at the right end of the pipe, and is smaller than 10 times of the outer diameter of the pipe. It suggests that the pipe is stable when considering the $L_{stable} < L_{10}[5]$ displacement criteria. However it seems that the displacement will still develop and the conclusion may be conservative. It should be noted that the instability in this context refers to an “accumulated damage” that may also get contribution from storms that are less severe than the design storm in a normal analysis. Never the less, the standard procedure tends to underestimate the displacement.

5.2 Procedure recommended by the PONDUS user manual

According to example 4 in the PONDUS manual[8], the waves are sorted into two sets, the first with 800 waves and the other with 500 waves. This procedure is penetration-oriented and is built up step by step by substituting the initial penetration depth taken from the previous simulation result.

- Step 1. 800-1000 waves with linear increasing hydrodynamic forces.
- Step 2. 500 waves with short start-up period (100s), use the penetration found in Step 1 as initial penetration.
- Step 3. If the penetration is still under development, repeat the analysis with 500 waves and penetration from previous step as the initial penetration.
- Step 4. Perform the design storm analysis when the penetration is stabilized.

5.2.1 Step 1, 800 waves

The simulation is performed for 800 waves with linearly increasing hydrodynamic forces. The time duration of the analysis is 11136s. The initial penetration of 0.0001m is calculated by equation 5.1. Simulation results are presented as follows.

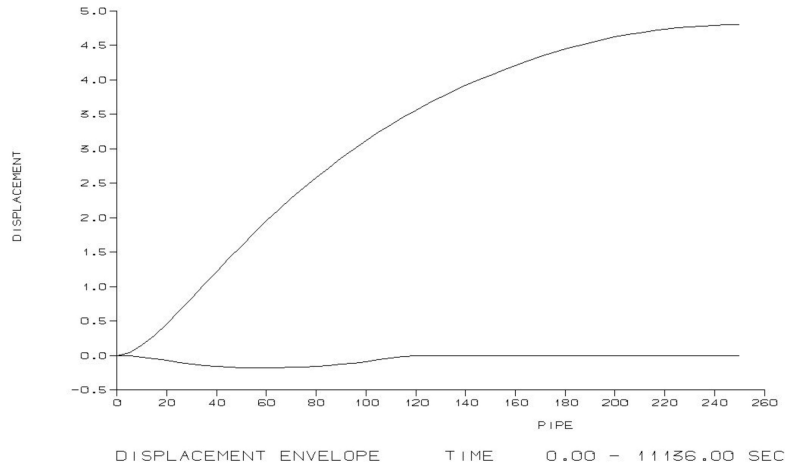


Figure 5.3: Displacement envelop curve vs the pipe length for the stiff-clay model (Step 1:800 waves)

As shown in figure 5.3, the maximum displacement is nearly 5m towards the right end node.

As it is shown in figure 5.4, the relative penetration increases steeply from 0 up to 0.045m through out the time-period. This value will be applied as the initial penetration in the next step.

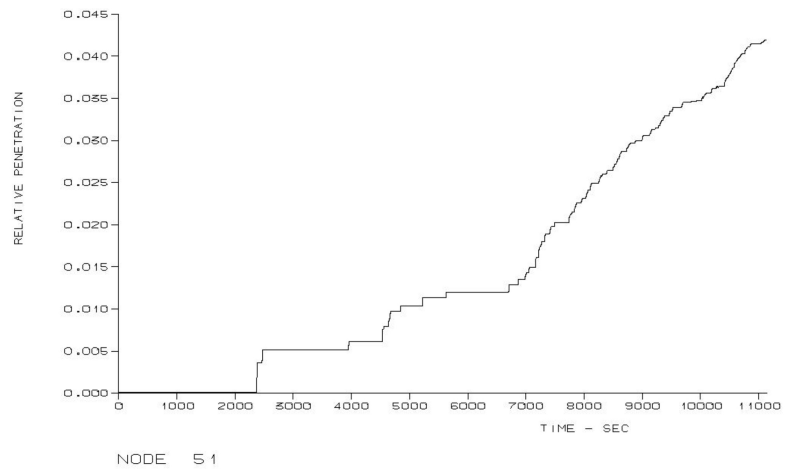


Figure 5.4: Relative penetration at node 51 for the pipe with the stiff-clay model (Step 1:800 waves)

5.2.2 Step 2, 500 waves

The simulation is conducted for 500 waves with 100s start-up period. The initial penetration is taken as 0.045m from Step 1.

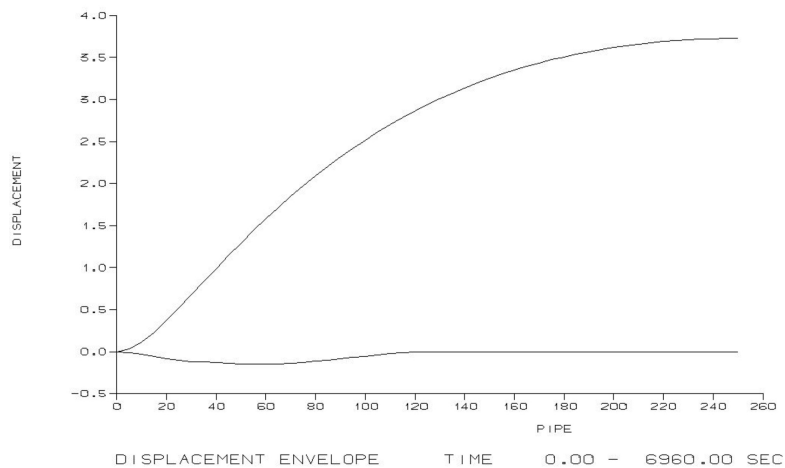


Figure 5.5: Displacement envelop curve vs the pipe length for the stiff-clay model (Step 2:500 waves)

As shown in figure 5.5, the maximum displacement increases gradually to 3.7m at the right end node, which is actually decreased comparing to Step 1. This is due to the increased initial penetration which increases the passive resistance soil force and restrains the movement of the pipe.

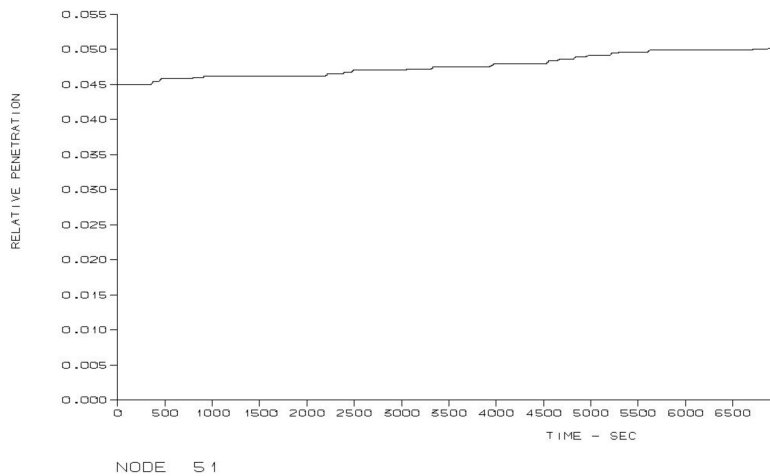


Figure 5.6: Relative penetration by time at node 51 for the pipe with the stiff-clay model (Step 2:500 waves)

The penetration depth increases from 0.045m to 0.05m, which develops with a smaller gradient compared to that in 800 waves. In order to get a stabilized penetration, a repeated analysis with 500 waves is performed in Step 3 with the maximum penetration depth from Step 2 as the initial penetration.

5.2.3 Step 3, 500 waves

The simulation is repeated for 500 waves. The initial penetration is 0.05m taken from Step 2. The simulation results for Step 3 are presented as follows.

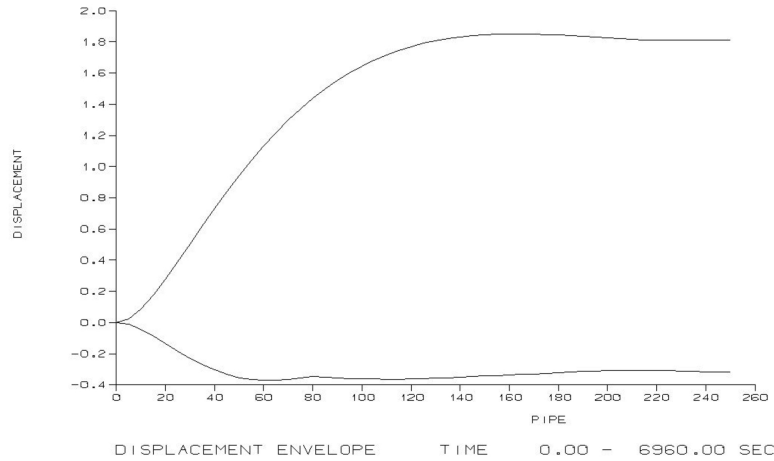


Figure 5.7: Displacement envelop curve vs the pipe length for the stiff-clay model (Step 3:500 waves)

As shown in figure 5.7, the maximum displacement is 1.82m and occurs at about 150m from the left end, then decreases slightly towards the right end node. It became smaller compared to that in Step 2 as the initial penetration is set to be larger. It further proves the contribution from the initial penetration depth in restraining the movement of the pipe.

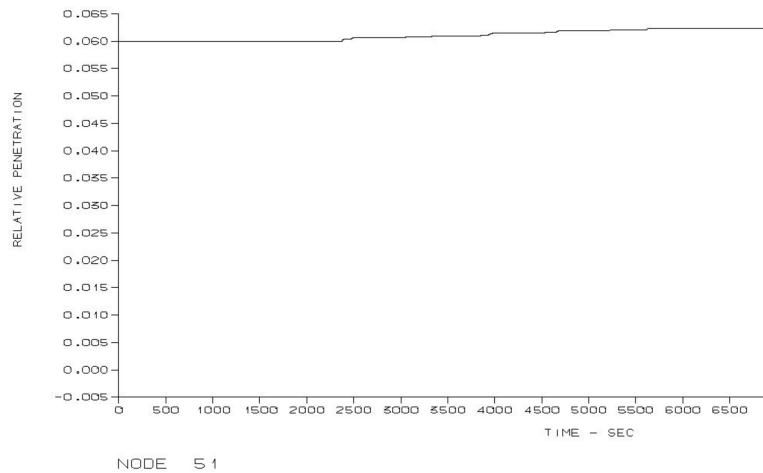


Figure 5.8: Relative penetration by time at node 51 for the pipe with the stiff-clay model (Step 3:500 waves)

According to figure 5.8, the penetration is almost constant. Therefore the penetration depth of 0.061m will be applied as the initial penetration for Step 4.

5.2.4 Step 4, 3-hour design storm analysis

The simulation is conducted for a 3-hour design storm analysis. The initial penetration is 0.061m from Step 3, which ensures a stable relative penetration depth. The simulation results for this step are presented as follows.

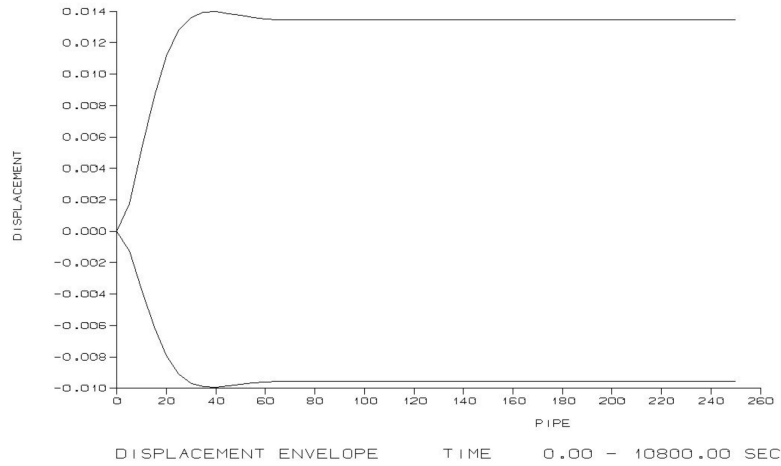


Figure 5.9: Displacement envelop curve vs the pipe length for the stiff-clay model (Step 4)

The total displacement for the PONDUS recommended procedure is $5+3.7+1.82+0.012 = 10.5m$

As shown in figure 5.9, the maximum displacement drops down to 0.014m as the initial penetration from Step 3 is applied. The depth of 0.061m provides adequate passive resistance and the pipeline will not move during the design storm.

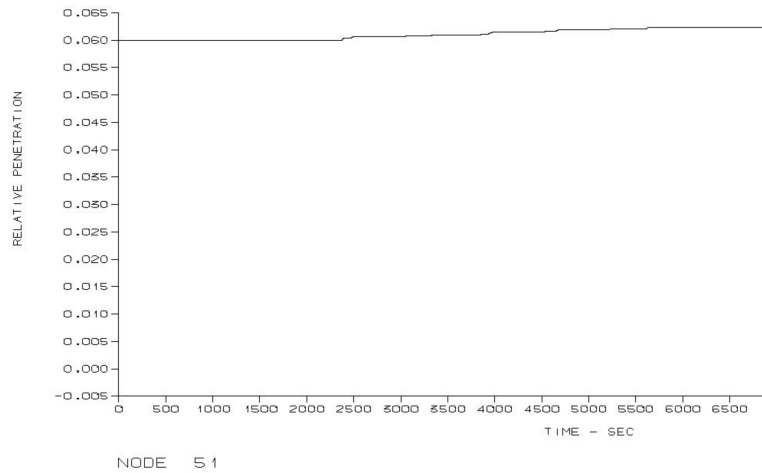


Figure 5.10: Relative penetration by time at node 51 for the pipe with the stiff-clay model in 500 waves (Step 4)

The relative penetration stayed at 0.061m, which equals to the initial penetration. The analysis of step 4 indicates the pipe will be stable in the design storm when the stabilized penetration from Step 3 is considered as the initial penetration. The accumulated displacement is about 10.5m.

5.3 Procedure recommended by DNV-RP-F109

According to DNV [5], the storm sea scenario can also be modeled by introducing a linear ramp function on wave induced particle velocity and acceleration, so that the load increases from zero to full load during approximately the first 20 per cent of the analysis. The pipe will be subjected to moderate waves with small displacement that leads to increased penetration and passive resistance. As the 3-hour simulation is considered in the analysis in 20 percent of 3-hour (2160s). Thus the start-up period in PONDUS simulation is set to be 2160s.

As it is required in [5], very small time increments are applied to accurately capture the highly non-linear phenomenon with a large degree of the stick-slip response. Therefore the number of time-step is set as 0.001s for the clay soil.

As shown in figure 5.11, the maximum displacement is 5.7m at the right end node.

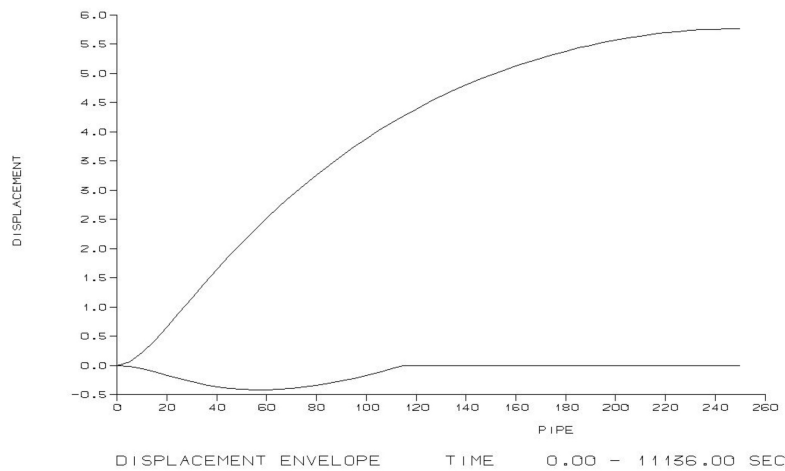


Figure 5.11: Displacement envelop curve vs the pipe length for the stiff-clay model

The results satisfy the L_{10} displacement criteria[5] for the pipeline, but it is not sufficient to draw a conclusion on whether the displacement of the pipeline will further increase if the simulation time increases. It is also important to find out whether the penetration becomes stable at 2160s in the analysis.

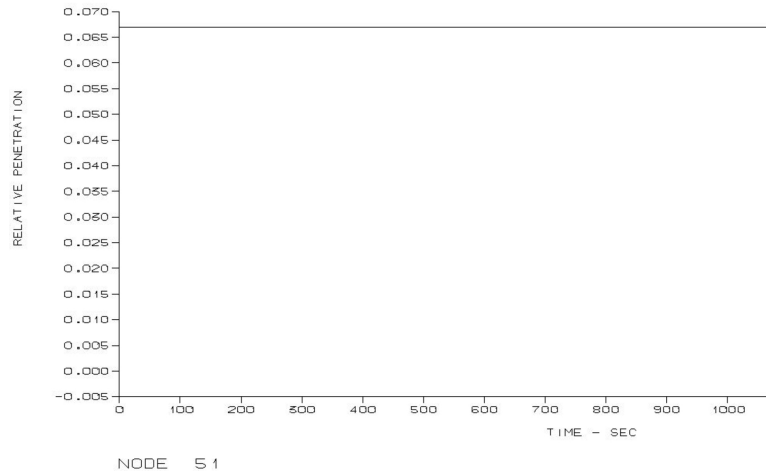


Figure 5.12: Displacement by time at node 51 for the pipe with the stiff-clay model

5.4 Comparison and discussion

A summary for the process and related results are listed in the table below:

Procedure no.	Displacement during 3-hour simulation with design storm [m]	Accumulated displacement [m]	Max. relative penetration [m]
1	5	5	0.046
2	0.014	10.5	0.065
3	5.7	5.7	0.067

Table 5.2: Case summary for different procedures

As it is mentioned in the short discussion for the first procedure, it seems that the pipeline fulfills the L_{10} displacement criteria[5]. However the development of the penetration and displacement is not stabilized, therefore there is no sufficient material for a conclusive assessment of on-bottom stability under this circumstance.

Considering the total steps of each procedure, the PONDUS recommended procedure is obviously the most sophisticated one, as the initial penetration is deducted step-by-step with several iterations. The initial penetration of 0.061m is used for the design storm analysis for procedure 2, and the penetration is about 0.07m in the DNV procedure. The penetration used for the design storm analysis for the current case is similar to procedure 2 and procedure 3.

The maximum displacement is 0.014m in the 3-hour design storm analysis. It shows that the pipeline is stable when the stabilized initial penetration is used in analysis. Procedure 2 has the largest accumulated displacement and is recommended in practice.

The procedure recommended by DNV considers the build-up effect of the initial penetration before the storm. It could be applied in the analysis when the penetration is stabilized after the start-up time (20% of 3-hour).

6 Mitigation methods

A subsea pipeline will be exposed to multiple structural failures and potential risks of damages in its life cycle. Most of the failure modes can be avoided by achieving the on-bottom stability criteria in the design phase. If the on-bottom stability criteria can not be fulfilled, secondary mitigation approaches will be applied to stabilize the on-bottom pipe from various aspects. There are 4 most applied methods recommended by DNV according to DNV-RP-F109 [5].

- weight coating
- trenching
- burial
- mattresses
- structural anchors
- intermittent rock berms

Those measures should be properly dimensioned throughout the design life of the pipeline for all relevant loads that described in section 2.5 . Weight coating is taken into consideration in this chapter as a primary stabilization method. However it is not always sufficient to stabilize the on-bottom pipeline, therefore additional methods should be considered as well. Various of secondary stabilization methods are available to restrict the displacement of the pipeline.

Trenching is often applied to reduce the hydrodynamic force acting on the pipeline. At the same time, the penetration of the pipe at the side of trenching increases the passive resistance force. However, the relatively higher cost and requirement of the equipment in deep water is a major issue for the operation. The trench effect is taken into account in the PONDUS simulation by applying equivalent penetration.

Referring to table 2.4, the most critical Case 1.3 is applied for the current investigation. Further more, $L_{stable} < D/2$, the virtual stability criteria [5] is considered to obtain the most conservative result.

6.1 Weight coating

According to the analysis results in section 3, the pipe does not satisfy the requirement of virtual stability criteria $L_{stable} < D/2$ in following load combinations:

- 10-year return currents and 100-year return irregular waves
- 100-year return currents and 10-year return irregular waves

Considering material cost and simplicity for operation, the diameter of the pipes concrete layer is increased to achieve virtual stability, which means extra layer of concrete has to be applied in order to increase the weight of the pipe, it exceeds the horizontal external force from waves and currents when the pipe is stable at the seabed.

6.1.1 Pipelines under combined load of 10-year return currents and 100-year return irregular waves with increased layer

Table 6.2 shows the pipe and environmental data for the pipeline under combined load of 10-year return currents and 100-year return irregular waves with increased layer.

Table 6.1: Pipe and environment data

Soil type: Simple Coulumb friction model		
Friction coefficient, μ	0.6	-
Int. diameter of pipe, D_{in}	571.8	mm
Concrete coating, t_{con}	75	mm
Wall thickness, t_{wall}	19.1	mm
Corrosion allowance, t_{cal}	1.5	mm
Corrosion coating, t_{cc}	5	mm
Marine growth, t_{mg}	0	m
Pipe roughness, k/D	0.001	-
Significant wave height, H_s	14.8	m
Peak wave period, T_p	15.9	s
Current velocity, U_{10}	0.44	m/s

Table 6.2: Pipe and environmental data for the pipeline under combined load of 10-year return currents and 100-year return irregular waves with increased layer

The thickness of the concrete layer is increased from $55mm$ to $75mm$, which makes the outer diameter of the pipe to $0.75m$.

The simulation results presented in figure 6.3 and figure 6.4 shows that the maximum displacement at $65m$ from the right end is $0.2m$, which is smaller than half of the outer diameter $D/2 = 0.5m$. Thus the virtual stability criteria in [5] is satisfied.

Pondus simulation results for the displacement of the pipeline are presented as follows.

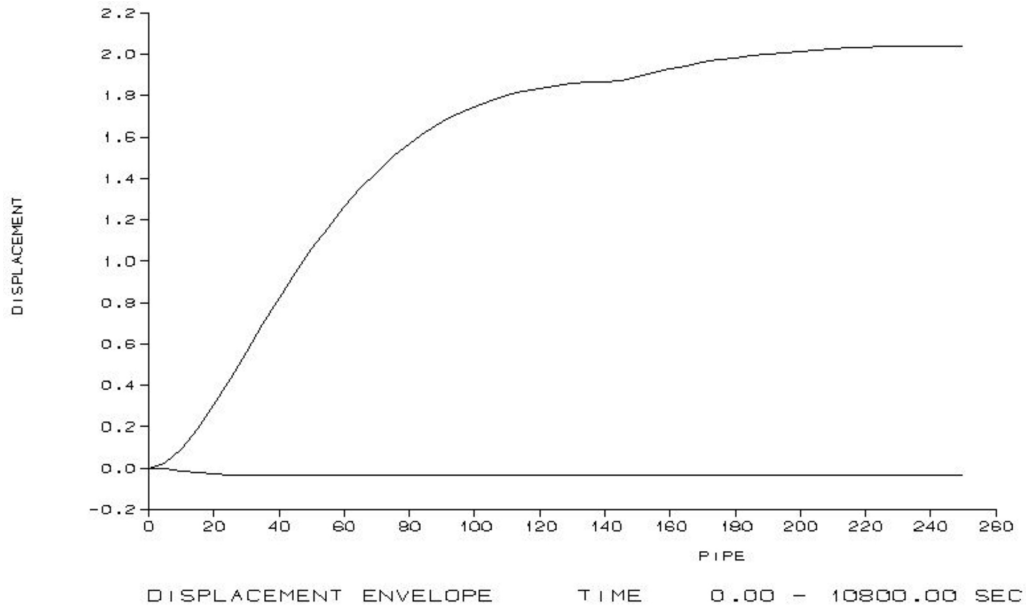


Figure 6.1: Displacement envelop vs pipe length of the pipeline with increased concrete layer under combined load of 10-year return currents and 100-year return irregular waves with increased concrete layer

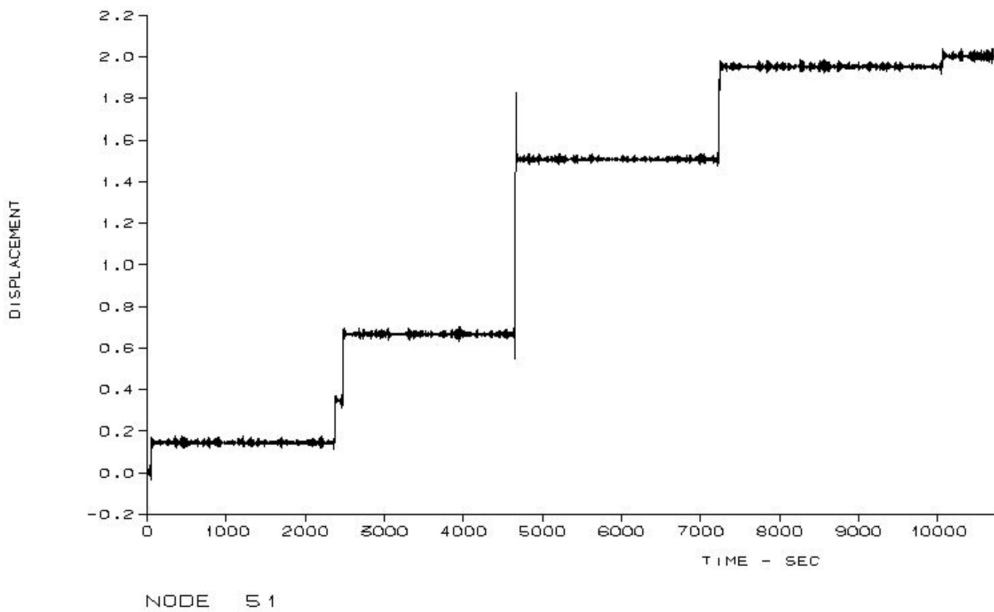


Figure 6.2: Displacement at node 51 vs time for the pipeline with increased concrete layer under combined load of 10-year return currents and 100-year return irregular waves with increased concrete layer ($D = 1.0m$)

The results show that this increment of pipe diameter to 0.75m is still not sufficient to achieve an acceptable displacement. It suggests that further increase of the concrete layer should be applied.

The thickness of the concrete layer is further increased that the outer diameter of the pipeline goes up to 1.0m.

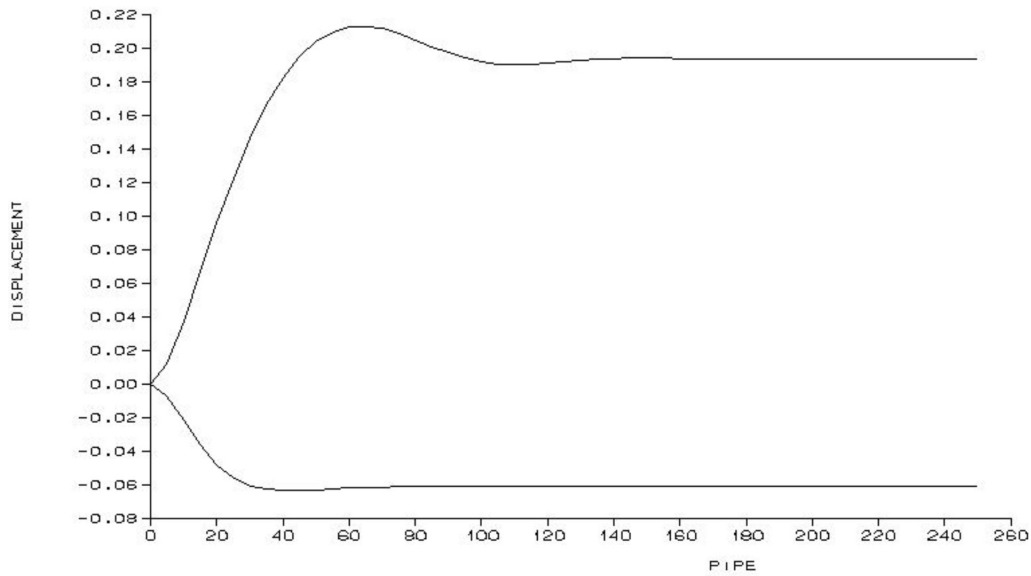


Figure 6.3: Displacement at node 51 vs time for the pipeline with increased concrete layer under combined load of 10-year return currents and 100-year return irregular waves with increased concrete layer ($D = 1.0m$)

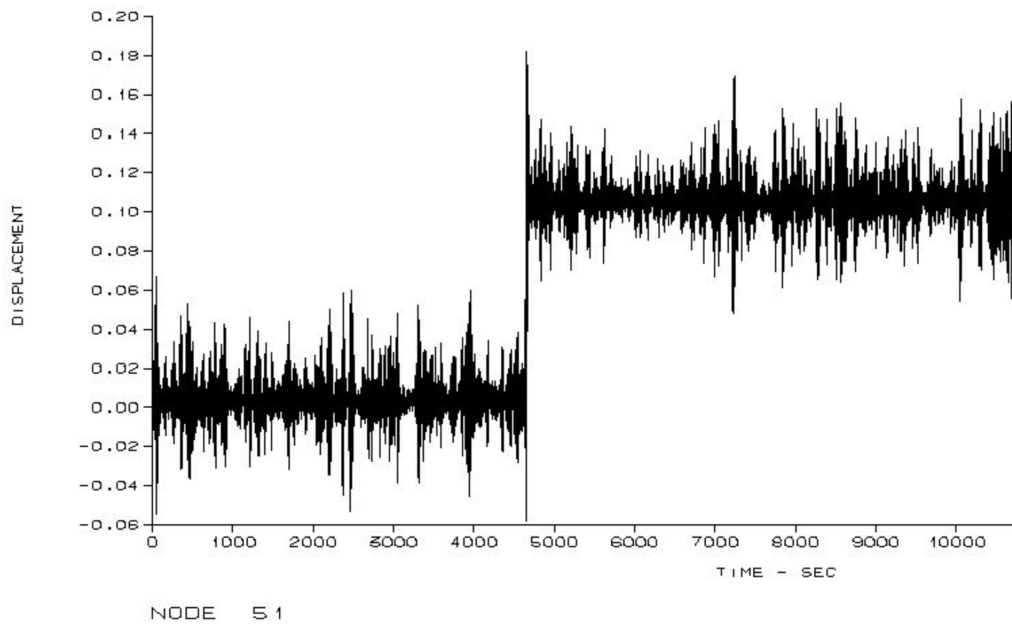


Figure 6.4: Displacement at node 51 vs time for the pipeline with increased concrete layer under combined load of 10-year return currents and 100-year return irregular waves with increased concrete layer

6.1.2 Pipelines under combined load of 100-year return currents and 10-year return irregular waves with increased concrete layer

A thicker concrete layer is to be applied and the outer diameter is increased slightly by 0.01m.

Table 6.4 shows the pipe and environmental data for the pipeline under combined load of 100-year return currents and 10-year return irregular waves with increased layer.

Table 6.3: Pipe and environment data

Soil type: Simple Coulomb friction model		
Friction coefficient, μ	0.6	-
Int. diameter of pipe, D_{in}	571.8	mm
Concrete coating, t_{con}	75	mm
Wall thickness, t_{wall}	19.1	mm
Corrosion allowance, t_{cal}	1.5	mm
Corrosion coating, t_{cc}	5	mm
Marine growth, t_{mg}	0	m
Pipe roughness, k/D	0.001	-
Significant wave height, H_s	12.6	m
Peak wave period, T_p	14.7	s
Current velocity, U_{100}	0.57	m/s

Table 6.4: Pipe and environmental data for the pipeline under combined load of 100-year return currents and 10-year return irregular waves with increased layer

With the 0.01m increase of the concrete layer, as shown in figure 6.5, the maximum displacement in figure 6.5 occurs at 110m from the right end. Combining with figure 6.6, the maximum displacement drops drastically by almost 50% to 0.22m, which meet the virtual stability criteria.

Pondus simulation results for the displacement of the pipeline are shown as follows.

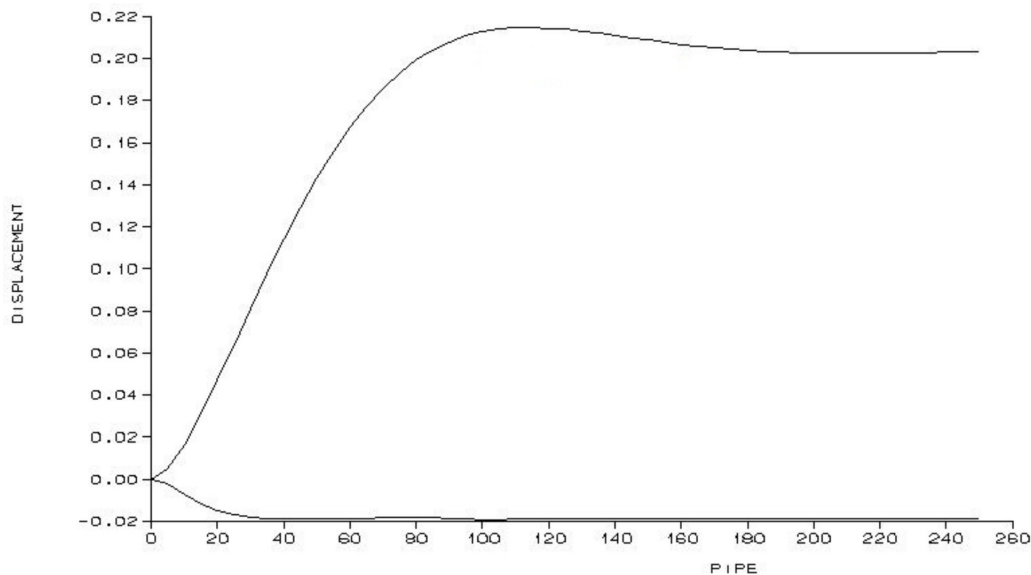


Figure 6.5: Displacement envelop vs pipe length of the pipeline with $D = 0.74$ under combined load of 100-year return currents and 10-year return irregular waves with increased concrete layer

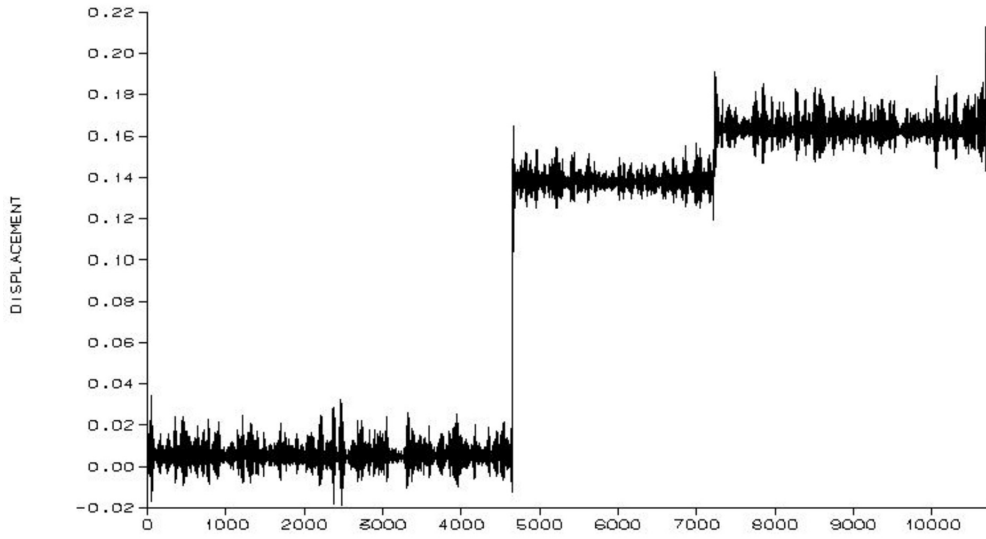


Figure 6.6: Displacement at node 51 vs time for the pipeline with $D = 0.74$ under combined load of 100-year return currents and 10-year return irregular waves with increased concrete layer

6.2 Anchoring

Anchoring is one of the most well-developed approach to intervene the substantial movement of the pipe. Rock bolts, strategic anchors and gravity anchors are often used to serve this purpose. A more appropriate simulation model can be obtained by implementing the secondary stabilization method as a part of the structure model. It restrains the displacement by inducing additional tension along the pipeline. A typical anchor weights from 50 to 350 tons. For the simulation model in PONDUS, a spring stiffness will be defined based on the anchor material, namely steel or concrete. Based on Case 1.3 in table 2.4, the pipe will be modeled with anchor restrictions in PONDUS considering the most conservative selection for spring stiffness, and a simple Coulomb model will be applied for the soil properties. The pipe and environmental data are shown in table 6.5.

Table 6.5: Pipe and environmental data

Soil type: Simple Coulomb friction model		
Friction coefficient, μ	0.6	-
Int. diameter of pipe, D_{in}	571.8	mm
Concrete coating, t_{con}	55	mm
Wall thickness, t_{wall}	19.1	mm
Corrosion allowance, t_{cal}	1.5	mm
Corrosion coating, t_{cc}	5	mm
Marine growth, t_{mg}	0	m
Pipe roughness, k/D	0.001	-
Significant wave height, H_s	14.8	m
Peak wave period, T_p	15.9	s
Current velocity, U_{10}	0.44	m/s

As there is no specification in standards on determination of anchor-spacing, the design for anchor arrangement is therefore conducted by iteration testing, which starts from applying one single anchor at the end node of the pipe, where the maximum displacement occurs. The simulation results are shown as follows.

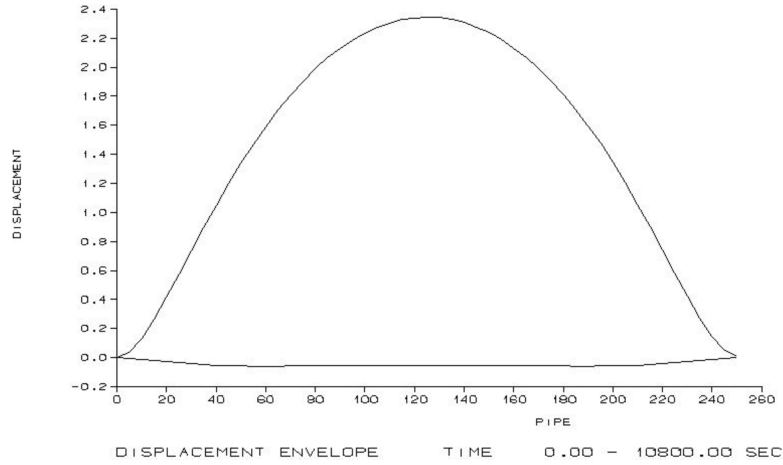


Figure 6.7: Displacement by length with one anchor at the end of the pipe

As it suggests from figure 6.7, the displacement at the end node of the pipe, where the maximum displacement use to occur, became 0 as the anchor restrains it from any movement. However the maximum displacement is transferred to the middle point of the pipe, which is still unacceptable. Thus another configuration with two anchors will be applied to the pipe, and together the two anchors are placed at node 16 and node 36, and the pipe is divided into 3 sections in this analysis.

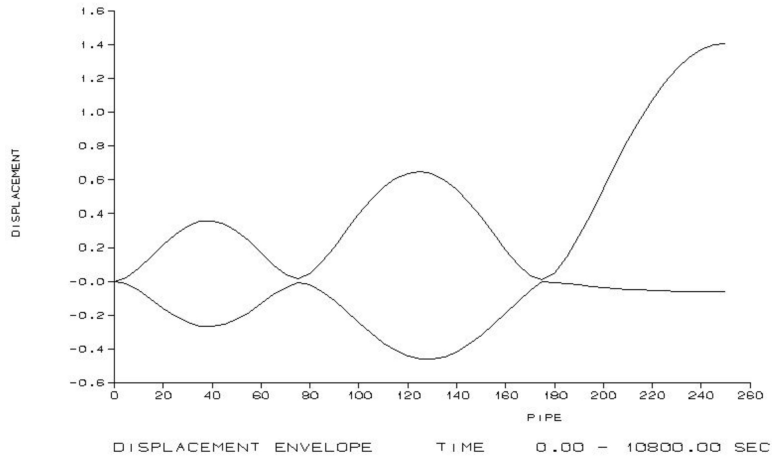


Figure 6.8: Displacement by length with double anchors

The double-anchor arrangement reduced the maximum replacement to a relatively lower value but still not able to meet the virtual stability requirement. This implies that more anchors are needed to obtain an acceptable value for the maximum displacement. After several iterations, an anchor-set of four is proven to be effective on limiting the movement of the pipe.

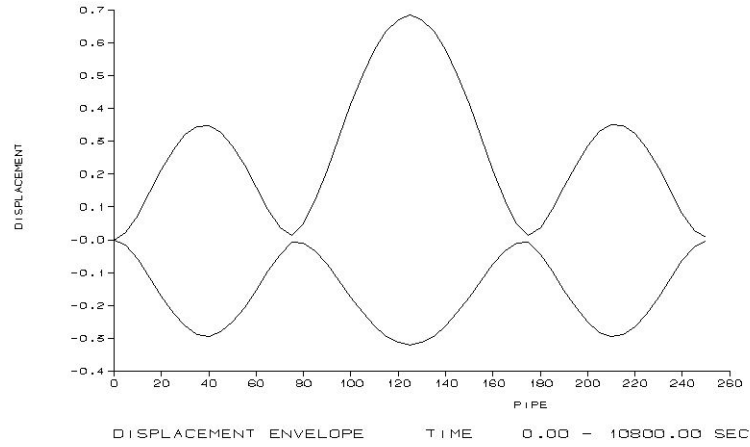


Figure 6.9: Displacement by length with 3 anchors

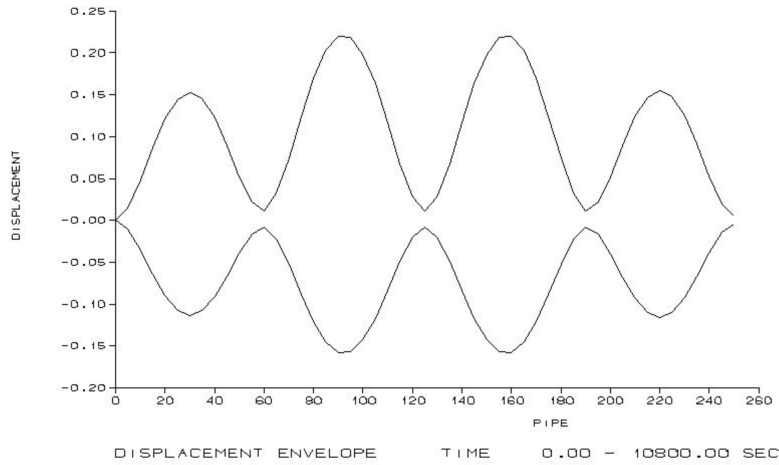


Figure 6.10: Displacement by length with 4 anchors

As it shows in figure 6.10, the pipe is divided equally to 4 sections with those 4 anchor, and shows a relative stable displacement with a sinusoidal shape. With the maximum displacement limited to 0.23m, the virtual stability criteria is met as well. Typical input files for the pipe with 4 anchors are given in Appendix B.

Considering the lack of specified terms in existing standards, manual iteration based on the shape of the displacement curve seems to be the only available choice for simulations in PONDUS. However, related algorithms or calculation formulas need to be developed in the future for anchor arrangement.

7 Conclusion and future work

A series of numerical studies have been conducted on several subjects regarding the on-bottom stability of a subsea pipeline in this thesis. The conclusion and recommendations for the future work will be given upon simulation results and discussions obtained from the present study.

7.1 Conclusion

- Comparisons between the impact of irregular and regular waves for the pipeline with simple Coulomb friction model.
 - Different load combinations should be considered according to the DNV guideline [5]
 - The explicit on-bottom stability criteria is referred based on the maximum displacement of the on-bottom pipeline as $L_{stable} < L_{10}$, where $L_{10} = 10D$ and D is the outer diameter of the pipeline.
 - With same values applied for the wave height and wave period of regular waves, the peak wave height and the significant wave period of irregular waves, the maximum wave induced water particle velocity is larger in irregular waves. It suggests that irregular waves should be considered in the hydrodynamic context to obtain a more realistic and reliable model in the on-bottom stability analysis.
 - When considering the environmental condition, 10-year return currents and 100-year return irregular waves are the most critical load combination for current study.
 - The stair-like development pattern of dynamic displacement is quite extinguishable when the pipe is exposed to underwater environment with irregular waves.
- Sensitivity level of soil parameters and correlations between essential reaction components.
 - Compared to the simple Coulomb friction model, a specified pipe-soil model is proven to be more realistic with specific soil parameters, as the maximum displacement is shown to be much larger with the simple Coulomb friction model than it is with a specified pipe-soil interaction model. The passive resistance force due to the pipe penetration contributes to the on-bottom stability of the pipeline. Underestimation of the on-bottom stability will lead to a considerably higher cost on modification and mitigation measures.
 - The displacement for different pipe-soil models (with the same combination of waves and current) is proven to be
 - Simple Coulomb friction model > pipe-sand model > pipe-clay model
 - In the present study, the right end is free in translation and the maximum displacement normally occurs at the right end nodes. However the different combinations of soil types along the route may change the pattern of the displacement along the pipe.

- The friction coefficient will affect the soil friction, and changes the initial time when the pipe line starts to move in lateral direction when the initial penetration is the same. The time history of displacement of pipeline is changed for different friction coefficients.
 - The relative velocity between water particle and pipeline is different at time instance when pipeline has large displacement. This will induce the difference in drag and lift forces when the relative velocity and relative acceleration is considered in the analysis.
 - When considering the energy-based soil model, the penetration is related to the accumulated displacement of pipeline. The smaller the friction coefficient is, the earlier the pipe will start to move. Moreover, the development of the penetration is relatively slow for large friction coefficients and the maximum value is also small.
 - The penetration and accumulated displacement tends to become larger as the friction coefficient decreases
- Comparison on different procedures for the on-bottom stability assessment of the pipeline during the design storm situation.
 - The initial penetration depth appears to be very important for the assessment of the on-bottom stability during the design storm condition.
 - Procedure 2, which is recommended by the PONDUS user manual [8], is proven to be the most realistic and feasible procedure for the on-bottom stability assessment for a design storm situation.
 - Modeling of mitigation measures.
 - Taking account of the cost and viability of operations, weight coating should be considered first as a primary stabilization method. It should also be noted that the increase of self-weight due to weight coating will affect the initial penetration. The increase of the outer diameter of the pipeline will affect the hydrodynamic coefficients and the hydrodynamic loads.
 - The allocation of anchors along the pipe is essential on the reaction mechanism and improvisation of the on-bottom-stability.

7.2 Future work

Due to the time limitation, only a pipeline with a typical diameter is studied in this thesis, suggestions for the future studies on this topic are as follows:

- Further studies on the on-bottom stability for umbilicals with relative small diameters should be carried out.
- More comparisons can be made between regular waves and irregular waves based on the relationship specified in DNV-RP-F109 [5] for the design single oscillation velocity amplitude and the design spectral velocity amplitude for a specified number of oscillation.

- The parameter study for soil properties could be further investigated. The basic mechanism and tendencies are revealed in the present study for different soil coefficients and different soil types along the route. The effect of different parameters will be even more clear if cases with larger displacement are considered.
- Studies on the anchoring mitigation measurement should be conducted by experiments. The optimization of the mitigation arrangement should be further investigated.

References

- [1] Chen, Q. (2015). Pipeline on-bottom stability design lecture notes. University in Stavanger, Norway.
- [2] D. Bruton, D. White, M. C. and Cheuk, C. (2008). *Pipe-soil interaction during lateral buckling and pipeline walking-the safebuck JIP*.
- [3] DNV-OS-F101 (2012). *Submarine pipeline systems*.
- [4] DNV-RP-C205 (2007). *Environmental conditions and environmental loads*.
- [5] DNV-RP-F109 (2010). *On-bottom stability design of submarine pipelines*.
- [6] Igland, R. T. (2006). *Airy's linear theory*. MARINTEK, SINTEF, Norway.
- [7] MARINTEK (1994). *PONDUS Technical Manual*.
- [8] MARINTEK (2015). *PONDUS user Manual*.
- [9] Richard, V. and Lund, K. M. (1995). *A soil resistance model for pipelines placed on clay soils*.
- [10] Sotberg, T. and Verley, R. L. (1992). *A soil resistance model for pipelines on sandy soil*.
- [11] Harald E. Krogstad and øyvind A. Arntsen (2000). *Linear Wave Theory*. Norwegian University of Science and technology, Norway.
- [12] Irman, A. A. (2015) *Non-linear Soil Models for Pipeline and Riser Analysis*. Norwegian University of Science and Technology, Norway.
- [13] Sumer, B. M. and Fredsøe, J. (2006). *Hydrodynamic around cylindrical structures*. World Scientific Publishing, Singapore.
- [14] Longoria, R.G., Beaman, J.J. and Miksad, R.W.(1991) *An experimental investigation of forces induced on cylinders by random oscillatory flow*. Trans. ASME, J. Offshore Mech. and Arctic Engrg.,113:275-285.
- [14] *Coastal Engineering Manual (CEM)*. United States Army Corps of Engineers' Coastal and Hydraulics Laboratory. <https://cdip.ucsd.edu/?nav=documentssub=indexitem=waves>
- [15] Bai, Q., Bai, Y. (2014) *Subsea Pipeline Design, Analysis, and Installation* Gulf Professional Publishing
- [16] Peregrine, D.H.(1976) *Interaction of water waves and currents. Advances in Applied Mechanics, 16:9-117*.
- [17] Jonsson, I.G. (1990) *Wave Current Interactions In The Sea. eds. B. Le Mehaute and D.M. Hanes* Wiley-Interscience, N.Y., Chapter 9A:65-120
- [18] Justesen, P., Hansen, E.A., Fredsøe, J., Bryndum, M.B. and Jacobsen, V. (1987) *Forces on and flow around near-bed pipelines in waves and current*. Proc. 6th Int.Offshore Mechanics and Arctic Engrg. Symp., ASME, Houston TX.

- [19] Bearman, P.W. and Obasaju, E.D. (1989) *Transverse forces on a circular cylinder oscillating in-line with a steady current*. Proc. 8th Int. Conf. Offshore Mechanics and Arctic Engineering, OMAE, The Hague. 2:253-258.
- [20] Moe, G. and Verley, R.L.P. (1980) *Hydrodynamic damping of offshore structures in waves and current*. 12th Annual Offshore Technology Conf. Paper No. OTC 3798, Houston, TX, 3:37-44.
- [21] Soulsby, R.L., Hamm, L., Klopman, G., Myrhaug, D., Simons, R.R. and Thomas, G.P. (1993) *Wave-current interaction within and outside the bottom boundary layer*. Coastal Engineering, 21:41-69
- [22] Sarpkaya, T. and Storm, M. (1985) *In-line force on a cylinder translating in oscillatory flow*. Applied Ocean Research, 7(4):188-196.
- [23] Sumer, B.M., Jensen, B.L. and Fredsøe, J. (1992) *Pressure measurements around a pipeline exposed to combined waves and current*. Proc. 11th Offshore Mechanics and Arctic Engineering Conf., Calgary, Canada, V-A:113-121

A PONDUS input file for Case 1.3

```
WAVESIM
FILES
' WAVE-FILE 1
  FC3_wav.dat
EXECUTION
' IRUN IDATE
  1 20160201
' IETA IVX IVY IAY IZARR
  1 1 1 1 1
PARAMETERS
' IGTYP NPOS NF NSTEP NTHET
  1 1 16385 32768 1
' JUMBO JUMDIR TR FL FH
  90 190 13500. 0.0314 0.1886
' THETL THETH DEPTH
  0. 180. 104.
SPECTRAL
' HS FP GAMMA THMEAN SCOS
  14.8 0.0628 3.3 90. -1
GRID
' NX NY XO YO ZO
  1 1 0. 0. 104.
' DX DY (BLANK IF ONE GRID POINT)

END
```



```
50PREPONDUS (5 LINES WITH DESCRIPTIVE TEXT TO FOLLOW)
PREPONDUS LONG PIPE/LONGCR.IRR. WAVES/NONMA/PIPE-SAND
INPUT FILE: fc3.ipre
OUTPUT FILE: fc3.opre
LANJING LI 2016-02-01
FILES
'  FILNAM1
  FC3_wav.dat
'  FILNAM2
  FC3_pre.dat
FORCE
'  ICOD DOUT CMA IOPCL FACVY FACDT ISIGN RHOW IRP
  2    0.73 0   0    1.00 1.00 1    1030. 1
CURRENT
'  VCURR ANGLE
  0.44 90.
PRINT
'  IPRINT IPRINT2 PTIME1 PTIME2
  0      0
END
```

50PONDUS (5 lines with descriptive text to follow)
 PONDUS LONG PIPE/LONGCR.IRR.WAV/NONMA/PIPE-SAND, JAN.2016
 INPUT FILE: FC3.ipon
 OUTPUT FILE: FC3.opon
 LANJING LI 2016-02-01

FILES

' IDENT FILENAME
 PON FC3_plot.dat
 INO FC3node51.dat 'time series results for node 51
 WA2 FC3_pre.dat
 OCT FC3timeseriesresults.ts 'startimes file to store the time
 series results for specified nodes and elements

EXECUTION

' IRUN ICOD TSTART IOPFAC FACH FACL ICOMP IREL STRTUP
 2 2 0

UNIT

' SCALE
 METERS

MATERIAL

' EMOD RNYC THERM RHOS RHOC RHOI YIELD RHOW
 2.1E11 0.3 1.2E-7 7.80E3 2813.34 800. 4.15E8 1030.

PIPEDATA

' PLEN NEL DEPTH XSTART INODF FSH
 250 50 104.
 ' I L HDIA SDIA STHICK RMASS WSUB
 0 0 0.73 0.61 0.0191

BOUNDARY

' BCOTL BCORL BCOTR BCORR IOPAX SKAL SKAR RMYL RMYR
 -1 -1 0 -1 1

SOIL

' I L ISOIL SKA RMY
 0 0 1 50.E3 0.60

TEPRTE

' IOFF
 1
 ' PRES TENS RTEMP TEMP
 0. 0. 0. 0.

SOLVE

' DT NTIMX IOPDIS
 0.01 1080000 1
 ' EPS MAXIT IOPINT ALPHA1 ALPHA2 ALPHA3 EPSNM
 0.00001 10 1 0. 0.02 0.02

PRINT

' IPRINT IPRINC PTIME
 1 0 0
 ' NNP NEP ITPR INODT ITPRT
 51 10 1000 51 10
 ' INP1 INP2 INPNNP
 1 2 3 4 5 6 7 8 9 10 11 12 13 14 15 16 17 18 19 20 &
 21 22 23 24 25 26 27 28 29 30 31 32 33 34 35 36 37 38 39 40 &
 41 42 43 44 45 46 47 48 49 50 51
 ' IEP1 IEP2 IEPNEP
 1 10 15 20 25 30 35 40 45 50

PLOT

' ISTEP ISTET ISTEOP
 1000 200 200
 ' NTN
 10
 ' INOD IDA IOCT

```
51      1      1
51      2      1
51      3      1
51      4      1
51      5      1
51      6      1
51      7      1
51      8      0
51     -2      0
51    -11      0
' NTE
2
' IEL      IDB
1          1
1          3
END
```

B PONDUS input file for Case 4.4

```
50PONDUS (5 lines with descriptive text to follow)
PONDUS LONG PIPE/LONGCR.IRR.WAV/NONMA/PIPE-SAND, JAN.2016
INPUT FILE: FC3.ipon
OUTPUT FILE: FC3.opon
LANJING LI 2016-02-01

FILES
' IDENT FILENAME
PON FC3_plot.dat
INO FC3node51.dat 'time series results for node 51
WA2 FC3_pre.dat
OCT FC3timeseriesresults.ts 'startimes file to store the time
series results for specified nodes and elements
EXECUTION
' IRUN ICOD TSTART IOPFAC FACH FACL ICOMP IREL STRTUP
2 2 0
UNIT
' SCALE
METERS
MATERIAL
' EMOD RNYC THERM RHOS RHOC RHOI YIELD RHOW
2.1E11 0.3 1.2E-7 7.80E3 2813.34 800. 4.15E8 1030.
PIPEDATA
' PLEN NEL DEPTH XSTART INODF FSH
250 50 104.
' I L HDIA SDIA STHICK RMASS WSUB
0 0 0.73 0.61 0.0191
BOUNDARY
' BCOTL BCORL BCOTR BCORR IOPAX SKAL SKAR RMYL RMYR
-1 -1 0 -1 1
SOIL
' I L ISOIL SKA RMY
0 0 1 50.E3 0.60
TEPRTE
' IOFF
1
' PRES TENS RTEMP TEMP
0. 0. 0. 0.
SPRING
' I L STRANS SROT
13 13 9.81E6 0
' I L STRANS SROT
26 26 9.81E6 0
' I L STRANS SROT
39 39 9.81E6 0
' I L STRANS SROT
51 51 9.81E6 0
SOLVE
' DT NTIMX IOPDIS
0.01 1080000 1
' EPS MAXIT IOPINT ALPHA1 ALPHA2 ALPHA3 EPSNM
0.00001 10 1 0. 0.02 0.02
PRINT
' IPRINT IPRINC PTIME
1 0 0.
' NNP NEP ITPR INODT ITPRT
11 10 60000 51 100
' INP1 INP2 . . . . . INPNNP
1 6 11 16 21 26 31 36 41 46 51
' IEP1 IEP2 . . . . . IEPNEP
```

```
1    10    15    20    25    30    35    40    45    50
PLOT
' ISTEP    ISTEP
  2160     1200
' NTN
  10
' INOD     IDA    IOCT
  51       1      1
  51       2      1
  51       3      1
  51       4      1
  51       5      1
  51       6      1
  51       7      1
  51       8      0
  51      -2      0
  51     -11      0
' NTE
  2
' IEL     IDB
  1       1
  1       3
END
```